ABSTRACT

TENDULKAR, SAMEER SUDHAKAR. Design and Analysis of High-Throughput Microfluidic Devices for Scalable Production of Encapsulated Tissue and Biological Materials. (Under the direction of Dr. Melur K. Ramasubramanian and Dr. Fuh-Gwo Yuan.)

Current applications of the microencapsulation technique include the use of encapsulated islet cells to treat Type 1 diabetes, and encapsulated hepatocytes for providing temporary but adequate metabolic support to allow spontaneous liver regeneration, or as a bridge to liver transplantation for patients with chronic liver disease. Microcapsules can also be used for controlled delivery of therapeutic drugs. The two most widely used devices for microencapsulation are the air-syringe pump droplet generator and the electrostatic bead generator, each of which is fitted with a single needle through which droplets of cells suspended in alginate solution are produced and cross-linked into microbeads. A major drawback in the design of these instruments is that they are incapable of producing sufficient numbers of microcapsules in a short-time period to permit mass production of encapsulated and viable cells for transplantation in large animals and humans. The objective of this research is to design and develop a scalable high throughput microfluidic device to increase the production rate by simultaneously producing multiple droplets.

Accordingly, a parametric study was conducted to compare an earlier developed *Encapsulator machine* to understand the effect of various parameters affecting the process of microencapsulation. Prototype microfluidic device with eight droplet producing zones was proposed. Computational Fluid Dynamics (CFD) analysis of the proposed microfluidic design was performed using commercially available CFD solvers namely SolidWorks® Flow simulation. The prototype microfluidic device was fabricated using stereo lithography

process. This microfluidic device was used to produce droplets with diameters ranging from 0.45mm to 0.9mm with aqueous solutions of sodium alginate at various concentrations of 0.75% to 3% (wt. /vol.) and then gelled in a $CaCl_2$ cross linking bath. The polymorphism present was less than 10%.

Defects observed in mass production of microcapsules have been characterized. The reasons behind the formation of satellite droplets and observation of stress lines on microcapsules have been identified. High speed video analysis was conducted to understand the effect of physical parameters namely flow rate of air, flow rate of alginate and concentration of alginate using dimensionless numbers namely Weber number and Capillary number to gain in-depth understanding of the droplet formation process. A single nozzle co-axial air flow device was fabricated and a 2D axis symmetric numerical model was developed to conduct CFD analysis of the droplet formation region. The detailed approach to reduce and eliminate these defects has been presented. Applicability of this encapsulation technique towards encapsulation of pancreatic islets and proteins (BSA) has been tested and high cell viability was observed after encapsulation.

Design and Analysis of High-Throughput Microfluidic Devices for Scalable Production of Encapsulated Tissue and Biological Materials

by
Sameer Sudhakar Tendulkar

A dissertation submitted to the Graduate Faculty of
North Carolina State University
in partial fulfillment of the
requirements for the degree of
Doctor of Philosophy

Mechanical Engineering

Raleigh, North Carolina

2013

APPROVED BY:

_____	_____
Dr. Melur K. Ramasubramanian Co-Chair of Advisory Committee	Dr. Fuh-Gwo Yuan Co-Chair of Advisory Committee
_____	_____
Dr. Lawrence M. Silverberg	Dr. Alexander Dean

DEDICATION

To Aai, Baba, Sachin….. And to NC State for the opportunity

BIOGRAPHY

Sameer Tendulkar was born in the beautiful scenic state of Goa, India. In 2003, he began his undergraduate studies in Mechanical Engineering in University of Mumbai (Mumbai, India). After completing his bachelor's in Mechanical Engineering in 2007, he came to North Carolina State University (Raleigh, NC) to pursue graduate studies in Mechanical Engineering. While in his Master's program, Sameer got an opportunity to work with Dr. Melur K. Ramasubramanian on microencapsulation project. The research topic fascinated him so much that he joined the Direct to PhD program in the Mechanical and Aerospace Engineering Department at North Carolina State University to pursue the research topic further. Sameer's research interests include biomedical device design, microfluidics, biomechatronics, microencapsulation, biomanufacturing, rapid prototyping, stereo lithography, microfabrication, fluid mechanics and robotics.

ACKNOWLEDGMENTS

My time at N.C. State has been a great opportunity for scientific education, development as a researcher, as well as professional and personal growth. It has been quite a journey and I could not have made it alone. It is my pleasure to acknowledge those who have helped me along the way.

First and foremost I express my gratitude to my advisor, Dr. Melur K. Ramasubramanian, for his guidance and support. He has always been supportive of my research ideas and has encouraged me to pursue them. In addition to his technical expertise, he has been an incredible source for developing research collaborations. I am most grateful for his respect and consideration for his students as individuals. I consider myself fortunate to have the opportunity to work and learn under his guidance and support. I am thankful for his positive outlook and constant encouragement that has helped me to sail through the times of adversity. His passion for research has been very inspiring and without his kind and generous concern for my well-being, I would not be where I am today.

Additionally I would like to acknowledge the members of my committee Dr. Yuan, Dr. Silverberg and Dr. Dean for their insightful discussions, time and support. I am especially appreciative of Dr. Yuan and Dr. Silverberg for their valuable feedback and suggestions throughout my doctoral career. I would also like to thank Dr. Ward for his advice during the early and mid-stages of my doctoral studies. My experience in the department would not have been the same without the help and support of the outstanding staff. Thank you Ms. Rand, Ms. White, Ms. Cross, Mr. Magnum, Ms. Nowell and Ms. Moore for all that you do to

keep things running smoothly. I would also like to thank Mr. Andres Meyers for his guidance and support while teaching undergraduate labs.

I thank Dr. Opara, Dr. Saul, John P. McQuilling, Dr. Sivanandane, Charlie Childers, Walter Wofford, Dr. Mirmalek-Sani, and Dr. Pareta from Wake Forest Institute for Regenerative Medicine for their help with the biology related research of my project. I am especially appreciative of Dr. Opara for his insightful discussions, guidance, time, patience and support. I would also like to thank Dr. Khan and Alina Higham for their guidance and help with regards to the rheology equipment and data collection. I thank Dr. Coutris, C. Leigh Herran, Stephen Bass, Jamie Cole and Michael Justice for all their help during my work at Clemson University. Also I would like to thank Mr. David Bentley of FineLine Prototyping, for his tremendous help with the fabrication of the microfluidic device.

My experience at NC State would not have been as fruitful without the professional development opportunities provided by the graduate school. I am especially appreciative of Dr. Bostrom for all of her guidance, time and support. I would like to thank Dr. Honeycutt for teaching me How to teach and helping me improve as teacher. I am indebted to all the students that I have taught throughout my graduate studies at NC State for helping me improve both personally and professionally.

I am indebted to the caring and support of the network of peers who helped me when I needed it the most. I would not be here today without your care, generosity and kindness. To Rushabh, Fahad, Nilesh, Suresh, Ajay, Ravi, Keyur, Abhay, Kshitin, Pratik, Shailesh and all past residents of 2512-207/8; Aaron, Jenny, Eddie (a.k.a. Vball Nut), Ada, Zach, Deepak, Sameer, Kevin, Billy, Magaly, Veena, John, Scott, Ken and other volleyball teammates;

Meghambari, Vinay; I cannot thank you enough and am eternally grateful for your altruism. None of this would have been possible without the guidance of the above-mentioned people and without the caring and support of my research group: Swapnil Gupta, Kalyan Katuri, Ranjeet Agarwala, Karthik Tiruthani and Guang Chen. I am especially appreciative of Swapnil Gupta for all his help with experiments and the myriad discussions that we participated in as lab colleagues.

Finally, I thank my family for their support. I am grateful to my parents Sudhakar and Smita Tendulkar for their hard work, many sacrifices and commitment to family and education that have provided me the opportunity to pursue my dreams and made this journey possible. I also thank my brother Vasant Tendulkar for his tremendous patience, help and support especially near the end of my doctoral studies.

TABLE OF CONTENTS

LIST OF TABLES

LIST OF FIGURES

Chapter 1 Introduction

1.1 Diabetes

Diabetes is a disorder of metabolism in which the body is unable to process glucose, main source of energy for the body. There are two types of diabetes. Type 1 diabetes is an autoimmune disease, in which the immune system attacks and destroys the insulin-producing beta cells in the pancreas. The pancreas then produces little or no insulin. This is known as the "Insulin-Dependent Diabetes Mellitus (IDDM)." In type 2 diabetes, the body cannot effectively use the insulin being produced, a condition called insulin resistance. This is known as the "Non-Insulin-Dependent Diabetes Mellitus (NIDDM)." Regardless, the end result is that the body is unable to regulate sugar levels in the blood and cells do not have enough energy for metabolism (Cihakova 2001; Fisher 2006).

1.2 Islet tissue and cure for Diabetes

1.2.1 Islet tissue

Islets are cells clusters located in the pancreas. They consist primarily of beta cells, alpha cells, delta cells, and pancreatic polypeptide cells. Roughly there are about ten thousand individual cells in an islet cluster. Beta cells are the most abundant, about 80%, in islets and they are the only cells in the body that make insulin. People with Type 1 diabetes still have islets but the beta cells have been destroyed. An islet is anywhere from 50 μm to 150 μm in effective diameter. Replacing the beta cells (by replacing the islets) would mean that people with type 1 diabetes would no longer need to take insulin shots (Soon-Shiong et al. 1994). About a million islet cells are needed for a human transplant. In general, four to six

donor pancreases are needed for one human transplant as the islets comprise of only about 2% of all the tissue in a pancreas (Opara 1998). The process of isolating viable islet tissue from a donor pancreas is not efficient to capture all the islets since the process is a selective enzyme digestion of the rest of the organ. An attractive option to meet this demand is to use islets from a different source for ex: porcine islets which are available in abundance.

1.2.2 Cure for Diabetes

There are four general approaches that might accomplish a cure for diabetes (Opara & Kendall Jr 2002). The first is the complete pancreas and islet transplantation. In this case, a donor pancreas is implanted into a diabetic or islet cells from a donor are infused into a vein that drains in the pancreas. In this case, the primary problem is organ rejection. In order to prevent organ rejection, immunosuppression drugs have to be administered and their side effects and complications have to be dealt with. The second method involves a mechatronics solution where the blood sugar level is measured using an embedded sensor and a microcomputer determines the amount of insulin needed and pumps the metered quantity into the blood stream from a reservoir. This method is still in its early stages of offering and faces a host of issues involving reliability and safe operation. The third approach is to genetically engineer the cells to evade the immune system of the host and avoid immunosuppressive drugs. This is not currently developed far enough to make an assessment of the effectiveness and side effects. The fourth approach is the use of encapsulated islets; bio-artificial pancreas has living, functional islets or cells in an artificial biocompatible material. This method has been shown to work when microencapsulated islets were transplanted into small animals and primates (Sun et al. 1996). The transplantation of the organs and tissue across species

boundaries is known as xenotransplantation. In the case of finding a cure for diabetes, the bioartificial pancreas seems to hold the most promise (Fisher 2006; Pareta et al. 2012).

1.3 Microencapsulation

Microencapsulation is described as a process of enclosing micro-particles of solids or droplets of liquids or gasses in an inert shell, which in turn isolates and protects them from the external environment. The products obtained by this process are called microparticles, microcapsules and microspheres which are different in morphology and internal structure (Jyothi et al. 2010; Ghosh 2006) typically with a size range of 200-1000 μm in diameter (Pareta et al. 2012). Microfluidics on the other hand is the science and technology of systems that process or manipulate a small (down to micro and femto liters) volume of fluid using channels with dimensions of tens to hundreds of micrometers (Whitesides 2006). Microencapsulation has mostly been applied to large scale industrial processes of emulsification, coacervation, spray drying, fluidized bed coating, etc. mainly for applications in the chemicals (detergents, cosmetics, printing ink, etc.), textiles, food and paper industry (Tewes, Boury & Benoit 2006), albeit, there has been a long-standing interest in its application in cell therapy since Lim & Sun described microencapsulated islets as a bioartificial pancreas (Lim & Sun 1980). With recent advancements in the micro-fabrication technologies and the advent of microfluidics allowing researchers the ability to manipulate pico and femto liters of fluid volumes, microencapsulation has become one of the most exciting and promising technologies in the field of biomedical research. Several new applications of microencapsulation are being investigated along with novel microfluidic devices and biomaterials for the production of microcapsules.

A major reason for the tremendous interest in the microencapsulation technology is the ability of the user to prepare capsules from a wide variety of biomaterials with tunable properties specific to an application. For example, in the food industry, researchers have successfully encapsulated flavors and colors (Kandansamy & Somasundaram 2012) to provide improved taste and appeal of various food products. In the cosmetic industry, active ingredients present in shampoos or detergents have been encapsulated to protect them until they are delivered on activation by precipitating factors, for example water/dirt/proteins/biological materials to trigger their release thus making them more effective. Most recently, widespread use of the technique has been observed in the biomedical industry, where microencapsulation has been explored in drug delivery and controlled release (Tendulkar et al. 2012; Park, Ye & Park 2005; Wheatley et al. 1998; Machluf, Orsola & Atala 2000; Joki et al. 2001; Dai, Wang & Zhao 2005), biosensors (Chaudhary et al. 2011; McShane & Ritter 2010; Chinnayelka & McShane 2005; Kim et al. 2012), regenerative medicine (Opara et al. 2010; Tendulkar et al. 2012; Lim & Sun 1980), imaging aids (Wheatley et al. 1998; Sheeran & Dayton 2012; Sheeran et al. 2010), cell and tissue encapsulation (Lim & Sun 1980; Opara et al. 2010; Lim et al. 2010; Garfinkel, Harland & Opara 1998; Orive & Pedraz 2010; Kizilel et al. 2010; Beck et al. 2007; Vaithilingam & Tuch 2011; Mikos et al. 1994; Wang et al. 1997), gene therapy (Matte et al. 2011; Haberger & Feil 2006), microelectronics (Yoshizawa 2004; Donaldson 1976) and bio analysis (Eun et al. 2011; Ishii, Tago & Senoo 2010; Chabert & Viovy 2008).

Cell microencapsulation comes under the broader field of bioencapsulation which involves the immobilization of therapeutic cells using polymer scaffolds or semi permeable

hydrogel capsules that provide the cells with a favorable protective environment by allowing the exchange of nutrients and oxygen and protecting them from the host immune systems by blocking the antibodies and cytotoxic cells as shown in figure 1.1 (Lim et al. 2010; Orive et al. 2004). One of the earliest demonstrations of transplanted cells in immunoprotective membranes for organ replacement dates back to 1933, when Bisceglie enclosed tumor cells in a polymer membrane and transplanted them into a pig's abdominal cavity (Orive et al. 2004; Bisceglie 1933). The results showed that the cells survived long enough for it to be concluded that they were not destroyed by the immune system. Thirty years later, Chang introduced the idea of using encapsulation for the immunoprotection of transplanted cells and subsequently coined the term 'artificial cells' for referring to this concept (Chang 1964). This approach was successfully put into practice in the 1970s and 1980s to immobilize xenograft islet cells to aid in glucose control for diabetes in small animal models (Chick, Like & Lauris 1975; Lim & Sun 1980). Since then there have been tremendous efforts all over the world to advance and adapt this process; the wide range of therapeutic applications of cell microencapsulation technology includes: (i) treatment of classical Mendelian disorders, (ii) cancer treatment, (iii) diseases of the central nervous system (CNS), and (iv) bioartificial organs for the treatment of various diseases. Cell microencapsulation represents one of the strategies designed to overcome the present difficulties related to whole organ graft rejection and limited availability of human organs for transplantation. Additionally, it presents a new paradigm for local and systemic controlled release of drugs and growth factors. In the last few years, the principal application of the technology has been for the treatment of a wide variety of endocrine diseases, including anemia (Koo & Chang 1993), dwarfism (Chang,

Shen & Westcott 1993), hemophilia B (Liu, Ofosu & Chang 1993), kidney (Cieslinski & Humes 1994) and liver failure (Wong & Chang 1986), pituitary (Aebischer et al. 1986) and central nervous system insufficiencies (Aebischer et al. 1994) and diabetes mellitus (Lim & Sun 1980; Opara et al. 2010). More recently, microcapsules are also being used as new biodegradable scaffolds for stem cell proliferation and differentiation in vitro as well as in vivo administration (Orive & Pedraz 2010).

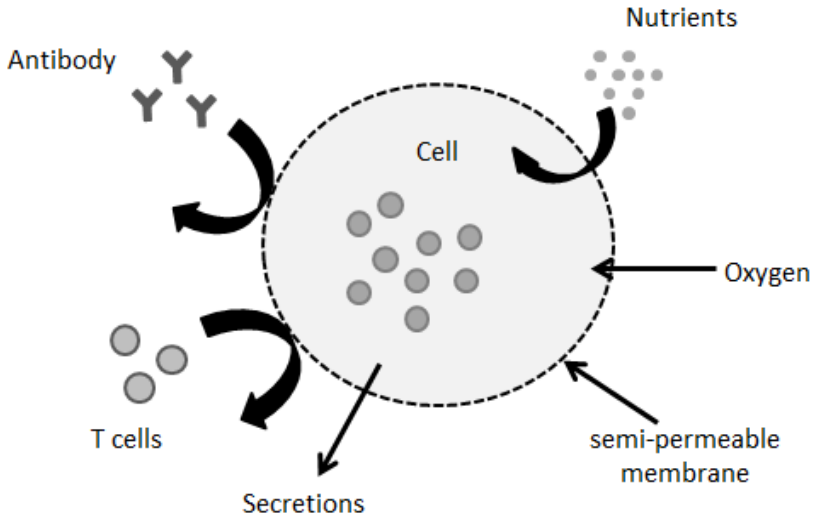

Figure 1.1: Microencapsulated cells protected by a polymer semipermeable membrane that allows nutrients and oxygen to diffuse across the membrane while blocking/restricting access to immune cells and antibodies.

1.4 Different Approaches to Microencapsulation:

A variety of methods have been investigated towards the encapsulation of different materials. Bulk microencapsulation processes traditionally implemented in the industry include processes like spray drying, hot melt, coacervation and phase separation, atomization, pan coating, solvent evaporation, fluidized bed/air suspension coating, and others (Jyothi et al. 2010; Garg et al. 2011). These traditional bulk microencapsulation

techniques used in the food and cosmetic industry, detergents, chemicals, textiles generally have low technical demands such as monodispersity of the output. Thus, these processes provide a less expensive, high throughput microencapsulation procedure for industrial purposes. However there is little or no control over the quality of individual microcapsules produced in these bulk processes. On the other hand, in instances where highly monodispersed, highly controllable microencapsulations are a requirement, microfluidics-based microencapsulation technologies are used. Additionally microfluidic technologies require much less volume of samples and reagents, they have shorter reaction times due to higher surface area to volume ratios and thus help towards reducing overall costs. The commonly employed microfluidic methods/devices for microencapsulation of cells and biological materials are coaxial air-flow droplet generator, electrostatic generator, vibration method, jet cutter and shear flow driven methods. To maintain the focus of this article on microencapsulation of cells using microfluidics we will emphasize the approaches involving the above mentioned microencapsulation methods illustrated in Figure 1.2.

1.4.1 Coaxial air-flow droplet generator:

In this method, droplets are generated as the alginate (dispersed phase) flowing in the inner nozzle gets sheared off by air flowing through the outer nozzle (continuous phase). The size of the droplets produced by this method depends on the flow rate of the dispersed phase, flow rate of continuous phase, outer diameter/wall thickness of the dispersed phase channel (Wolters et al. 1992; Koo et al. 2008; Anilkumar, Lacik & Wang 2001). De Vos et al. reported a scaled up version with four nozzles of the coaxial air-flow droplet generator which allowed for simultaneous production of multiple microcapsules thus helping towards

upscaling the production of microencapsulated islets (De Vos, Haan & Schilfgaarde 1997). In 2007, Sugiura et al. described a scaling up procedure for the coaxial air-flow method using a novel microfabricated device known as Micro-Airflow Nozzle (MAN). This device with 15 nozzles facilitated the simultaneous production of microcapsules (Sugiura et al. 2007).

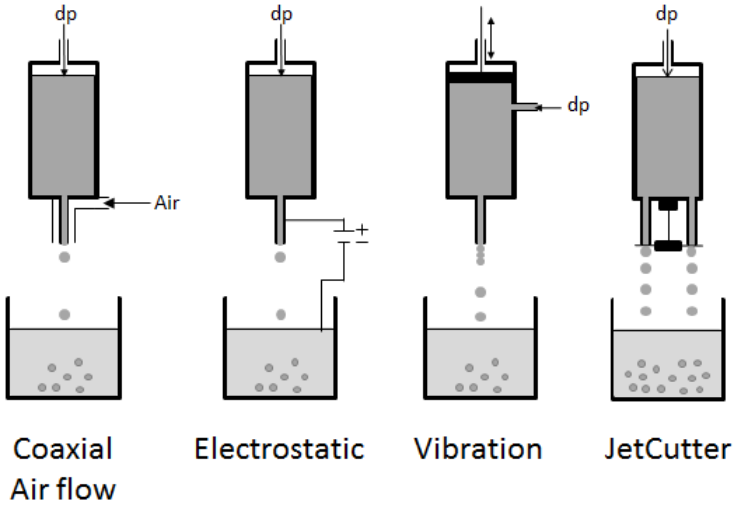

Figure 1.2: Schematic representation of the various microencapsulation methods.

1.4.2 Electrostatic droplet generator:

In this method, electrostatic forces are used to disrupt a liquid filament at the capillary needle tip and form a charged stream of small droplets (Bugarski et al. 1994; Manojlovic et al. 2006; Nedović et al. 2006; Poncelet et al. 1999; Keshavarz et al. 1992). The process of droplet formation depends on a number of parameters such as applied electrostatic potential, needle diameter, electrode distance and geometry, polymer solution flow rate as well as surface tension density and viscosity (Manojlovic et al. 2006; Poncelet et al. 1999). The first scaled up version of this process was described by Poncelet et al. with multiple needles

which allowed for the simultaneous production of several microcapsules (Poncelet et al. 1994). Recently, Deng et al. described a system with 250 sources/cm^2 density of nozzles and Arnanthigo et al. reported an 8 nozzle system for up scaling the production rates of microcapsules using electrospraying technique (Deng et al. 2006; Arnanthigo et al. 2009; Arnanthigo et al. 2011).

1.4.3 Vibration Method:

In the Vibration method, droplet generation is achieved by applying vibrations on a laminar fluid jet which breaks into small droplets when the appropriate wavelength is applied to it [63]. The droplet size depends upon the diameter of the nozzle, wavelength of the applied vibration, and viscosity of the fluid. This method is particularly not suitable for high viscous polymer solutions as droplet break up from the fluid column does not occur as the viscosity of the solution increases beyond a certain limit (Prüsse et al. 2008). Brandenberger and Widmer reported a scaled up version of this device with 13 nozzles for the encapsulation and immobilization of micro-organisms, enzymes, and cells with a production rate up to 5000 ml/hr. (Brandenberger & Widmer 1998).

1.4.4 Jet Cutter Method:

In the Jet cutter method, droplets are generated by mechanical cutting of a liquid jet by rotating cutting wires installed in a cutting tool. The diameter of the microcapsules produced depends on the nozzle diameter, rotation frequency of the cutting tool, as well as the number and diameter of the wires. As this method is based on physical cutting of the liquid jet by blades, about 5% of the encapsulating fluid/polymer is lost in the process (Prüsse et al. 1998; Prüsse et al. 2008). For low viscosity solutions the jet cutter method does

not produce beads in the normal configuration; however it is able to achieve excellent production rates with high viscosity solutions (Prüsse et al. 2008). Prusse et al. described a scale-up of this process for high throughput processing in industrial application (Prüsse et al. 1998).

1.4.5 Shear flow driven methods:

In shear flow driven droplet generation, the shearing force of one flowing fluid is used to form droplets. The two most common types of flow geometries implemented in such microfluidic devices are 'T-junction' and 'Co-flow/ Flow focusing' (Ben-Tzvi & Rone 2010). These methods are currently popular and widely utilized methods in academic research environments.

1.4.5.1 T-junction Geometry

In a typical T-junction configuration, the flow of dispersed phase is orthogonal to the flow of the continuous phase, as shown in Figure 1.3(a). The breakup of the dispersed phase fluid into droplets is caused by shear from the cross flow of the stream of a second immiscible fluid (continuous phase). This geometry was first used to produce highly monodisperse droplets in a microchannel by Thorsen et al. (Thorsen et al. 2001). Since then many studies have been conducted on T-junction geometry to gain in-depth understanding of the physics involved in the droplet formation process, the factors affecting the formation of droplets. Figure 1.3 (b), (c), (d), and (e) depict the schematic representations of the various T-junction geometries and their modifications employed in biomedical applications. The diameter of the microcapsules produced by this method depends on the flow rates of the fluids, channel widths, and the relative viscosity between the two fluids (Garstecki et al.

2006; Teh et al. 2008). The use of active elements (see figure 1.3 (c) for expanding the flexibility, control and range of reliable droplet production in T junction devices has also been reported (Lin, Lee & Lee 2008; Wu et al. 2009). Scaling up droplet formation using T junction devices has also been described for mass production with the highest throughput being 320ml/hr. for 256 droplet formation units (Sugiura et al. 2005; Zeng et al. 2010; Nisisako & Torii 2007). However, one of the challenges facing the scale up is to minimize the detrimental cross-talk between the different droplet formation units (Gu, Duits & Mugele 2011).

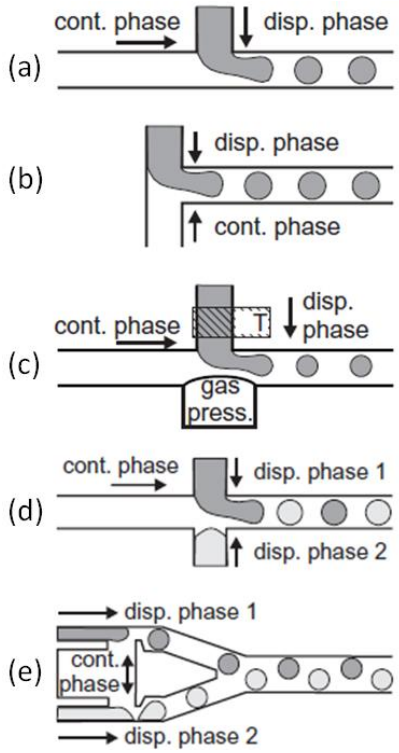

Figure 1.3: Schematic representation of various T Junction Geometries and various modifications employed in the biomedical field (a) basic T-junction geometry (b) a modified T junction geometry known as 'Head on' geometry where the dispersed phase and continuous phase are injected into the main channel from opposite sides (c) Active T-junction geometry (d) & (e) Demonstrates combination of two T-junctions (Seemann et al. 2012).

1.4.5.2 Co-flow / Flow focusing geometry

In co-flow/ flow focusing geometry, a stream of dispersed phase fluid is sheared onto droplets by a surrounding carrier/continuous phase fluid flow. The carrier/continuous phase fluid is designed to surround the dispersed phase fluid flow. The flow focusing device is a slight modification of the co-flow device where the continuous and dispersed phase fluids meet and then move through an orifice, where the continuous phase fluid forces the dispersed phase fluid into a narrow stream which breaks up into small droplets downstream of the orifice (Anna, Bontoux & Stone 2003; Gañán-Calvo & Gordillo 2001). Figure 1.4 is an illustration of co-flow and flow focusing devices. This geometry was first implemented for liquid gas flows by Alfonso M. Gañán-Calvo (Ganan-Calvo 1998). Later this technique was implemented for liquid-liquid systems by Umbanhowar et al. (Umbanhowar, Prasad & Weitz 2000), and then modified to a 2D flow focusing geometry by Anna et al. (Anna, Bontoux & Stone 2003). Since then many studies have been conducted to gain fundamental understanding of the co-flow/flow focusing geometry. The size of the microcapsules generated depends on channel geometry, flow rate of the fluids, and their viscosity (Utada et al. 2007; Ward et al. 2005). Attempts at scaling up this geometry have been made by Li et al. (Li et al. 2008), Hashimoto et al. (Hashimoto et al. 2008), and Kendall et al. (Kendall et al. 2012). They found weak hydrodynamic coupling between the different parallel flow focusing devices. The use of active element in co-flow/ flow focusing geometries has also been reported to increase the flexibility and operating range (Ganan-Calvo, Lopez-Herrera & Riesco-Chueca 2006; He et al. 2010).

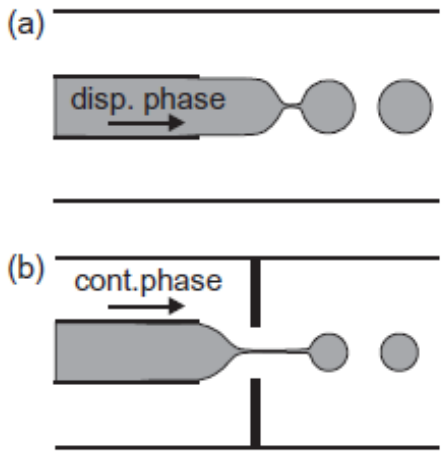

Figure 1.4: Illustration of the (a) co-flow and (b) flow focusing devices (Seemann et al. 2012).

1.5 Fabrication Methods:

A number of microfabrication techniques, initially developed for micro-electronics and micro-electro-mechanical systems (MEMS), are now employed by the biomedical field and being used for building microfluidic devices. Compared to the field of microelectronics, fabrication of the biomedical devices present more challenges due to the use of a variety of different materials, chemicals and fluids for different applications (Guttman & Khandurina 2004). Early microfluidic devices were composed of silicon and glass because of their good optical properties and well developed microfabrication technology and surface chemistry. Microfabrication of these devices required the use of wet and dry etching, photolithography, electron beam lithography, and other techniques all of which in turn require the use of clean room facilities and equipment making it an expensive and time consuming fabrication process (Fiorini & Chiu 2005). With the development and increase in the use of polymer materials like thermosets (SU-8, polyimide, etc.), thermoplastics (poly(methyl methacrylate)

(PMMA), polycarbonate (PC), cycloolefin polymers and copolymers (COP, COC)) and elastomers (poly(dimethylsiloxane) (PDMS)) researchers have been able to fabricate microfluidic devices using less complex techniques which paved the way for inexpensive disposable polymeric microfluidic devices. Recently some research groups have developed paper and wax based microfluidic approach also resulting in simple, low cost microfluidic devices for use in the biomedical field (Martinez et al. 2010; Zhang & Zha 2012; Kaigala et al. 2007). In the following sections we will review the most common methods used for the fabrication of disposable polymeric devices. Informational overviews as well as detailed descriptions of various microfabrication methods used for patterning fine structures and assembling microfluidic devices can be found in a number of recent publications (McDonald et al. 2000; Becker & Gartner 2000; Becker & Gartner 2008; Steigert et al. 2007; Thomas et al. 2010; Iliescu et al. 2012).

The microfabrication techniques used for the fabrication of disposable polymer microfluidic devices can be broadly characterized into replication and direct techniques. As a general rule, the choice of the fabrication method is determined by several factors such as available technologies/equipment, cost, speed, desired feature size and profile, and the preferred material substrate.

1.5.1 Replication Techniques

The various replication techniques used for microfabrication are hot embossing (Esch et al. 2003; Kimerling et al. 2006), injection molding (McCormick et al. 1997; Kim et al. 2006), photo/soft lithography (McDonald et al. 2000; Burns et al. 1998; Qin, Xia & Whitesides 1996) and others (Fiorini & Chiu 2005; Becker & Gartner 2008; Baharudin 2008).

Replication methods are based on replication of the master structure which is the first step in the fabrication of microfluidic devices. The commonly used microfabrication processes for the fabrication of the master are wet/dry etching, photoresist, polymer casting, LIGA, ultra precision micromachining, among others. Once a master is fabricated its typical lifetime is limited to a few ten to hundred replications at moderately complex designs and low aspect ratios. A detailed overview of the various processes used for the fabrication of the master and other replication technologies are provided in recent reviews (Becker & Gartner 2000; Becker & Gartner 2008; Iliescu et al. 2012). The most commonly used replica fabrication technique in the biomedical field for making microfluidic devices involves standard soft-lithography procedure along with polydimethylsiloxane (PDMS) polymer as it as it does not require routine access to a cleanroom for making most structures relevant to microfluidic devices (McDonald et al. 2000). In this method (as shown in figure 1.5), PDMS polymer is cast onto a master and cured at room temperature or at a slightly higher temperature. After removing the cured PDMS replica from the master, the PDMS mold is typically bonded to a glass substrate using various bonding techniques (gluing, lamination, laser/ultrasound welding, etc.) and contacted by tubing which can be simply pushed through the PDMS rubber. Some advantages of this technique include its simplicity of fabrication, low background fluorescence and good biocompatibility of PDMS. The most frequently used photoresist for soft-lithographic procedure to create the master is the negative resist SU-8 which is available in different viscosities to directly generate a wide range of structure heights starting from about 1μm to several hundred micrometers in a single step (Fiorini & Chiu 2005; Becker & Gartner 2008; Baharudin 2008; Seemann et al. 2012).

Replication techniques are less expensive, high volume fabrication methods and are more or less adaptations of the corresponding fabrication processes from the macrofabrication technology. Over the past decade these methods have allowed for and have been instrumental for the commercialization of microfluidic devices and enabling them to be available as disposables.

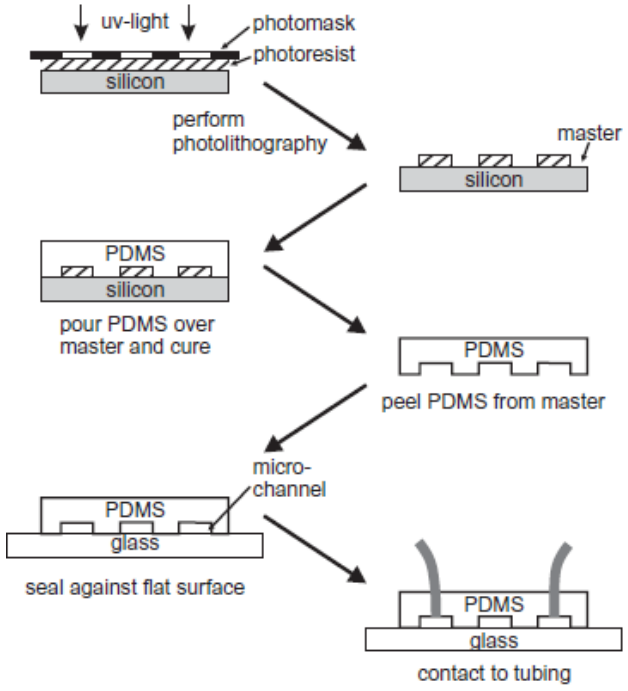

Figure 1.5: Illustration of various steps involved in the fabrication of a microfluidic device using standard soft-lithography technique and PDMS polymer (Seemann et al. 2012).

1.5.2 Direct Techniques

In contrast to the above mentioned replication techniques, which allow the repetitive production of a polymer device from a single mold, several other techniques exist, which micromachine each single device individually. Direct techniques include microfabrication methods like laser ablation (Malek 2006; Malek 2006; Metz et al. 2004), X-ray lithography

(Sun & Kwok 2006), and stereo-lithography (Bertsch, Lorenz & Renaud 1999; Maruo, Ikuta & Korogi 2003). These methods allow rapid fabrication of low-cost highly customizable single devices as no prior master fabrication step is required, thus eliminating that time-consuming and expensive step of replication techniques. However the fabrication throughput is limited by the fabrication time for each individual device. More detailed information regarding these methods can be obtained from recent reviews (Fiorini & Chiu 2005; McDonald et al. 2000; Becker & Gartner 2000; Becker & Gartner 2008; Baharudin 2008). Other microfabrication aspects to be considered include sealing steps to form complete devices with enclosed micro-channels by direct bonding, anodic bonding, lamination, gluing, laser and ultrasonic welding (Guttman & Khandurina 2004; Becker & Gartner 2000; Iliescu et al. 2012).

Recently some researchers have published the use of paper and tape as the base material in the fabrication of three dimensional extremely low-cost, easy to use analytical devices aimed at providing a new class of affordable point-of-care diagnostic devices for use in developing countries (Martinez et al. 2010; Martinez, Phillips & Whitesides 2008). They have also shown wax printing as a simple micro patterning process for making paper-based microfluidic devices (Carrilho, Martinez & Whitesides 2009). Paper based microfluidic devices have also been fabricated using printed circuit technology (Zhang & Zha 2012). Another research group has used copper substrates or gold compact disks using rapid marker masking to replace photolithography for making low-cost rapid prototyped microfluidic devices (Abdelgawad & Wheeler 2008).

With the recent advances in stereo lithography microfabrication technology, it is now possible to fabricate microfluidic channels with low surface roughness and reduce the build time required for the fabrication of each device. In a recent publication by Tendulkar et al., a completely monolithic 3D microfluidic device has been fabricated using the stereo lithographic 3D printing process (Tendulkar et al. 2012). The biggest advantage of stereo lithography process is that the entire device is fabricated as one single monolithic device thus avoiding the additional steps of alignment and sealing which are required for the complete fabrication of microfluidic devices fabricated using the other above mentioned microfabrication technologies. This helps in preventing any misalignment and leakage issues that might arise later during the working/use of the microfluidic device.

1.6 Applications of microencapsulation:

1.6.1 Industrial applications

The first major industrial application of microencapsulation was in the paper industry towards manufacturing of carbonless paper in 1950's (Yoshizawa 2004). Carbonless paper is prepared by coating one side of the paper with microcapsules containing ink precursors which would rupture when pressure is applied while writing (White 1998). In the food industry, microencapsulation has been used to encapsulate colors, flavors, lipids, probiotics, antioxidants, antimicrobials, milk proteins, and other substances to make them more attractive and pleasant, and to add to the nutritional value of food (Kandansamy & Somasundaram 2012). In the textile industry, microencapsulation has found wide spread use. Some of the major applications include coating of textiles with colors/dyes, antimicrobial coatings, fragrances with skin softeners, insect repellents, vitamins, phase change materials,

antibiotics and other drugs (Nelson 2002). In the electronics industry, microencapsulation is used in manufacturing ultra-flat mounted electronics, e-ink, and microencapsulated electrophoretic display system (Comiskey et al. 1998; Yoshizawa 2004).

In the past decade, however the biomedical field has seen the most exciting wide spread use of the microencapsulation technology. These can be broadly divided into therapeutic applications of cell and biological materials and other biological processing and applications.

1.6.2 Therapeutic applications of cell and biological materials

The strategy of encapsulation of cells has been used for the following therapeutic purposes namely (a) development of bioartificial organs, (b) cure for cancer and (c) treatment of other disorders like anemia, dwarfism, hemophilia, diabetes mellitus, Parkinson's, Huntington's, Alzheimer's, etc. Recent focus and efforts by scientists from all over the world are being put towards development of bioartificial organs like pancreas, kidney (Cieslinski & Humes 1994), liver (Wong & Chang 1986) and parathyroid (Aebischer et al. 1986).

The construction of genetically modified cells has opened new avenues for the treatment of classical Mendelian disorders such as dwarfism, hemophilia and lysosomal-storage disease. However, one crucial limitation of these gene therapy approaches is that genetically modified cells often arise from allogenic or xenogenic source and thus their use leads to the formation of antibodies against the gene products because the host's immune response regards the replaced enzyme as a foreign antigen. To overcome this problem, a single treatment of anti-CD4 antibody could be coadministered with the microcapsules, thereby prolonging the therapeutic effect of the gene product (Orive et al. 2003). The

appropriate selection of the cell source for a specific application depends on functional requirements, processing, storage, availability and cost (Murua et al. 2008).

Several studies using cell microencapsulation have been performed for the treatment of cancer, which is the second leading cause of death in the Western world. In one study microencapsulated cells capable of expressing inducible nitric oxide synthase (iNOS) caused tumor suppression in mice, triggering the upregulation of Fas, Fas ligand and similar proteins in the tumor, which resulted in the activation of apoptotic pathways (Xu, Liu & Charles 2002). In another, encapsulated cells were transfected with cytochrome P450 to activate ifosfamide enzymatically. In a clinical trial Lohr et al. reported the use of microcapsules to enable the continuous and localized delivery of chemotherapies, avoiding systemic toxicity. Such a cell-based treatment would help in protecting the recipient from the dire side effects of chemotherapy and help towards speeding up the recovery time for patients (Löhr et al. 2001). Targeting might also be favored by linking the anti-neoplastic molecule to the Fv region of an antibody with affinity to a specific tumor line. Using this approach, C2C12 myoblasts were able to secrete, during 21 days, a fusion protein composed of interleukin 2 and the Fv region of an antibody with affinity to the oncogene HER-2/neu (Cirone et al. 2002). Thus one of the main advantages of the use of encapsulated cells for the treatment of cancers is that therapeutic molecules can be locally delivered in a sustained manner from implanted cells since the cells are enclosed in microcapsules and are thus protected from host immune rejection.

Microencapsulated cells can be implanted into damaged areas of the brain to achieve local, targeted and long-term delivery of drugs or proteins. Many studies have demonstrated

the preclinical feasibility of encapsulation as a means of delivering biological factors to the CNS including the use of primary chromaffin cells for pain, PC12 cells for Parkinson's disease, genetically-engineered cells secreting trophic factors for Parkinson's (PD), Huntington's (HD), Alzheimer's disease (AD) and ALS. In general, these studies demonstrate that encapsulated cells can be immunoisolated and remain viable for extended periods of time to produce significant neuroprotective and behavioral benefits.

An area of increasing interest in which microencapsulation of stem cells could be a promising therapeutic strategy is tissue replacement therapy, a relatively new research area with very limited data. Stem cell integration upon implantation in the host tissue and to maintain the undifferentiated state to afterwards direct their differentiation could become the main objectives of the technology. Although most of the published data are only from in vitro approaches, some in vivo studies have been developed such as the implantation of encapsulated bone marrow mesenchymal stem cells to improve the formation of the osseous and cartilaginous architecture (Cai et al. 2007; Kaigler et al. 2006) and the transplantation of encapsulated embryonic stem cells (ESC) in order to overcome the rejection that may take place when transplanting ESCs into recipients with different major histocompatibility antigens (Dean et al. 2006).

1.6.3 Other biological processing and applications

Microencapsulation technology has also found wide spread application in the development of other biological techniques like imaging, biosensors, bioanalysis, among others. Kendall et al. recently, reported a scaled up microfluidic device for producing dual layer micro bubbles for use in medical imaging and drug delivery (Kendall et al. 2012).

Sheeran et al. have described the use of microcapsules containing perfluorobutane which are used as phase-change contrast agent for low energy ultra sound imaging (Sheeran et al. 2010). Wheatley et al. has reported use of hollow biodegradable polymeric microcapsules as contrast agents and also listed strategies for their use in imaging and drug delivery (Wheatley et al. 1998). The use of alginate microcapsules as biosensors has also been reported by Chaudhary et al. (Chaudhary et al. 2011). They fabricated near-infrared dissolved core alginate microsphere sensors by emulsion process and coated them using layer-by-layer assembly and showed that these glucose sensors had approximately 1.5 times more sensitivity than that observed by visible dye sensors while not affecting the biocompatibility of the materials. McShane and Ritter reported the use of nanoengineered capsules as they show promise as carriers for optical sensing reagents, providing a wall of separation between the environment and encapsulated probes while allowing small molecule analytes (McShane & Ritter 2010). They have demonstrated prototype biosensors to stably entrap macromolecular luminescent components within polyelectrolyte microcapsules and observe reversible reactions with target species. Kim et al. presented a microfluidic-based strategy that would be potentially suitable to produce microcapsules with various bioactive microbial spores for on-site biosensor analysis (Kim et al. 2012). Eun et al. have described a high throughput cell analysis and isolation system made by encapsulating bacterial cells in agarose microparticles around 30μm in diameter followed by fluorescence-activated cell sorting (FACS) (Eun et al. 2011). Using this approach they were able to reduce the time and quantity of antibiotics required for isolation of mutants 8 to 150 times respectively, compared to conventional techniques using nutrient agar plates. Chabert and Viovy proposed an approach

in which single cells were encapsulated into small droplets and self-sorted with high purity and yield using a microfluidic platform based on passive hydrodynamic effects (Chabert & Viovy 2008). Their system works with highly concentrated suspensions and with whatever the distribution of cells is in the solution. They also demonstrate the practical applicability of their system by directly encapsulating and sorting cancerous T-lymphocytes out of whole-blood mixture. Zeng et al. reported a high performance single cell genetic analysis system in which they generated microcapsules containing cells and primer functionalized microbeads which then were further processed to be used for solid PCR. These microcapsules were then lysed and the beads pooled and rapidly analyzed by multicolor flow cytometry (Zeng et al. 2010).

Many more exciting applications of microencapsulation technology using microfluidics are being researched across the world by various scientists. Since the microfluidics platform is such a versatile resource an increasing number of its applications in the biomedical field will certainly emerge in the near future.

1.7 Microencapsulation of islets for transplantation

A major focus of the application of microencapsulation technology in cell therapy has been in the development of a bioartificial pancreas for the treatment of diabetes. There has been a long-standing interest in the replacement of the destroyed β-cells in Type 1 diabetes since the descriptions of viable procedures to isolate pancreatic islets from rats (Lacy & M. 1967) and humans (Ricordi et al. 1988). However, routine use of islet transplantation in diabetic patients has been stalled by the need to use risky immunosuppressive drugs to prevent transplant rejection and the limited availability of human organs. The concept of

immunoisolation of islets by microencapsulation prior to transplantation evolved as a strategy to overcome these two major barriers to transplantation. The resulting construct is frequently referred to as a bioartificial pancreas (Lim & Sun 1980; Opara et al. 2010), which would help diabetic patients avoid multiple daily insulin injections that are required to maintain normal blood sugar and also help in preventing the undesirable side effects such as unwanted weight gain and increased episodes of hypoglycemia (Opara et al. 2010).

Lim and Sun first described the concept of immunoisolation for a bioartificial pancreas in 1980 (Lim & Sun 1980). Since then a lot of research groups have reported various levels of success with transplantation of immobilized cells in small animal models. Also, promising results obtained in allo- and xeno-transplantation approaches are encouraging (Lim & Sun 1980). A large clinical trial by Living Cell technologies, Ltd., that begun in Russia as a phase 1 trial has now been extended to a phase II trial in New Zealand and Argentina (Technologies 2010).

1.8 Challenges faced by microencapsulation technology and need for scale up devices

Since the introduction of the microencapsulation technology in the biomedical field by Bisceglie in 1930's (Bisceglie 1933) for immune protection of transplanted cells, it has made significant progress towards acceptance and applicability in various fields. However there are certain challenges that still prevent this versatile technology from wide-scale use. Some of the pressing challenges facing the use of microencapsulation technology for encapsulation of cells and other biological materials are scale up devices for microencapsulation, internal oxygen and nutrients transfer limitation to encapsulated cells, optimal transplantation site,

reduction of the total transplant volume, ability to monitor implanted capsules, complete encapsulation of all the cells, reduction of inflammatory response after transplant of the encapsulations, availability of unlimited islet donor sources, more efficient islet isolation procedures, and better purification and storage techniques (Pareta et al. 2012). In various studies over the last decade, researchers across the globe are examining different strategies to address the above mentioned issues. For the scope of this dissertation, the focus has been limited to discussion regarding the requirement of scale up devices for microencapsulation.

1.9 Scale up devices for microencapsulation

One of the biggest challenges facing cell microencapsulation is scaling up of the process. The two most widely used devices for microencapsulation are the air-syringe pump droplet generator (Wolters et al. 1992) and the electrostatic bead generator (Bugarski et al. 1994; Hsu et al. 1994). Each of these devices is fitted with a single needle through which droplets of cells suspended in alginate solution are produced and cross-linked into spherical microbeads. A major drawback in the design of these instruments is that they are incapable of producing sufficient numbers of microcapsules in a short-time period to permit mass production of encapsulated and viable cells for transplantation in large animals and humans (De Vos, Haan & Schilfgaarde 1997). A prolonged process of encapsulation of cells adversely affects the viability of the cells. A multi needle approach to producing more than one encapsulated cell at a time as a scale up of the process has been described with four needles (De Vos, Haan & Schilfgaarde 1997). While this scale up is a step forward in accelerating the production of encapsulated cells, production rates at several orders of magnitude higher are required to meaningfully produce sufficient quantities of encapsulated

and viable cells to serve millions of patients requiring cell transplantation. For instance, for transplantation in human subjects, it has been estimated that for the 1 million islets needed for transplantation in a diabetic human subject, about 100 hours would be required to complete the encapsulation of this number of islets, assuming one islet/microcapsule. In practice, it has actually been estimated that the duration of the process would be closer to 200 hours because of the additional steps involved in the encapsulation procedure, following the generation of the initial cell containing alginate microspheres (De Vos, Haan & Schilfgaarde 1997).

Some of the recent studies however have reported some promising approaches to scaling up of the production rates of microencapsulated islets. Brandenberger and Widmer reported the use of vibrational technology and multi nozzle design for scaling up the production of alginate beads (Brandenberger & Widmer 1998). Their system uses 13 nozzles for production of microcapsules in the range of 0.2-1mm. While they reported that their system has a productivity of 5000ml/hr., with less than 4% error droplets, the system is limited to fluids with viscosities less than 200 mPas. The system described was built up of various different parts that gave rise to alignment and sealing issues. Poncelet et al. (Poncelet et al. 1994), Deng et al. (Deng et al. 2006), and Arnanthigo et al. (Arnanthigo et al. 2011) have all described scale up processes for electrostatic droplet generator and electrospraying process. Poncelet, et al. described a parallel plate electrostatic droplet generator with a 20-needle design (Poncelet et al. 1994). Satellite droplets production was observed as smaller droplets were produced using a 26 gauge needle and the volume of the satellite droplets was less than 10% of the total droplets produced. It is however as a good manufacturing practice not to

have any/minimize the satellite droplets from being generated during production of microcapsules containing cells. Also it was observed that, in order to generate droplets of a particular diameter, as the number of needles used for generation of droplets is increased, a corresponding higher voltage is required to generate droplets from these needles. Deng et al. managed to achieve a remarkable packing density of 250 nozzles/cm2, with droplets produced in the range of 10-12 µm with a relative standard deviation less than 0.15 (Deng et al. 2006). However the throughput of this system is very low in the range of 1cc/hr. per nozzle or less for small droplet generation and the maximum flow rate reported in the study was less than 16cc/hr. The device design is such that it gives rise to edge effects in the electric field distribution. The fabrication process to make the chip with such high nozzle density would require complex alignment and sealing processes to avoid any system leaks during operation. Arnanthigo et al. reported a scale up of the model by using 8 outlets and a circular fluid feeding reservoir design with droplet diameters in the range of 17- 25µm with flow rates ranging from 0.5 to 4 ml/hr. and relative standard deviation less than 0.2 (Arnanthigo et al. 2009; Arnanthigo et al. 2011). The device is made up of different parts with the nozzles made of polyether ether ketone (PEEK). Thus alignment and sealing issues could possibly arise during actual operation of this device. Prusse et al. presented the Jet-cutter device for scale up of the production rates of the microcapsules (Prüsse et al. 2008; Prüsse et al. 1998). This device was able to achieve production rates about ten times higher than a single nozzle vibration-based device and around ten thousand times higher than single nozzle devices based on the coaxial and electrostatic technologies. However this technique

does not make droplets with low viscosity solutions and approximately 5% of the fluid is lost due to cutting and processing issues when using this encapsulation technique.

Kendall et al. reported a scale up device having 8 outlets generating high throughput droplets with diameter in the range of 18.6-22.3µm with polydispersity less than 9% (Kendall et al. 2012). The device is fabricated using standard soft lithographic techniques and PDMS. It is a four layer device with the top three layers made from PDMS and the last one being a glass slide. Oil is used for the generation of droplets. As oil is infused at the bottom layer and gas in the top layer, perfect alignment and sealing of the channels is necessary for optimal working of the device as misalignment would drastically affect its performance. Li et al. has demonstrated an instrument using four parallel flow focusing devices (Li et al. 2008). The microfluidic device is made up of three layers with standard soft lithographic techniques. The device generated droplets with coefficient of variation less than 5%. Surfactant Span 80 in light mineral oil was used as the continuous phase to generate droplets. Lorenz et al. reported a microfluidic device with five outlets capable of producing multiple droplets simultaneously using T-junction geometry (Lorenz et al. 2008). The device is fabricated using standard soft lithographic techniques and PDMS. They used various silicon oils and surfactant Span 80 to generate droplets. The flow rates achieved for the device varied from 250-400 µl/min. It was observed that as the produced droplet size increased the polydispersity of the droplets also increased. The device showed signs of droplet quality deterioration after running continuously for a period of 70 minutes as the droplets started wetting the channel floor. Nisisako and Torii presented production module comprising a glass microfluidic chip with planar microfabricated 16–256 droplet-formation units (DFUs)

and a palm-sized stainless steel holder having several layers for supplying liquids into the inlets of the mounted chip (Nisisako & Torii 2007). Using the T-junction geometry based module having 128 cross-junctions (i.e., 256 DFUs) arranged circularly on a 4 cm x 4 cm chip, they could produce droplets of photopolymerizable acrylate monomer at a throughput of 320.0 mL/hr. having a mean diameter of 96.4 mm, with a coefficient of variation (CV) of 1.3%. Another co-flow module having 128 co-flow geometries could produce biphasic Janus droplets of black and white segments at 128.0 mL/hr. with a mean diameter of 142.3 mm, with a CV of 3.3%. This co-flow module could also be applied in the mass production of homogeneous monomer droplets.

Chabert and Viovy presented a high throughput microfluidic device based on flow focusing and hydrodynamic effects. Their device is fabricated using soft lithography techniques (Chabert & Viovy 2008). They demonstrated flow rates varying from 50-200µl/hr. to generate droplets of diameter varying from 7-17µm. They also demonstrated successful encapsulation of 70-80 percent of the injected cell population with <1% contamination by empty droplets and sorting cancerous T-lymphocytes out of a whole blood mixture. Sugiura et al. have reported two different scale up devices based on micro-nozzle arrays (Sugiura et al. 2007; Sugiura et al. 2005). In the first design, oil is used to generate droplets from both alginate and calcium chloride which are then cross linked at a different location in the flow. This device has 104 nozzles and alginate flow rate of 5ml/hr. was used to generate droplets with diameters from 50-200 µm and with a coefficient of variation less than 10%. This design was fabricated using micromachining techniques and the different parts were then assembled to form the entire microfluidic device. In the second design, called

the micro air-flow nozzle, fifteen concentric air flow and alginate channels were used to produce alginate microcapsules with diameter in the range of 100-300 μm and with coefficient of variation less than 7.5%. The optimal productivity of the device was 5ml/hr. and when it was increased to the theoretical value of 100ml/hr. leakage issues were observed. Most of the scale up techniques based on T-junction and flow focusing geometries mentioned above use standard soft lithographic techniques, micromachining techniques (DRIE, etc.) for fabrication of the different parts/layers of the device. These layers are then assembled, aligned and sealed together using adhesion techniques mentioned in the earlier section of this paper. These allow for alignment and leakage issues to occur during the actual operation of the device. Also these methods utilize oil and surfactants to produce microcapsules. The use of oil and surfactants is not desirable for the production of the microcapsules for immunoisolation and transplantation due to the additional steps and time required towards retrieval of the capsules before proceeding with further coating steps (Eun et al. 2011; Sugiura et al. 2007). Some researchers have used acidified oil along with surfactants during encapsulation, and these act as irritants for the cells and affect their viability after encapsulation due to acidity and low gas permeability (Kim et al. 2009).

1.10 Need for new approach

It is clear from the above literature review that there are many different types of scaled up devices for microencapsulation. However, most of them produce microcapsules in size ranges less than 100 μm in diameter making them highly unsuitable for microencapsulating islets with an average diameter around 150 μm. Some of the current designs that do manage to encapsulate islets use oil with/without surfactants to achieve the desired highly

monodispersed capsules. The use of oil with/without surfactants affects the cell viability in long term and is hence not favored for transplant/implant purposes. This situation raises an urgent need for a radically different approach to producing viable encapsulated cells in sufficient quantities rapidly for routine application in human cell therapy.

To address these requirements, the novel biomedical device should be able to produce highly monodisperse droplets containing pancreatic islets. Avoid the use of oil and surfactants to produce monodisperse droplets. The design should be scalable to achieve high throughput rates. The device should be cheap, disposable and be fabricated with minimum assembly requirement.

1.11 Dissertation Overview

Chapter-2 discusses the materials used for encapsulation. The various materials available for encapsulation, 'alginates' as the most suitable material for encapsulation, rheological properties of alginate and selecting the most suitable material model to model the non-Newtonian behavior of aqueous solutions of sodium alginates of varying concentrations (wt. / vol.) are also described in Chapter-2.

Chapter-3 discusses about the design of the prototype device. Summary of parametric study of original high throughput system, design stages including computational model and analysis of the prototype microfluidic device are also discussed in Chapter-3

Chapter-4 discusses about the parametric study and high speed video analysis of the microfluidic device. The effect of various parameters namely flow rate of air and alginate, concentration of alginate using dimensionless numbers and various issues with the microencapsulation process are also discussed in Chapter-4

Chapter-5 discusses about the computational model of the microfluidic device. The effect of viscosity and concentration of alginate solutions, flow rates of alginate and air are discussed in detail with the help of dimensionless numbers namely capillary number and weber number are also discussed in Chapter-5

Chapter-6 discusses about the actual process of pancreatic islet encapsulation and transplant. The preparation of islets for transplantation, encapsulation of islets, preparation of Alginate-PLO-Alginate (APA) capsules used for transplants, encapsulation of proteins and other biological materials is also discussed in Chapter-6.

Finally, in Chapter-7 a summary of the overall results is presented. Based on the findings, future ventures that can potentially improve the performance of the high throughput microfluidic device are recommended and possible applications are also discussed.

Chapter 2 Materials for Microencapsulation

2.1 Introduction

Microencapsulation of various materials into spherical hydrogel microcapsules of alginate has found applications in drug delivery, biosensors, microelectronics, bioanalyses, coded imaging aids, cell delivery and cell transplantation due to its biocompatibility and physical properties. It is emerging as an efficient technology in the treatment of diabetes, hormone and protein deficient diseases. Some of the major applications include the use of alginate encapsulated islet cells as a form of bioartificial pancreas to treat individuals afflicted with Type 1 diabetes; development of a reliable bioartificial liver in the form of encapsulated hepatocytes, for providing temporary but adequate metabolic support to allow spontaneous liver regeneration, or as a bridge to orthotopic liver transplantation for patients with fulminant hepatic failure; use of microcapsules in controlled drug delivery for both clinical and experimental therapeutics (Tendulkar et al. 2012).

A variety of polymers are used for microencapsulation of which Alginates are probably the most studied and recognized component for entrapment. Alginates are binary, linear copolymers of (1→4) linked β-D-mannuronic acid (M) and α-L-guluronic acid (G) residues of widely different composition and sequence. Alginates have for decades been used as medical devices in various products and research has been conducted on alginate gel beads as entrapment devices for the transplantation. Entrapment by alginate is a mild, simple and safe method for immobilizing any type of cell (ex. Bacteria, yeast, fungi, animal cells and even embryos) while retaining maximal biocatalytic flexibility (Draget & Taylor 2011;

Nussinovitch 2010; Mancini, Moresi & Sappino 1996; Skjak-Braek, Smidsrod & Larsen 1986).

In this chapter, a list of the various polymers used for encapsulation is provided in the materials used for encapsulation section. A particular group of hydrogels "Alginates" which were used for the purpose of encapsulation for the course of this research are discussed in detail in the Materials used for encapsulation section. Rheology of alginate is discussed in detail by experimentally determining the apparent viscosity of alginate as a function of Shear rate for different brands of sodium alginate (with varying molecular weights) and at different concentration of aqueous solutions of sodium alginate. Mathematical models available in literature typically used to model non Newtonian behavior of alginate solutions have been discussed and the model which best fits the experimental data has been selected for computational modeling of the microfluidic device in the subsequent chapters.

2.2 Materials used for Microencapsulation

With the current advancement in encapsulation techniques various materials are being used for encapsulation of cells and other biological materials. These materials can be broadly classified as follows: **Hydrogels** (namely Agar, Agarose, κ-Carrageenan, Alginates, Chitosan, Cellulose, etc.), **Proteins** (namely Collagen, Gelatin, Hen Egg White, Fibrin, etc.), **Synthetic polymers** (namely Polyacrylamide, Polyvinyl Alcohol, Polyethylene glycol Methacrylate, polyisocyanates, polyurethane, etc.), etc. Based on the desired characteristics of microcapsules, one would select the particular material for encapsulation. Hunt & Grover (2010) and Nussinovitch (2010) have provided more detailed description regarding above mentioned different encapsulation materials, their sources, particular applications and the

characteristics of the beads obtained. In this report more importance and focus is given to understanding the properties of "Alginates" as they pertain to the current research focus of our lab.

2.3 Alginates

Alginates are perhaps the most studied and recognized component for entrapment. Alginates occur both as structural components in marine brown algae as well as capsular polysaccharides in some bacteria. Alginates constitute a family of linear binary copolymers, consisting of (1 → 4) linked β-D-mannuronic acid (M) and α-L-guluronic acid (G) residues (see figure 2.1 (a) and (b)). Regions can consist of one unit or the other, or both monomers in alternating sequence, i.e., M blocks, G blocks, or heteropolymeric MG blocks, respectively (see figure 2.1(c)). Chemical composition and sequence may vary widely between algae species and even different parts of the algae and the time of year when it is harvested. Alginate forms gels with a number of divalent cations. This is the most important feature of alginate's physical properties, the selective binding of multivalent cations, which is the basis for gel formation and the fact that the sol/gel transition of alginates is not particularly influenced by temperature. For our particular application under food and biotechnological purposes, calcium is particularly suitable because of its non-toxicity (Nussinovitch 2010; Draget & Taylor 2011).

Alginate monomer composition (ratio of M to G blocks) and sequence have a profound effect on the final properties of calcium alginate gels since selective binding of ions is a pre requisite for gel formation. By varying the composition of the gel one can influence its stiffness and cell adhesion properties. Figure 2.2 shows the gel strength as a function of

the average length of G blocks larger than one unit. Noticeable effects are observed when the length of G blocks changes from 5 to 15, which coincides with typical G-Block lengths found in commercially available alginates. This can also be explained as the hydrogel formation occurs following electrostatic interaction between the carboxylic moieties on the G blocks of alginate and multivalent cations, thus generally the longer the average length of the G blocks, the higher the ratio of G:M, the stiffer the resulting gel (Draget, Skjak-Braek & Smidsrod 1994).

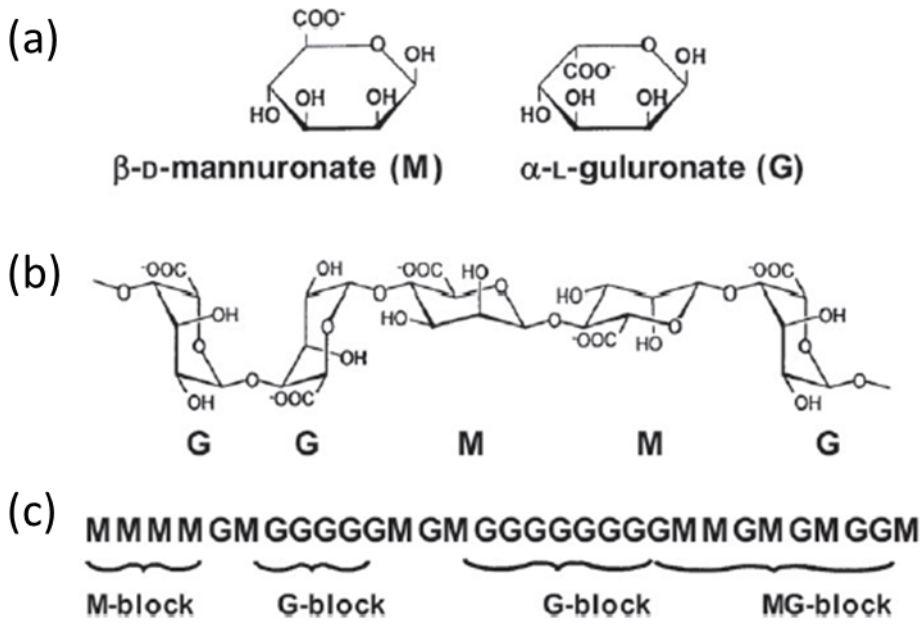

Figure 2.1: Structural Characteristics of alginates: (a) alginate monomers (b) chain conformation (c) block distribution (Draget & Taylor 2011)

Cell adhesion to alginate gels can be increased by covalently modifying the polymer with molecules such as RGD (Hunt & Grover 2012). Another advantage is that high molecular weight alginates having a variety of initial composition and sequential structures

can be tailored by enzymatic modification in vitro to yield polymers with a high content of guluronic acid (Skjak-Braek, Smidsrod & Larsen 1986).

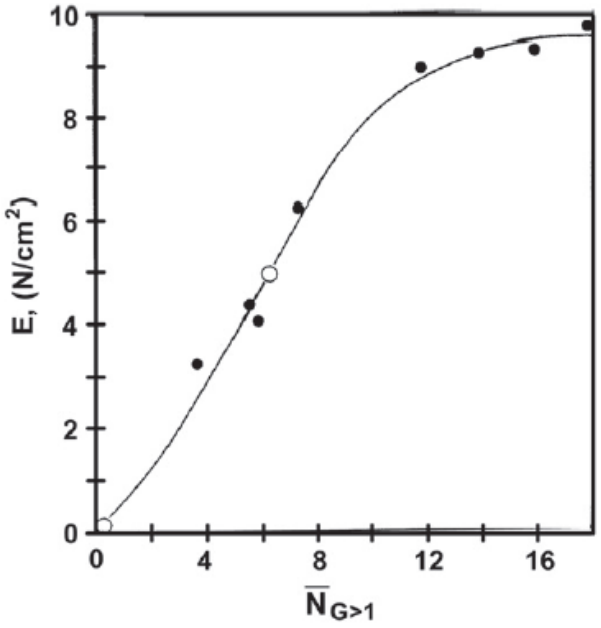

Figure 2.2: Mechanical Properties of alginate gels as function of average G-Block length (Draget & Taylor 2011)

2.4 Rheology of Alginate

Sodium Alginates have for many years found wide applications in the pharmaceutical and biomedical areas due to their abundance, low price and compatibility with biomedical systems. Pharmaceutically sodium alginates are generally used as suspending and thickening agents in suspensions, water-miscible gels, lotions and creams, as emulsion stabilizers or as gel-forming agents in combination with divalent metal ions such as calcium (Fu et al. 2010). Of particular interest are applications in the development of alginate-based controlled release drug delivery systems such as matrix tablets, microcapsules, etc. Over the last couple of

decades, new knowledge about the impact of chemical composition, rheology and sequential arrangement of alginate on biological systems points towards more advanced biomedical devices as well as pharmaceutical properties of alginate in its own right (Draget & Taylor 2011). In this section, we will discuss in detail about the rheology of aqueous sodium alginate solutions by experimentally determining the viscosity vs. shear rate plots for different brands of alginate (with varying molecular weight) and at concentrations varying from 0.75% -3% (wt. /vol.). Hereafter in this dissertation aqueous solutions of sodium alginate are referred as alginate solution and their concentrations are mentioned as (wt. /vol.) unless otherwise specifically mentioned.

2.4.1 Preparation of Sodium Alginate Solutions

For all the experiments performed in this study and hereafter for all experiments reported in this dissertation a standardized procedure was developed and used to prepare alginate solutions to maintain uniformity throughout the experiments. Sodium alginate (powder form) representing a wide range of viscosities and purity was procured from Sigma-Aldrich (Missouri, USA), Acros Organics (New Jersey, USA), Nova-Matrix (Sandvika, Norway) respectively to prepare solutions of varying concentrations (wt. /vol.) for this study. The following procedure was used to prepare alginate solutions:

- Take 50 ml Falcon tube, place on balance, TARE to zero.
- Next measure appropriate amount of sodium alginate (for ex: 0.5 gram for making 1% wt. /vol. of sodium alginate solution).
- Add 50 ml of distilled water (Food Lion, NC, USA) to the falcon tube.

- Add magnetic stirrer to the tube and place on the magnetic stir plate overnight for complete mixing.

Accordingly, various concentrations of alginate solution were prepared, namely 0.75%, 1%, 2%, 3% using sodium alginate from Sigma-Aldrich, 0.75% using sodium alginate from Acros Organics, 0.75% Ultrapure LVM Alginate from Nova-Matrix.

2.4.2 Experimental Setup

Three different grades of the sodium alginate solutions at concentrations namely 0.75%, 1%, 2% and 3% were prepared using the earlier mentioned procedure and steady shear measurements were performed on these solutions using a controlled stress rate rheometer (AR-2000, TA Instruments, New Castle, DE) with a cone-and-plate accessory (ϕ = 40mm; θ= 2º) made of Stainless steel. The sample temperatures were maintained at 25±0.1ºC by a Peltier temperature-control system except for the last sample which was done at 10±0.1ºC.

2.5 Results and Discussion

In this study, the rheological measurements of the different solutions of sodium alginate of varying concentration (0.75%, 1%, 2% and 3%) were analyzed in more detail to understand the effect of shear stress and shear rate on the apparent viscosity of alginate solutions. First the effect of concentration of the alginate solution on apparent viscosity made from the same source (Sigma- Aldrich, USA) was studied followed by the study of change in apparent viscosity of alginate solution (0.75%) prepared from sodium alginate acquired from different sources. The results obtained from these experiments are discussed in detail as follows.

2.5.1 Effect of concentration of Alginate on apparent viscosity

The steady shear rheological properties of the alginate solutions at 1%, 2% and 3% concentrations at 25ºC are depicted in figure 2.3 where apparent viscosity (η_{app}) was plotted as a function of shear stress. It was observed that the apparent viscosities of the alginate solutions of the varying concentrations are significantly different from each other. Thus, these alginate solutions will show significant differences in their rheological behavior under different conditions corresponding to a specific process or use. As shown in figure 2.3 the apparent viscosities of all the alginate solutions decrease with increasing shear stress demonstrating the shear-thinning nature of alginate solutions at these concentrations. This was consistent with the previous observations of shear thinning behavior of solutions of sodium alginate at these concentrations (Fu et al. 2010; Florian-Algarin & Acevedo 2010; Draget & Taylor 2011)

The apparent viscosity of alginate solutions at 1%, 2% and 3% wt. /vol. concentrations at 25ºC was plotted as a function of the shear rate as depicted in figure 2.4. It was observed that the shear thinning effect for different concentrations of alginate solutions start at different shear rates. This emphasizes the importance of determining the apparent viscosities at concentrations and shear rates relevant to formulations, e.g. apparent viscosities at low shear (e.g. 1–50 s^{-1}) can be useful in the development of a suspension formulation while apparent viscosities at high shear (> ~5,000 s^{-1}) are more appropriate for solutions used in coating or spray-drying processes. For our particular application of droplet formation we are concerned with apparent viscosity in the high shear rate region due to the high shear rates experienced by the droplets during break up from the nozzle.

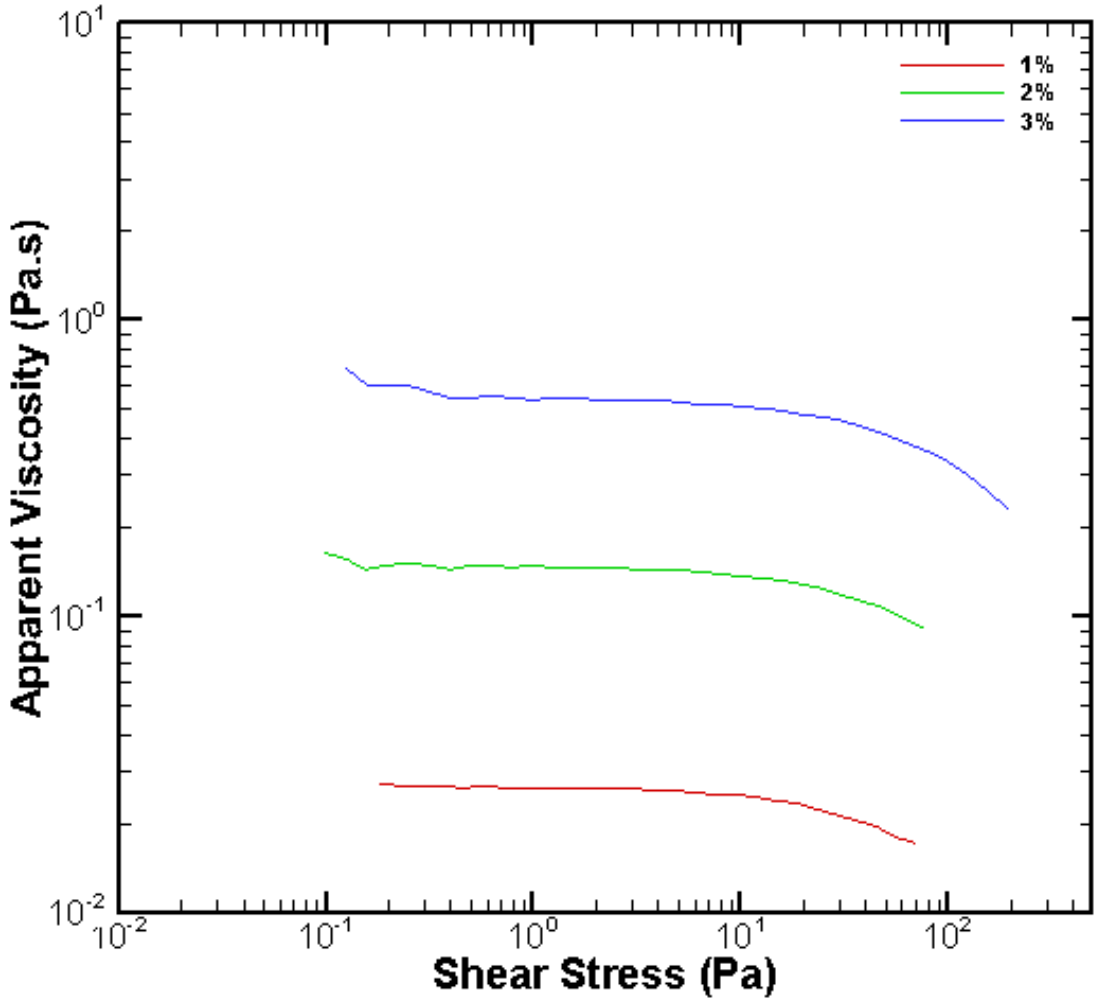

Figure 2.3: Steady shear results of sodium alginate solutions at three concentrations at 25°C: apparent viscosity as a function of shear stress for 1%, 2% and 3% wt. /vol. solutions.

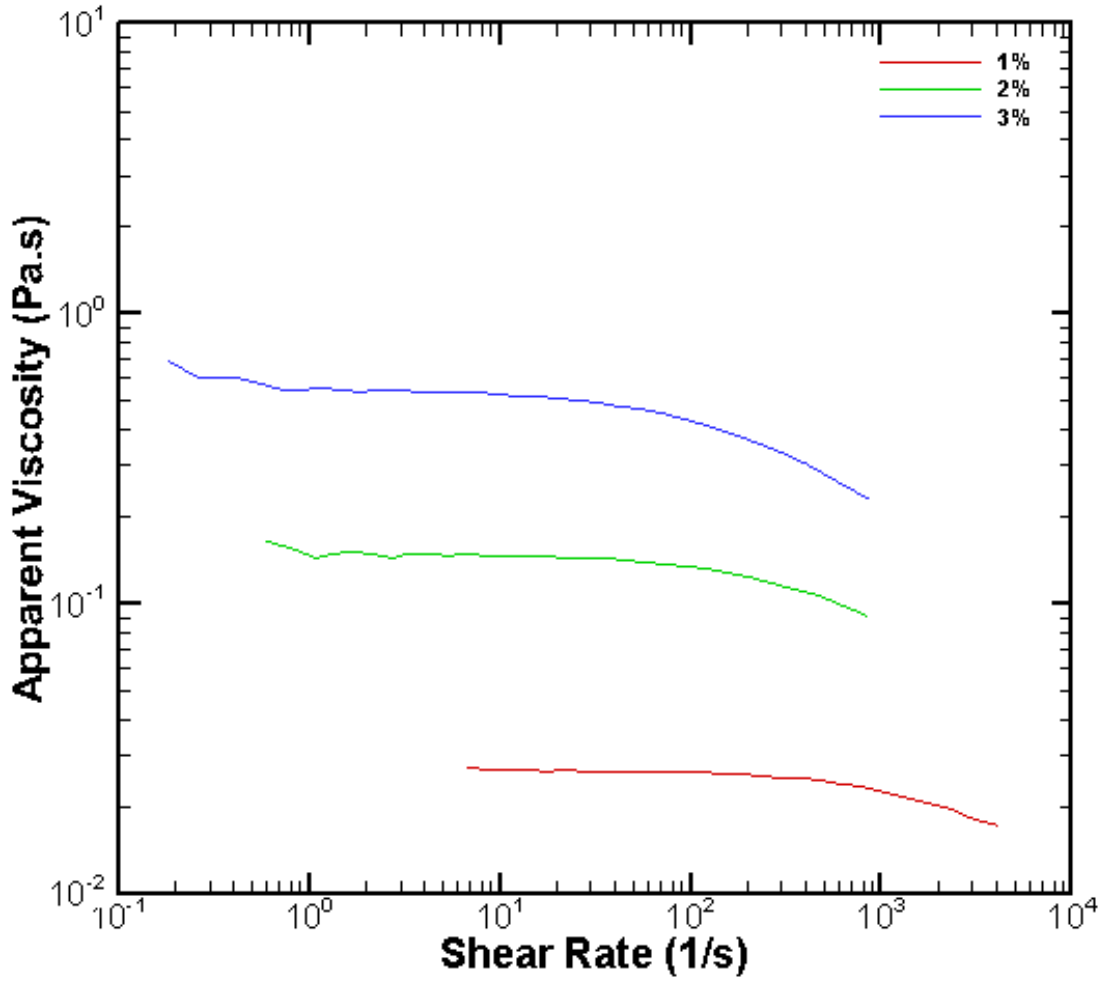

Figure 2.4: Apparent viscosity as a function shear rate for solutions of alginate for 1%, 2% and 3% wt. /vol. solutions at 25ºC.

Figure 2.5 shows the applied shear stress and the corresponding shear rates produced in alginate solutions thus, reinforcing the shear thinning behavior observed for different concentrations of the sodium alginate solutions.

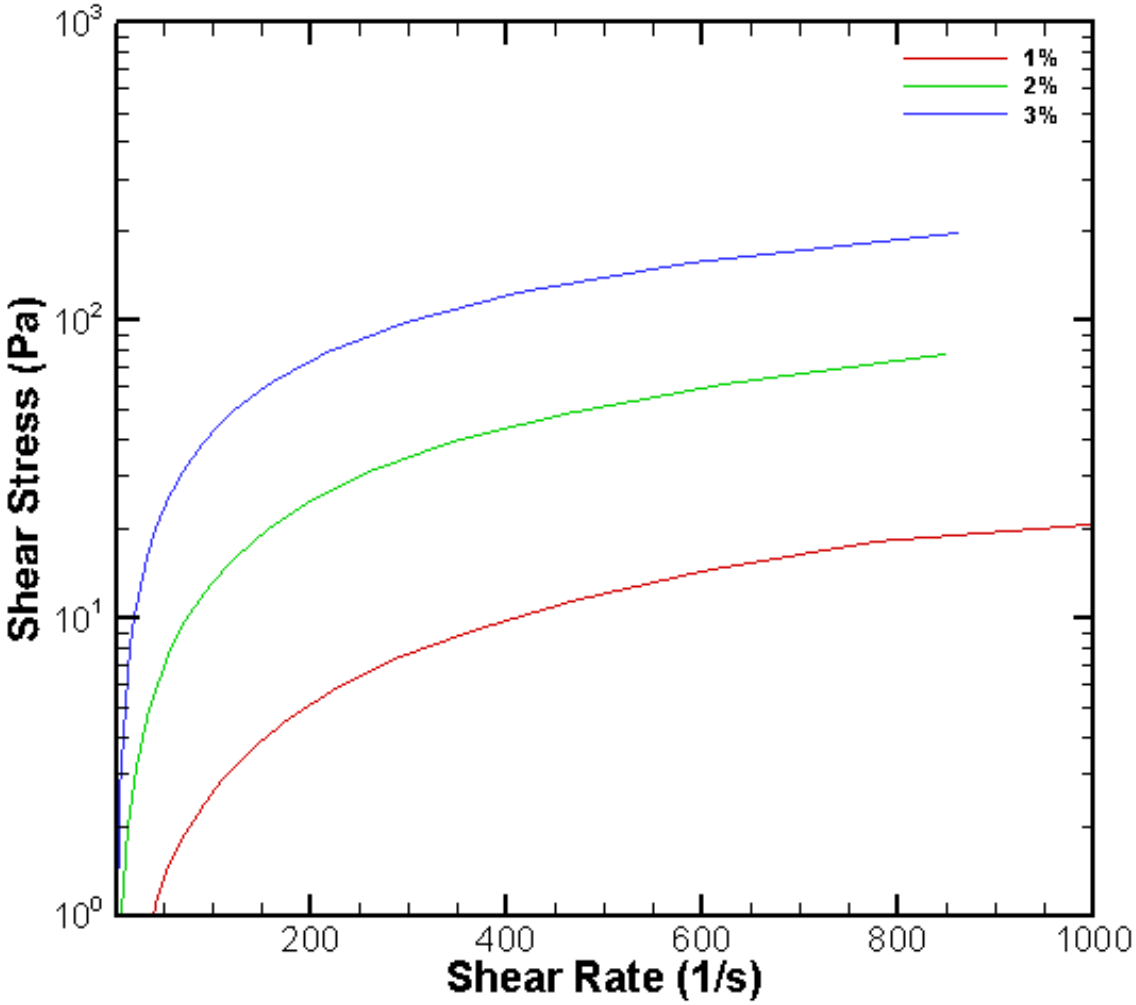

Figure 2.5: Shows shear stress applied to alginate solutions and the corresponding shear rates observed.

2.5.2 Comparison of apparent viscosity for the same concentration of alginate solution prepared from alginate obtained from various sources

The steady shear rheological properties of the solutions of alginate at 0.75% concentration at 25ºC are depicted in figure 2.6 where apparent viscosity is plotted as a function of shear rate. It was observed that the apparent viscosities of the alginate solutions

of the same concentration obtained from different sources are significantly different from each other and hence these alginate solutions would show significantly different rheological behavior under different conditions corresponding to a specific process or use. As shown in figure 2.6, the apparent viscosities of all the alginate solutions decrease with increasing shear stress demonstrating the shear-thinning nature of alginate solutions at these concentrations. This was consistent with the previous observations of shear thinning behavior of solutions of sodium alginate at these concentrations (Fu et al. 2010; Yaniv 2009). The results obtained above are consistent for the most part with the expectation that higher the relaxation time would mean higher average molecular weight (Graessley, Hazleton & Lindeman 1967) which would result in higher apparent viscosities. The relaxation time was calculated using the procedure provided in (Graessley, Hazleton & Lindeman 1967) where the relaxation time was measured when the numerical value of apparent viscosity reaches to 90% of the numerical value of zero shear viscosity. Table 2.1 summarizes the physical properties of alginate obtained from different sources.

Table 2.1: Physical properties of aqueous solutions of 0.75% (wt. /vol.) of alginate obtained from different sources, at 25 ºC

Concentration of Alginate Solution (wt. /vol.)	**Density (kg/m^3)**	**Relaxation time (s)**
0.75% Sigma	1001.6	1×10^{-3}
0.75% Acros	1010.5	0.025
0.75% Ultrapure	1020.9	0.529

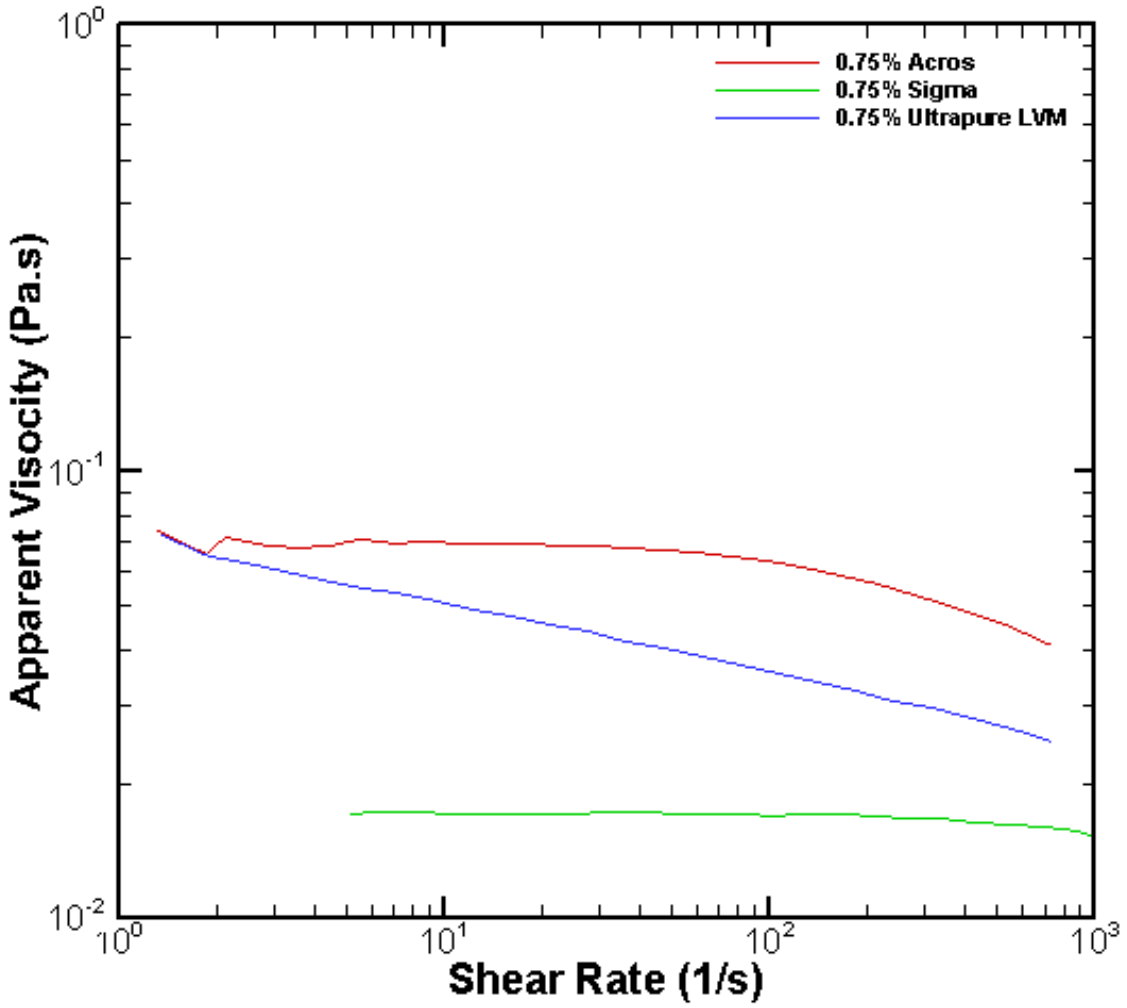

Figure 2.6: Steady shear results of sodium alginate solutions at 0.75% concentration at 25°C prepared from sodium alginate obtained from different sources: apparent viscosity as a function of shear rate for 0.75% solutions.

2.6 Mathematical Models to describe non-Newtonian behavior of aqueous solutions of sodium alginate

The data obtained in the previous section was then utilized towards preparing materials models to describe the non-Newtonian behavior of sodium alginate solutions. Although a variety of mathematical models exist in literature to describe the behavior of non-

Newtonian fluids, the three most commonly used mathematical models for modeling non-Newtonian behavior of shear thinning fluids are Power law model (Ostwald deWaele Equation), Carreau model and Cross WLF model. These mathematical models will be discussed in more detail below and the most suitable model is selected based on the best fit to the experimental data obtained from the rheological experiments.

2.6.1 Power Law model or Ostwald de Waele Model

Often the relationship between shear stress (σ) − shear rate ($\dot{\gamma}$) plotted on log-log co-ordinates for a shear-thinning fluid can be approximated by a straight line over an interval of shear rate i.e.

$$\sigma = m(\dot{\gamma})^n \qquad \textbf{2.1}$$

or, in terms of the apparent viscosity,

$$\eta = m(\dot{\gamma})^{n-1} \qquad \textbf{2.2}$$

Obviously, 0 < n < 1 will yield $(d\eta/d\dot{\gamma})$ < 0, i.e., shear-thinning behavior fluids are characterized by a value of 'n' (power-law index) smaller than unity. Many polymer melts and solutions exhibit the value of 'n' in the range 0.3-0.7 depending upon the concentration and molecular weight of the polymer, etc. Even smaller values of power-law index (n ∼ 0.1−0.15) are encountered with fine particle suspensions like kaolin-in-water, bentonite-in-water, etc. Naturally, smaller is the value of 'n'; more shear-thinning is the material. The other constant, 'm' (consistency index) is a measure of the consistency of the substance. Although, eq. (2.1) or (2.2) offers the simplest approximation of shear-thinning behavior, it predicts neither the upper nor the lower Newtonian plateaus in the limits of $\dot{\gamma} \to 0$ or $\dot{\gamma} \to \infty$. Besides, the values of 'm' and 'n' are reasonably constant only over a narrow interval of

shear rate range whence one needs to know a priori the likely range of shear rate to be encountered in an envisaged application. The power law model fit for the experimental data is depicted in figure 2.7 (Chabbra 2006).

2.6.2 Carreau Model

In this model, in addition to the power law index 'n' and consistency index 'm', two other important factors are considered. First is the zero shear viscosity (η_0) i.e. $\eta \rightarrow \eta_0$ at $\dot{\gamma} \rightarrow 0$ and second is infinite shear viscosity (η_∞) i.e. $\eta \rightarrow \eta_\infty$ at $\dot{\gamma} \rightarrow \infty$ which are respectively the upper and lower limits of the shear thinning fluid viscosity. In this model, viscosity is expressed as

$$\eta = \eta_\infty + (\eta_0 - \eta_\infty)(1 + \dot{\gamma}^2\lambda^2)^{(n-1)/2} \qquad \textbf{2.3}$$

where λ is the time constant, η_0 and η_∞ are the zero and infinity shear viscosities, and 'n' is the power law index. The Carreau model curve fit for the experimental data is depicted in figure 2.7 (Chabbra 2006; ANSYS Inc. 2011).

2.6.3 Cross-WLF Model

Based on the assumption that the shear-thinning behavior is caused by the formation and breakdown of "structural linkages or units," (Cross 1965) put forward an equation. For one-dimensional steady shearing, this three-constant equation can be written as,

$$\eta = \frac{\eta_0}{1 + (\lambda\dot{\gamma})^{1-n}} \qquad \textbf{2.4}$$

where λ is natural time (i.e. inverse of shear rate at which fluid starts exhibiting non-Newtonian behavior), $\eta_0$is the zero shear rate viscosity and 'n' is the consistency index. The

Cross-WLF model curve fit to the experimental data is depicted in figure 2.6 (Chabbra 2006; ANSYS Inc. 2011).

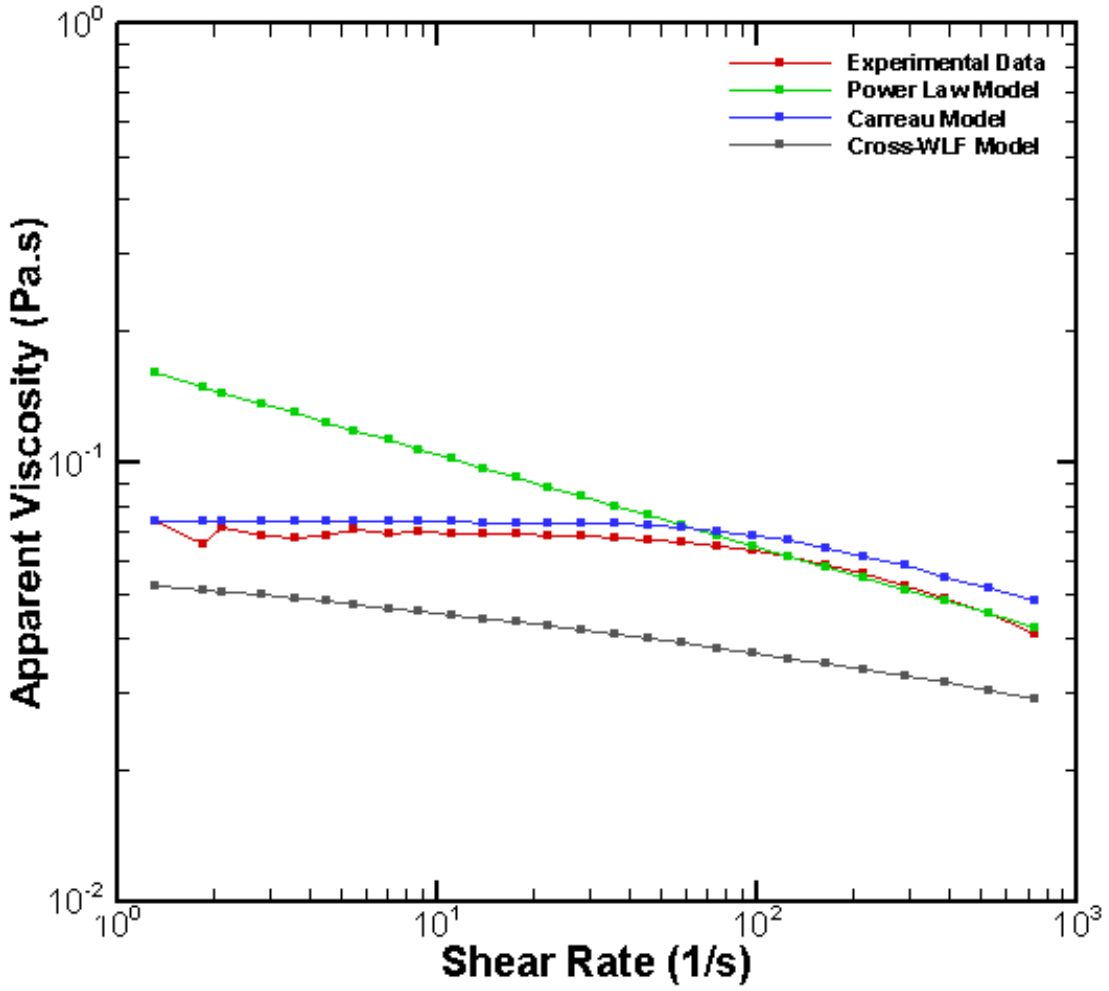

Figure 2.7: Different non-Newtonian viscosity mathematical model curve fits to the experimental data for 0.75% (wt. /vol.) concentration of Alginate from Acros Organics at 25 ºC, Power law model, Carreau model, Cross-WLF model.

From figure 2.7, it is observed that the power law models the non-Newtonian behavior of alginate solutions well in a very short region pertaining to the non-Newtonian

behavior of the fluid, however it over estimates the apparent viscosity value at lower shear rates and doesn't account for the plateau behavior observed at zero and infinite shear rates. While both the Carreau model and Cross WLF model for apparent viscosity show similar trend as the experimental data, the Carreau model provides a much better fit over the entire range of the experimental data. Similar consistency was observed using the Carreau model for higher concentrations of the alginate solutions too and hence will be the preferred model to be used for modeling the shear thinning behavior of sodium alginate solutions at different concentrations in the computational study.

2.7 Conclusion

In summary, there are various materials available for microencapsulation and of which alginates are the most widely preferred and used for encapsulation of cells and biological materials due to their availability (abundance), low price and compatibility with biomedical systems. The study of rheological properties of sodium alginate solutions of varying concentrations and of the same concentration but prepared from varying sources of sodium alginate was conducted and the findings have been discussed and documented. Different models available for modeling non-Newtonian behavior of the sodium alginate have been mentioned and Carreau model was selected based on best fit to the experimental data.

Chapter 3 Design of the Prototype Microfluidic device

In Chapter 1, the major issues related to mass production of microcapsules have been listed. These issues can be classified into two groups (a) Issues related to process of microencapsulation and (b) Issues related to fabrication of the microfluidic devices used for microencapsulation. These issues raise an urgent need for a radically different approach to producing viable encapsulated cells in sufficient quantities rapidly for routine applications in human cell therapy. In this chapter, we summarize the results of a high throughput encapsulation system based on the vibration method. The insight gained from these results along with the knowledge gained from the literature survey conducted in chapter 1 of microfluidic systems used for microencapsulation are combined together to design, develop and prototype a microfluidics based high throughput encapsulation system.

3.1 The 'Encapsulator Machine'

The first step towards designing the high throughput microfluidic device was to understand the existing high throughput encapsulation system i.e. the "Encapsulator Machine" (Ramasubramanian 2004). Figure 3.1 shows the picture of the Encapsulator. The "Encapsulator Machine" was based on the principle of vibration method. In this system, a volume of fluid was pumped through an array of nozzles by vibrating the fluid column with the help of compressed air. This induced Rayleigh instability in the laminar jets produced by the nozzles which break-up to form micro droplets/capsules. This was a very high throughput manufacturing system with the ability to process hundreds of milliliters of encapsulation material in a matter of seconds.

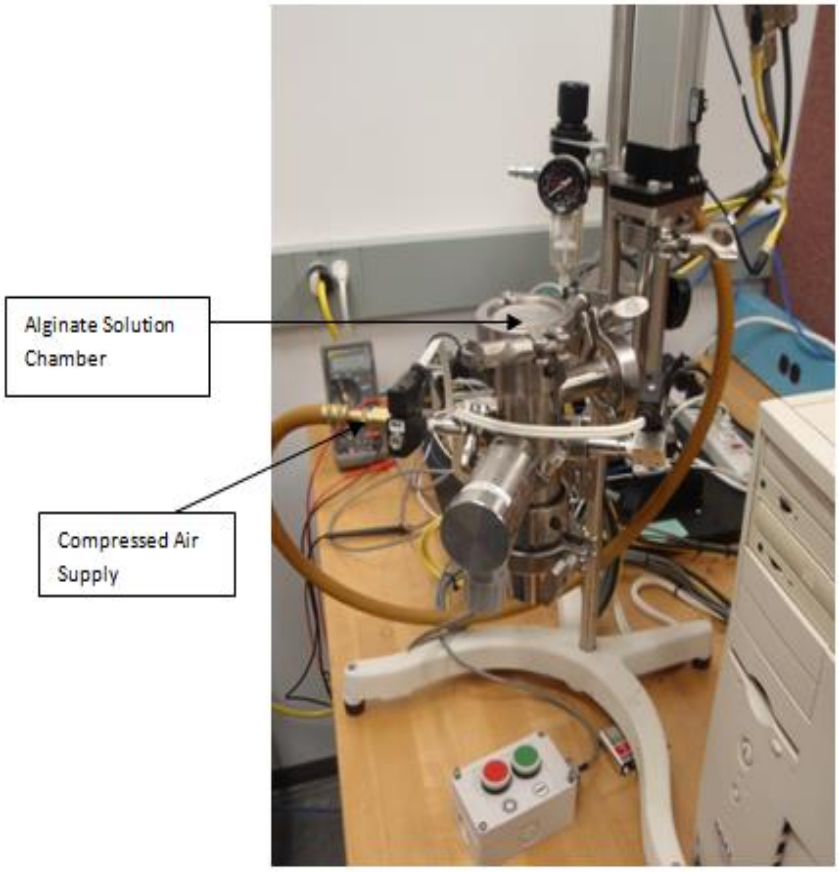

Figure 3.1: High throughput macrofluidic system based on vibration method: The "Encapsulator Machine".

A detailed parametric study was conducted on this system to understand the effects of the various factors (change in concentration of the alginate solution, compressed air pressure used to vibrate the fluid column, distance of the collection plate from the nozzles and hydrophobicity of the nozzles) affecting the process of microencapsulation. Figure 3.2 shows the results obtained from the parametric study performed using the Encapsulator Machine.

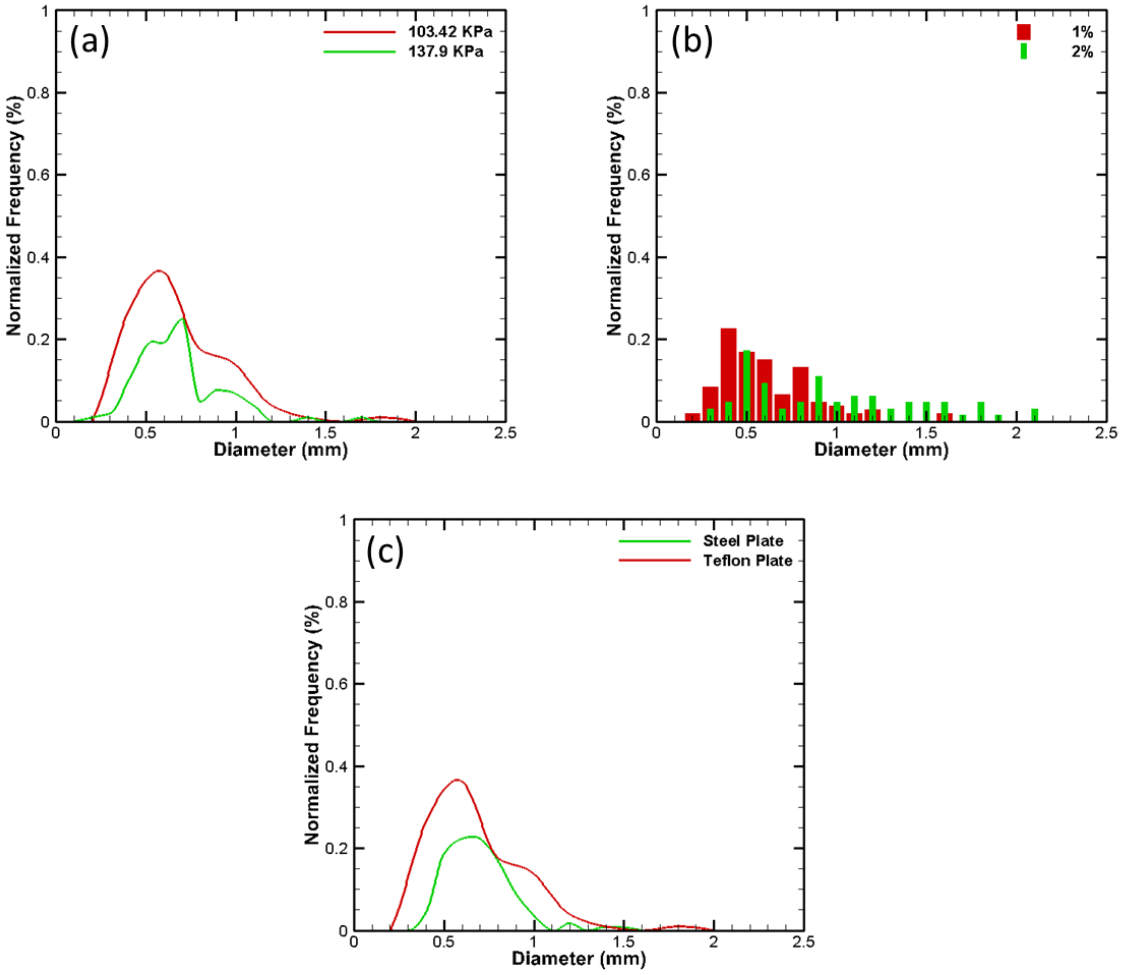

Figure 3.2: Parametric study results obtained using the Encapsulator Machine (a) Effect of change in air pressure; (b) Effect of change in concentration of the alginate solution using a Teflon plate; (c) Effect of Hydrophobicity of the nozzle.

As the concentration of the alginate solution was increased a corresponding increase was observed in the diameter of the microcapsules produced for both the steel and Teflon plates. The increase in the air pressure used to vibrate the fluid column led to a corresponding increase in the diameter of the droplets produced. With the increase in hydrophobicity of the nozzles (i.e. from steel plate to Teflon plate), a corresponding increase in the distance of the

collection plate from the nozzles was required to obtain spherical microcapsules as it allowed enough time for surface tension to cause the cylindrical fluid columns to form spherical droplets/capsules. Detailed discussion of the results for the parametric study of the "Encapsulator Machine" can be found in (Tendulkar 2010).

A major limitation of the high throughput Encapsulator machine was its sensitivity to the concentration of alginate solution. As the concentration of the alginate solution was increased to above 2% the Encapsulator machine produced long tubular strands as opposed to spherical micro beads as shown in figure 3.3 (b). Another limitation of the Encapsulator machine was the inability to precisely control the operation of each individual nozzle. This made it difficult to obtain highly monodisperse diameter distribution of the microcapsules. Polymorphism was observed in the capsules produced using the Encapsulator machine as shown in figure 3.3 (a).

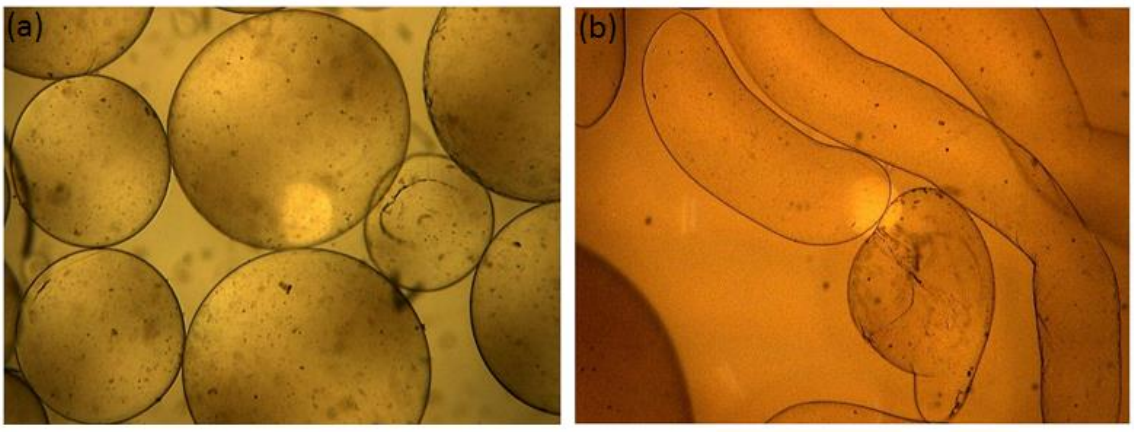

Figure 3.3: Shows (a) an example of polymorphism observed during microencapsulation process; (b) the tubular structure observed as the concentration of alginate solution is increased above 2%.

3.2 Design constraints for the microfluidic device

The parametric study of the Encapsulator machine helped to gain in-depth understanding of the high throughput macrofluidic system. It also made it clear that it would be very difficult to gain precise control over the droplet formation zone where the individual microcapsules are formed. Thus, for macrofluidic systems the most important tradeoff was between the precise control of droplet formation region to that of the high throughput of the system. On the other hand, literature review in chapter 1 indicated the highly monodispersed microcapsule generation obtained by using planar microfluidic devices. The operating parameters of these microfluidic devices to repeatedly produce precise and highly monodispersed droplets has been well documented in the literature. Thus, it was decided that a prudent way to attack this problem would be to scale up a microfluidic device to achieve the high throughput encapsulation rates of the macrofluidic systems combining the benefits and advantages of both the microfluidic systems (precision control over individual droplet formation zone) and macrofluidic systems (high throughput encapsulation rates).

Once the basic approach to the problem was decided, a look into other design constraints was taken to gain a thorough understanding of the complete research problem of microcapsule production. Accordingly, the other important constraints for the research problem are mentioned below.

(1) Use of air as the continuous phase fluid for the production of microcapsules.

(2) Size of the microcapsules should be in the range of 500 μm.

(3) Use of high air pressure for droplet formation should be avoided so as to keep high viability of the cells/pancreatic islets during encapsulation.

(4) Scalable design to increase the throughput for industrial scale implementation.

(5) A suitable fabrication process for making cheap microfluidic devices with minimum or no assembly requirement.

An attempt has been made to address all the above mentioned design requirements using the following approach.

3.3 Design of the co-axial air flow device

Figure 3.4 shows the prototype of the both the single inlet single outlet cross flow and co-flow geometries fabricated in Dr. Ramasubramanian's laboratory respectively. In cross flow device geometry (see figure 3.4 (a)), the flow of continuous phase is perpendicular to the flow dispersed phase. The most common example of cross flow geometry is the T-junction geometry. In co-flow geometry (see figure 3.4(b)), the flow of continuous phase is parallel to the flow of the dispersed phase. These single channel microfluidic devices produced highly monodispersed droplets/ microcapsules and both had similar potential for scale up. However, the cross flow geometry worked better when the viscosity ratio of the dispersed phase to continuous phase was low (ex: alginate, canola/sunflower oil combination, water-mineral oil combination). When the viscosity ratio is very high (ex: alginate and air combination with a viscosity ratio $\frac{\rho_{alginate}}{\rho_{air}} \geq 1400$) the alginate solution stuck to the surface of air channels leading to a free surface/ stratified flow as compared to forming micro droplets. Since one of the design requirements/constraints was to use 'air' as continuous phase, the co-flow geometry was selected for scale up.

Figure 3.4: (a) Prototype of the cross flow microfluidic device; (b) Prototype of the co-flow microfluidic device.

It was decided to scale up the single channel co-flow device to 8 droplet formation zones/regions or 8X as the first step after the successful implementation of which the device design can be scaled up further to 16X, 32X, 64X … 2^nX droplet formation zones. The next step in the design process thus, included designing the scaled up alginate part and air part of the microfluidic device from single inlet single outlet to having single inlet and 8 outlets. The design steps in this direction are discussed in detail as follows.

3.3.1 Design of the alginate head for the microfluidic device

The design of the alginate head was based on stokes flow (or creeping flow) through capillary tubes draining a big reservoir of highly viscous fluid spaced sufficiently close to each other to achieve uniform flow rate distribution across each capillary tube outlet. This type of design approach was chosen so as to suppress, if not entirely eliminate any cross talk between individual alginate outlets and also to minimize the effect caused due to clogging or choking of individual alginate outlets on the performance of the entire device. The design of the alginate head used for this study is shown in figure 3.5. Figure 3.5 (a) shows an isometric view of the alginate head of the microfluidic device. Figure 3.5 (b) shows the reservoir and capillary based design and the location of individual alginate channels. Commercial CAD

tool SolidWorks® was used to design the alginate head design. SolidWorks® Flow simulation tool was used to perform computational study on this design.

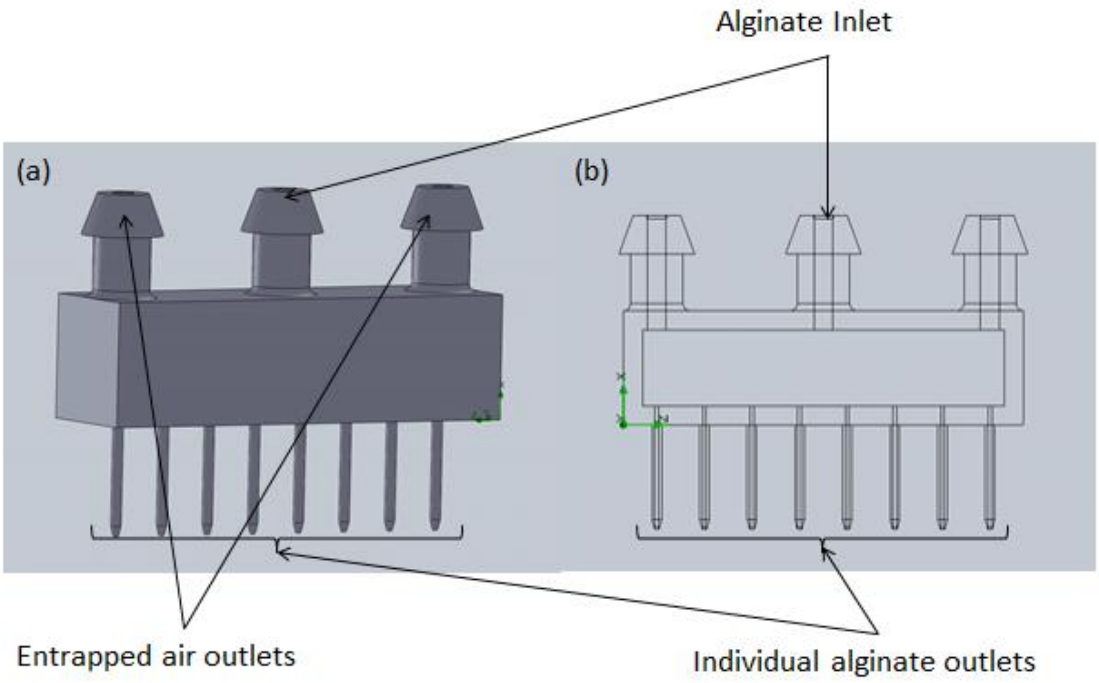

Figure 3.5: (a) and (b) show two different views of the alginate head design having single inlet and 8 outlets.

3.3.2 Design of the air plenum for the microfluidic device

The next step in the design process included the design of microfluidic air plenum with single inlet and 8 outlets to provide co-axial air flow to the 8 droplet formation zones one for each of the 8 alginate outlets. Commercial CAD tool SolidWorks® was used to build five different air plenum designs based on the most commonly used macrofluidic air plenums to determine which one would scale down for microfluidic air plenum design. SolidWorks® Flow simulation tool was used to perform computational study on the different air plenum

designs for the scale up of the microfluidic device. Figure 3.6 (1) - (5) depicts five air plenum designs studied for the prototype microfluidic device.

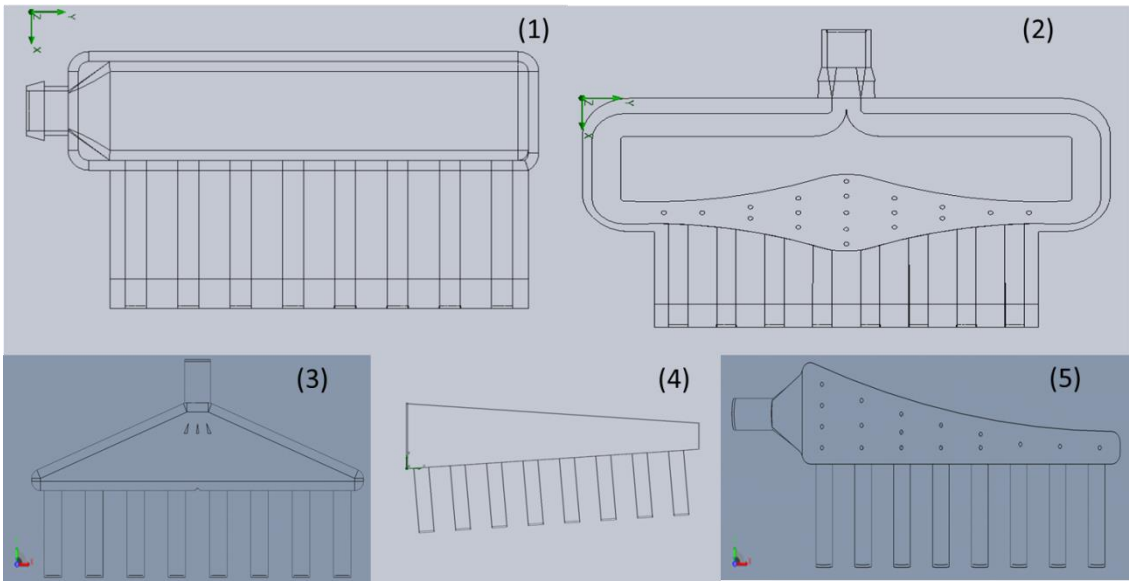

Figure 3.6: (1)-(5) depict various air plenum designs studied for the scale up of the microfluidic device

3.3.3 Numerical model setup for alginate head and air plenum

3.3.3.1 Governing Equations

The Navier-Stokes equations are used to model the flow in both the alginate and air channel. The flow in both the channels is assumed to be isothermal and incompressible. The flow of alginate is in the laminar regime (Stokes flow) while that of air changes from laminar to turbulent depending on the inlet boundary conditions applied. The basic equations used namely conservation of mass and conservation of Momentum are written as follows:

$$\frac{\partial \rho}{\partial t} + \frac{\partial}{\partial x_i}(\rho u_i) = 0 \qquad \textbf{3.1}$$

$$\frac{\partial \rho u_i}{\partial t} + \frac{\partial}{\partial x_j}\left(\rho u_i u_j\right) + \frac{\partial p}{\partial x_i} = \frac{\partial}{\partial x_j}\left(\tau_{ij} + \tau_{ij}^R\right) + S_i; i = 1,2,3 \quad \textbf{3.2}$$

$$S_i = S_{gravity} = -\rho g_i \quad \textbf{3.3}$$

where u is the velocity, ρ is the density, τ_{ij} is the stress tensor, p is the pressure and g_i is the acceleration due to gravity. The fluid used for simulating air part is Newtonian (air) and assumed to be incompressible.

For Newtonian fluids the viscous shear stress tensor is defined as:

$$\tau_{ij} = \mu\left(\frac{\partial u_i}{\partial x_j} + \frac{\partial u_j}{\partial x_i} - \frac{2}{3}\delta_{ij}\frac{\partial u_k}{\partial x_k}\right) \quad \textbf{3.4}$$

Following Boussinesq assumption, the Reynolds-stress tensor has the following form:

$$\tau_{ij}^R = \mu_t\left(\frac{\partial u_i}{\partial x_j} + \frac{\partial u_j}{\partial x_i} - \frac{2}{3}\delta_{ij}\frac{\partial u_k}{\partial x_k}\right) - \frac{2}{3}\rho k\delta_{ij} \quad \textbf{3.5}$$

Here, δ_{ij} is the kronecker delta function, μ is the dynamic viscosity, μ_t is the turbulent eddy viscosity and k is the turbulent kinetic energy. In the frame of the $k-\varepsilon$ turbulence model, μ_t is defined using two basic turbulence properties, namely the turbulent kinetic energy (k) and the turbulent dissipation (ε),

$$\mu_t = f_\mu \frac{C_\mu \rho k^2}{\varepsilon} \quad \textbf{3.6}$$

Here, f_μ is the turbulent viscosity factor, defined as

$$f_\mu = \left[1 - exp\left(-0.025R_y\right)\right]^2\left(1 + \frac{20.5}{R_T}\right) \quad \textbf{3.7}$$

Where,

$$R_T = \frac{\rho k^2}{\mu \varepsilon} \quad \textbf{3.8}$$

$$R_y = \frac{\rho \sqrt{ky}}{\mu} \quad \textbf{3.9}$$

and y is the distance from the wall.

The turbulence kinetic energy and dissipation transport equations for the $k - \varepsilon$ model read

$$\frac{\partial \rho k}{\partial t} + \frac{\partial}{\partial x_i}(\rho u_i k) = \frac{\partial}{\partial x_i}\left(\left(\mu + \frac{\mu_t}{\sigma_k}\right)\frac{\partial k}{\partial x_i}\right) + S_k \quad \textbf{3.10}$$

$$\frac{\partial \rho \varepsilon}{\partial t} + \frac{\partial}{\partial x_i}(\rho u_i \varepsilon) = \frac{\partial}{\partial x_i}\left(\left(\mu + \frac{\mu_t}{\sigma_\varepsilon}\right)\frac{\partial \varepsilon}{\partial x_i}\right) + S_\varepsilon \quad \textbf{3.11}$$

Where the source terms $S_k$and S_ε are defined as,

$$S_k = \tau_{ij}^R \frac{\partial u_i}{\partial x_j} - \rho\varepsilon + \mu_t P_B \quad \textbf{3.12}$$

$$S_\varepsilon = C_{\varepsilon 1}\frac{\varepsilon}{k}\left(f_1 \tau_{ij}^R \frac{\partial u_i}{\partial x_j} + \mu_t C_B P_B\right) - C_{\varepsilon 2} f_2 \frac{\rho \varepsilon^2}{k} \quad \textbf{3.13}$$

Here, P_B represents the turbulent generation due to buoyancy forces and can be written as

$$P_B = -\frac{g_i}{\sigma_B}\frac{1}{\rho}\frac{\partial \rho}{\partial x_i} \quad \textbf{3.14}$$

Where the constant $\sigma_B = 0.9$, $C_B = 1$ when $P_B > 0$ and 0 otherwise;

$$f_1 = 1 + \left(\frac{0.05}{f_\mu}\right)^3 \quad \textbf{3.15}$$

$$f_2 = 1 - exp(-R_T^2) \quad \textbf{3.16}$$

$$C_\mu = 0.09, C_{\varepsilon 1} = 1.44, C_{\varepsilon 2} = 1.92, \sigma_\varepsilon = 1.3, \sigma_k = 1$$

To obtain the steady state solution of the flow field, the governing equations were solved numerically on commercially available SolidWorks® Flow simulation tools with rectangular parallelepiped mesh cells using cell centered finite volume method. A second-order upwind method was used for spatial approximations at the solid/fluid interface. Time-implicit approximations of the continuity and convection/diffusion equations are used together with the operator-splitting technique which is also used to resolve the problem of pressure – velocity decoupling, while a SIMPLE-like approach is used to solve the discrete pressure equation by taking into account the boundary conditions for velocity. More details about the discretization's and the final form of discretized equations used can be found here (SolidWorks 2011).

The basic boundary conditions used were (a) Velocity boundary condition at the inlet of the air plenum, volume flow rate at the inlet of the alginate head and static pressure boundary condition (atmospheric pressure) at the outlet of both the air-plenum and the alginate head. Walls of both the air plenum and alginate head were modeled as smooth with no slip boundary condition. Four goals were used for checking the accuracy and convergence of the air plenum models namely, average static pressure at inlet and outlets, average velocity at outlets and pressure drop across inlet and outlets. For the alginate head model, except for average velocity at outlet goal, average mass flow rate at outlet was used as a convergence goal all other goals used were same.

The material models developed in chapter 2 were used for the study of alginate head. The properties for air were used from the Flow simulation material data base. The values of the various properties used for varying concentrations of alginate solutions and air are listed

in Table 3.1. Some of the other properties which were common to all the alginate solutions were surface tension = 0.0728 N/m, specific heat = 4187 J/kgK, thermal conductivity = 0.6 W/mK and density of 1000kg/m^3.

3.3.3.2 Validation

For validating the approach to the problem, the basic model of flow through a straight pipe was validated using the SolidWorks® Laminar and Turbulent flow in pipe validation examples. The flow through the straight pipe was modeled and successive mesh refinements for selecting the final mesh were done until the change in individual variables of interest namely pressure drop was less than 5%. The data was compared to the experimental data provided in the validation examples and approach to the problem as validated. The details of the validation examples and the conditions used can be found here (SolidWorks 2011).

Table 3.1: Material properties used for air and non-Newtonian (Carreau) model of aqueous solutions of sodium alginate of 1%, 2% and 3% (wt. / vol.) concentrations.

Material	Property	Symbol	Value	Units
1%	Zero shear viscosity	η_0	0.001	Pa.s
	Infinite shear viscosity	η_∞	0.02637	Pa.s
	Power law Index	n	0.88	
	Time constant	K_t	0.009116	s
2%	Zero shear viscosity	η_0	0.001	Pa.s
	Infinite shear viscosity	η_∞	0.1644	Pa.s
	Power law Index	n	0.881	
	Time constant	K_t	0.046512	s
3%	Zero shear viscosity	η_0	0.001	Pa.s
	Infinite shear viscosity	η_∞	0.6838	Pa.s
	Power law Index	n	0.817	
	Time constant	K_t	0.083403	s
Air	Density	ρ	1.225	kg/m^3
	Viscosity	η	1.85E-5	Pa.s
	Specific Heat ratio	$\frac{C_p}{C_v}$	1.399	
	Molecular Mass	M	0.02896	kg/mol

3.3.4 Results and Discussion

3.3.4.1 Design of the Alginate head of the microfluidic device

The alginate head design depicted in figure 3.5 was analyzed using the SolidWorks® Flow simulation tool. 3D simulations of the alginate head design were conducted to study and analyze the flow distribution through the individual 8 outlets of the alginate head. The material models developed in chapter 2 to emulate the behavior of non-Newtonian fluids namely the aqueous solutions of sodium alginate of varying concentrations (1% to 3%) were used in this study.

The alginate head design was simulated for different flow rates of alginate solutions namely 15, 30, 60 and 90 ml/hr. and for each of the 1%, 2% and 3% concentration of the alginate solutions. Reynolds number at the inlet of the alginate head for this computational study was in the range of $0.0002 \leq Re_{inlet} \leq 0.7$ and thus, in the range of Stokes flow regime. Figure 3.7 shows a cut surface plot of the velocity magnitude of alginate solution 2% concentration at a flow rate of 30 ml/hr. It was observed from the simulations that the flow through the individual alginate channels was fully developed and that there was no cross talk observed between the alginate outlets. Also, the reservoir body acts as a good insulator and damps out any disturbances at the individual outlets from being transmitted back to the inlet.

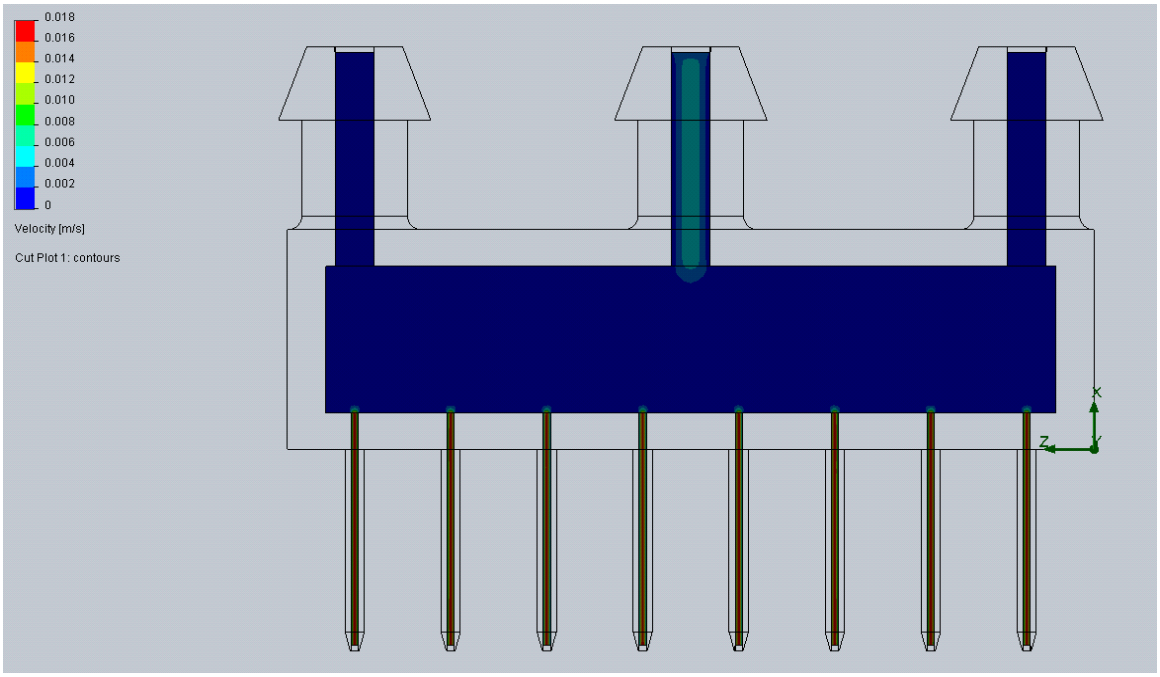

Figure 3.7: Shows the plot of velocity magnitude of 2% concentration of alginate solution through the alginate head at flow rate of 30ml/hr.

The plot for the alginate velocity profiles at each of the individual outlets of alginate solution 2% concentration across each of the individual 8 channels at two different flow rates of 30 ml/hr. and 90 ml/hr. is provided in figure 3.8. A uniform velocity distribution is observed with a standard deviation in the average velocity values across individual channels less than 13%. Figure 3.9 provides a close up view of the fully developed velocity profiles across individual channels for flow rates of 30 ml/hr. and 90 ml/hr. for 2% concentration of alginate solution. Thus, this design of the alginate head provided good scale up from the single inlet singe outlet design to single inlet to 8 outlets and was used towards fabrication of the final prototype microfluidic device with 8 co-axial air flow droplet formation zones.

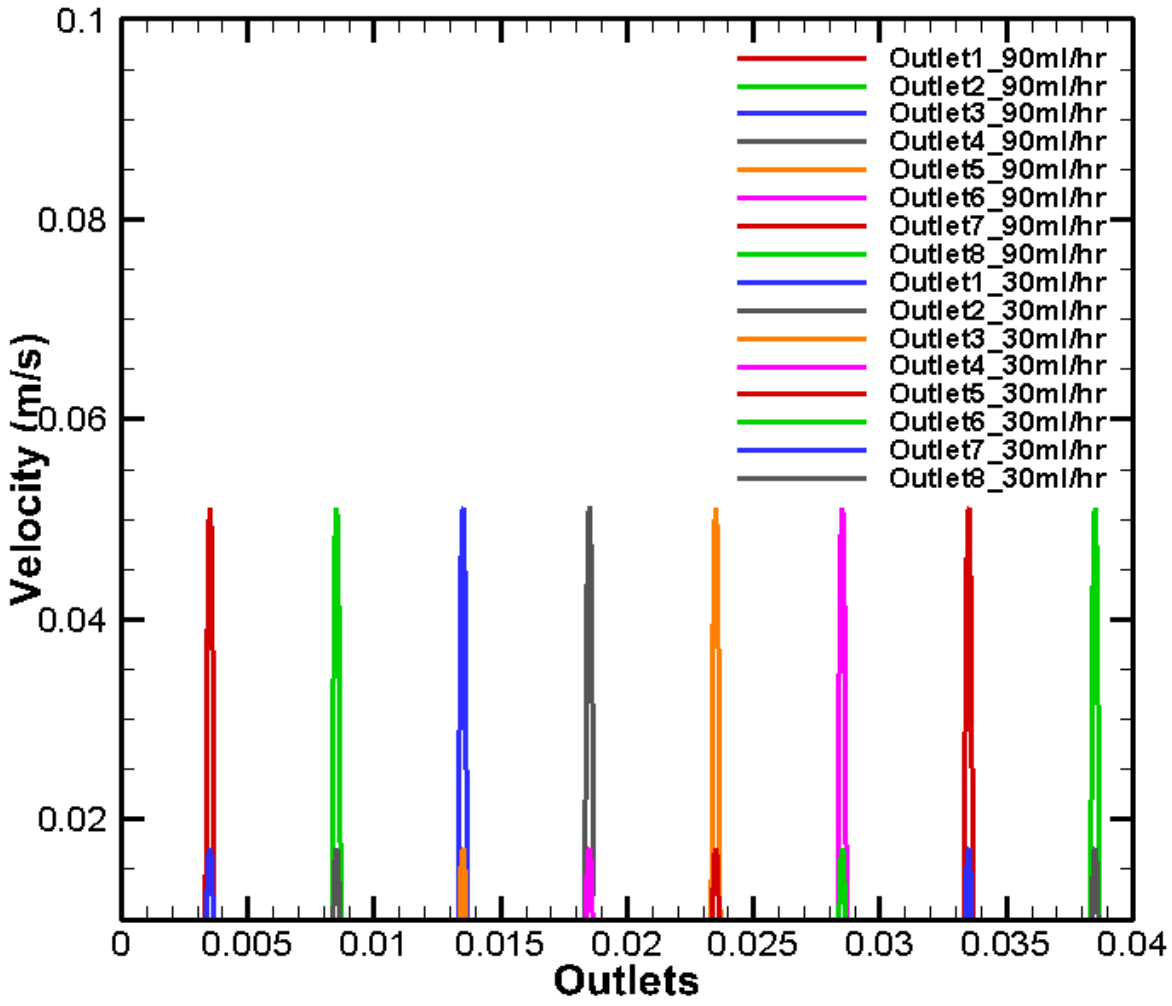

Figure 3.8: Shows the velocity profiles for flow of alginate solution (2%) at individual outlets for flow rates of 30ml/hr. and 90 ml/hr.

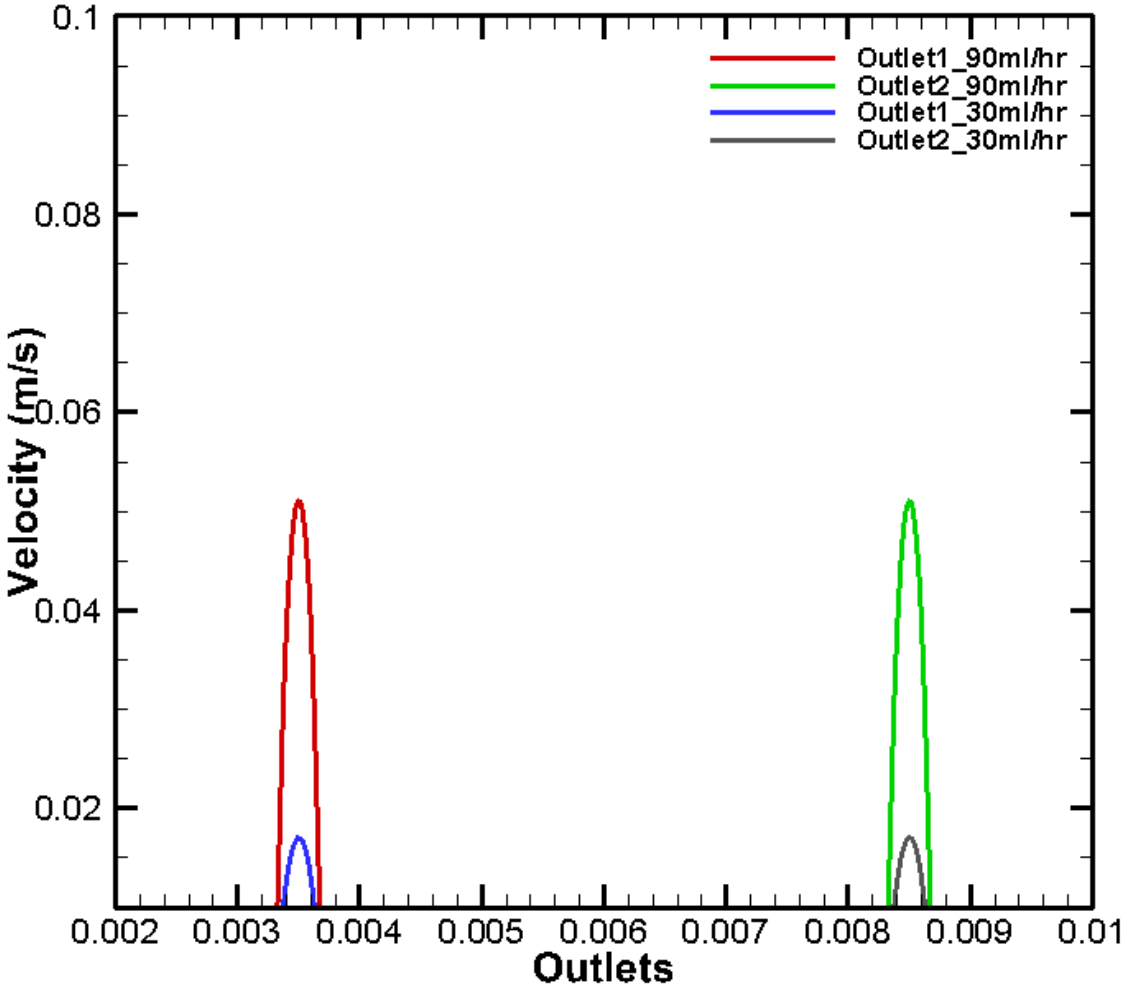

Figure 3.9: Close up view of the velocity profiles for flow of alginate solution (2%) at individual outlets for flow rates of 30ml/hr. and 90 ml/hr.

3.3.4.2 Design of the air plenum of the microfluidic device

To study and understand the air pressure distribution through the different air plenum geometries 3D simulation of air flow through them was carried out at air pressures ranging from 0.1 - 3psi (0.689 - 20.684 kPa). This range of air pressures was selected as they represent a wide range of Reynolds number (Re_{inlet}) for the air plenum design. The results

obtained from these simulations are discussed in detail below and the performance of the different air plenum geometries is analyzed and compared based on the pressure distribution observed near the individual air channel outlets. Figure 3.10 (a) & (b) shows the pressure distribution observed for the air plenum designs 2 and 1 simulated during the computational study at air pressure of 0.1 psi (0.689 kPa) and 3 psi (20.684 kPa) respectively.

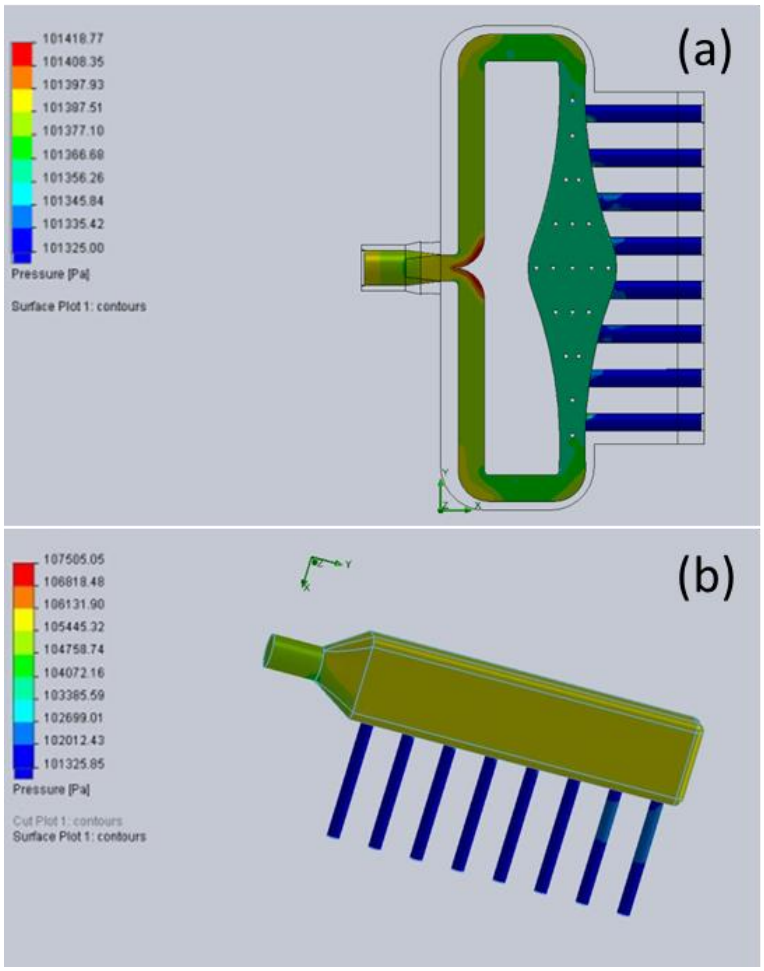

Figure 3.10: (a) Air Pressure distribution for design 2 of the air plenum simulated for air flow analysis at air pressure of 0.1psi (0.689kPa) (b) Air Pressure distribution for design 1 of the air plenum simulated for air flow analysis at air pressure of 3psi (20.684 kPa).

The results for pressure distribution obtained from 3D simulations of the air plenum designs at 0.1 (0.689kPa) and 3 psi (20.684 kPa) of air pressure are shown in figure 3.11 and 3.12 respectively. It was observed that the air pressure distribution across different air plenum designs was very uniform at 0.1 psi (0.689 kPa) and 3 psi (20.684 kPa). The air plenum design 4 showed the maximum difference between average pressure distribution across 8 channels of about 15 Pa. All other air plenum designs showed much smaller air pressure difference across all their air channels (less than 2 Pa see figure 3.11). At an air pressure of 3psi (20.684 kPa) all the other designs fared similar to 0.1 psi (0.689 kPa) condition as depicted in figure 3.12, however design 4 was excluded from this plot as at this air pressure range convergence issues were observed in the simulation study due to vortex crossing at the outlets of the air plenum which led to random fluctuations in the average air pressure distribution across its outlets. Thus, the results of the average air pressure across individual channels showed that either of the air plenum designs 1, 2, 3 and 5 would work appropriately for the selected air pressure range. However the average velocity plots across individual air channels showed that design 1 and 2 have much better average velocity distribution as compared to the other designs for both 0.1 (0.689 kPa) and 3 psi (20.684 kPa). Hence, designs 1 and 2 were selected for fabrication and further analysis with experiments to select the better of the two designs.

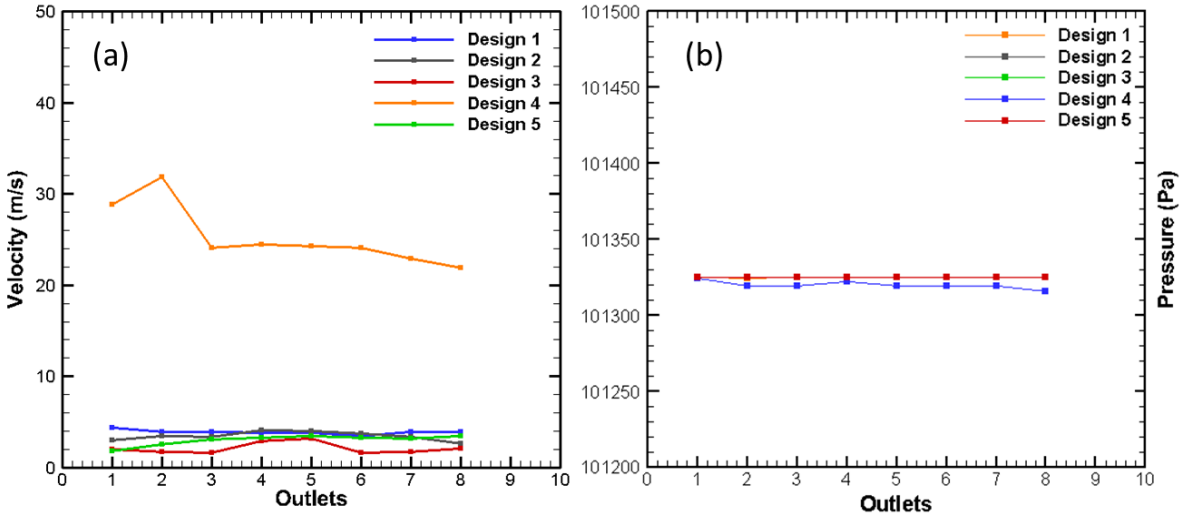

Figure 3.11: Average air pressure distribution across the outlets of the different air plenum designs at 0.1 psi (0.689 kPa).

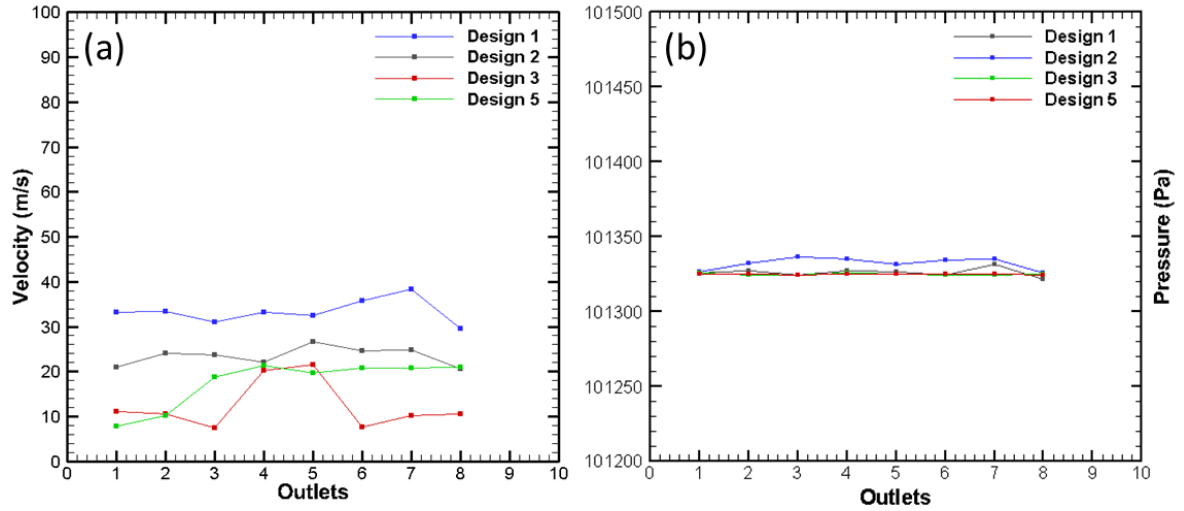

Figure 3.12: Average velocity and air pressure distribution across the outlets of the different air plenum designs at 3 psi (20.684 kPa).

The two air plenum designs namely Design 1 and Design 2 were then fabricated using rapid prototyping technology of 3D printing. Parametric studies were conducted on these two

devices and experiments revealed that the microcapsules produced using the microfluidic device with air plenum design 1 produced slightly better monodispersed output as compared to the microfluidic device fabricated with air plenum design 2. Figure 3.13 shows the diameter distribution of the microcapsules produced by these microfluidic devices with air plenum designs 1 and 2. The encapsulation conditions used were 1.5% concentration of alginate solution and air pressure of 1 psi (6.894 kPa). Microcapsules produced had an average diameter of 742 µm with standard deviation of 0.0386 (for design 1) and 764 µm (for design 2) with standard deviation of 0.0544.

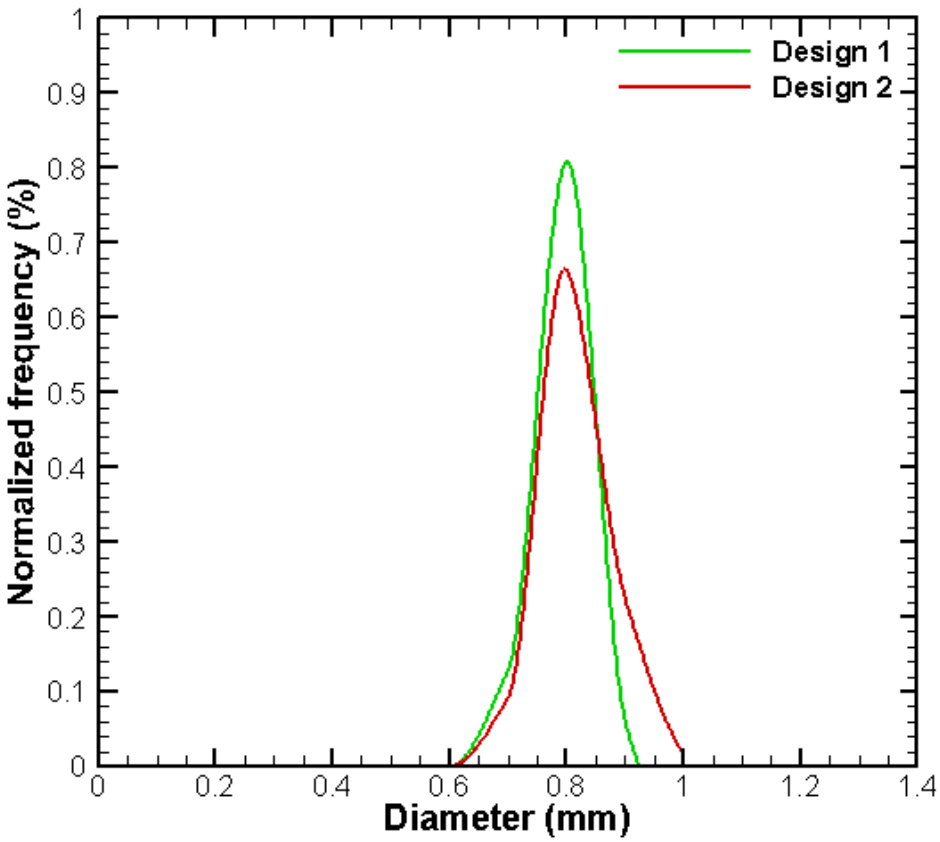

Figure 3.13: Droplet diameter distribution for microcapsules produced using designs 1 and 2 using 1.5% concentration of alginate solution at 1psi (6.894 kPa) air pressure.

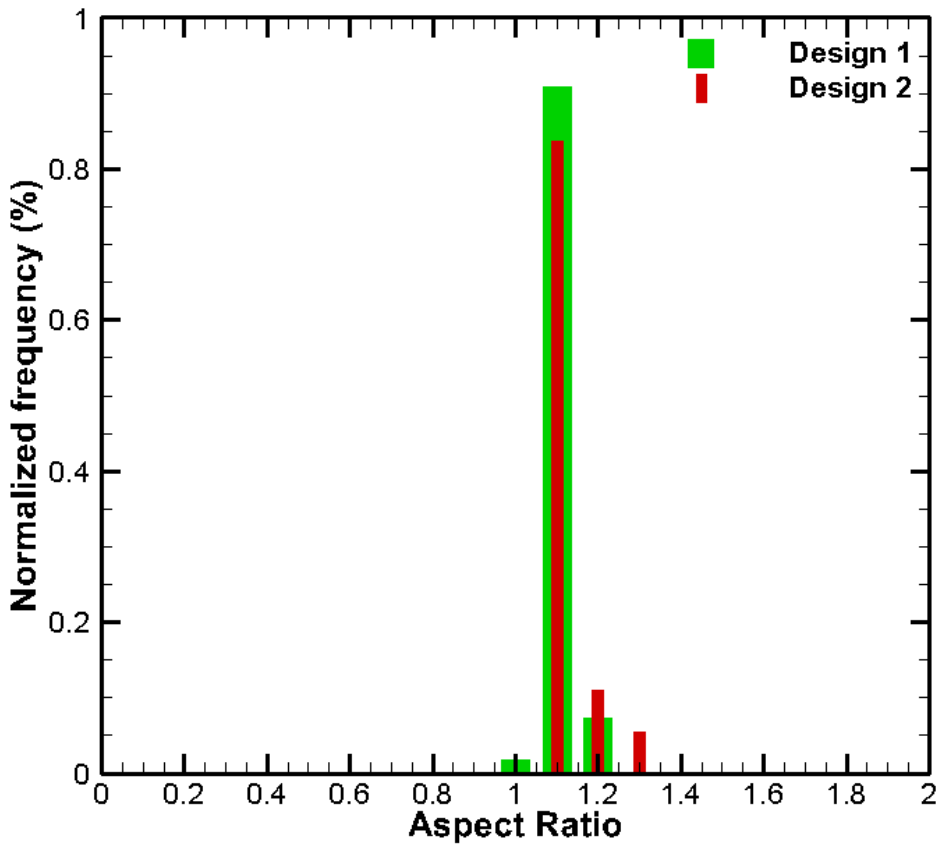

Figure 3.14: Aspect Ratio of the microcapsules produced using designs 1 and 2 using 1.5% concentration of alginate solution at 1psi (6.894 kPa) air pressure.

Figure 3.14 shows the aspect ratio distribution of the microcapsules produced using air plenum designs 1 and 2. It can be observed that microcapsules produced using air plenum design 1 had an aspect ratio closer to 1 as compared to the microcapsules produced using air plenum design 2. Thus, it was concluded from the experimental results that air plenum design 1 performed better than design 2 and hence will be selected as the air plenum design towards the prototyping of the 8 channel scale up microfluidic device.

3.4 Conclusion

In summary, in this chapter, the parametric study results of the high throughput vibration method based macrofluidic device were summarized. Preliminary data from the coaxial air based microfluidic device with one droplet formation zone was used and computational SolidWorks® flow simulation tools were used to design and analyze the scale up microfluidic device with 8X droplet formation zones. Additional experiments were conducted on two separate air plenum designs namely Design 1 and Design 2 which were selected for further study and based on the results obtained air plenum design 1 was selected for prototyping the final microfluidic device to be discussed in the next chapter.

Chapter 4 Parametric Study and High speed video Analysis

4.1 Introduction

The prototype model of the microfluidic device developed in chapter 3, was fabricated using 3D printing rapid prototyping process. This microfluidic device was then thoroughly analyzed further to gain in depth knowledge and understanding of the working of the microfluidic device and the effect of individual parameters on droplet formation. In this chapter, the effect of each individual parameter is discussed in detail. High speed video analysis was conducted to take a closer look at the droplet formation region and to understand the effect of dimensionless numbers namely capillary number (Ca), Weber number (We) and Reynolds number (Re). These findings are summarized in results and discussion section and suggestions towards improvement are provided to help improve the microfluidic device design.

4.2 Materials and Methods

4.2.1 Prototype design and fabrication

The schematic diagram of the device is shown in Fig. 4.1. The microfluidic chip capable of producing highly monodisperse droplets consists of a 3D air supply and multi-nozzle outlet for microcapsule generation. It has one alginate inlet and compressed air inlet (Fig. 4.1(a)). The outlet has 8 nozzles (Fig. 4.1(b)), each having 380 micrometers inner diameter which produce hydrogel microcapsules. These nozzles are concentrically surrounded by air nozzles with 2 mm inner diameter (Fig. 4.1(c)). There are two tubes connected at the top to allow the entrapped air bubbles to escape through them as the alginate

solution fills up the chamber. Once all the entrapped air escapes through the two tubes, the valves on the tubes are closed to prevent the alginate from rising in these tubes. In order to generate hydrogel microcapsules, alginate solution is introduced into the alginate chamber and compressed air is introduced in the air inlet.

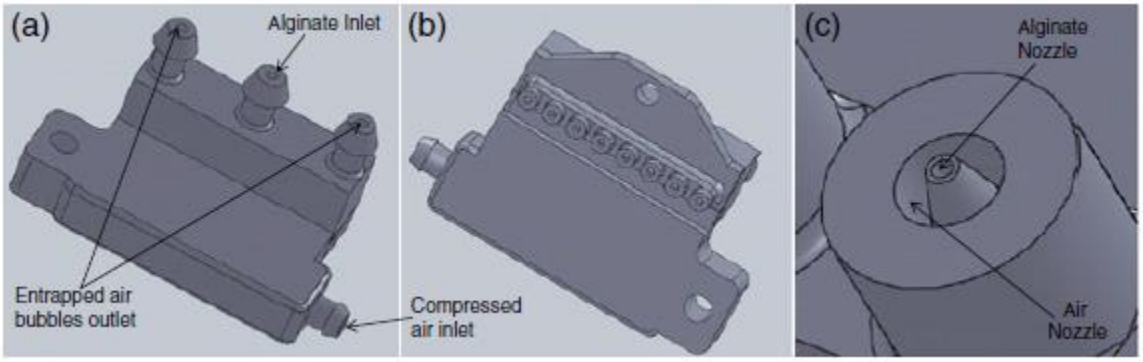

Figure 4.1: (a) Isometric Top View (b) Isometric Bottom View and (c) close up view of the co-flow outlets in the microfluidic device.

Figure 4.2 shows the alginate-cell mixture and compressed air flowing through the microfluidic device. The air enters the microfluidic device along the Z direction, then takes a 90° turn along the Y direction and then turns another 90° where it co-flows along with the alginate-cell mixture (inner nozzle) in the two concentric nozzles. The alginate-cell mixture enters the device along the X direction as shown to fill the inner chamber where it gets splits up into smaller streams and flows through the inner channels in the co-flow section, surrounded by air flow (outer nozzle). A variable flow pump 115 V (Thermo Fisher Scientific Inc., USA) is used to pump alginate solution into the microfluidic device. Tygon® tubing (Fisher Scientific, USA) is used to connect in-house air supply to the air channel and

peristaltic/syringe pump to the alginate chamber. A pressure regulator is used to control the flow rate of air.

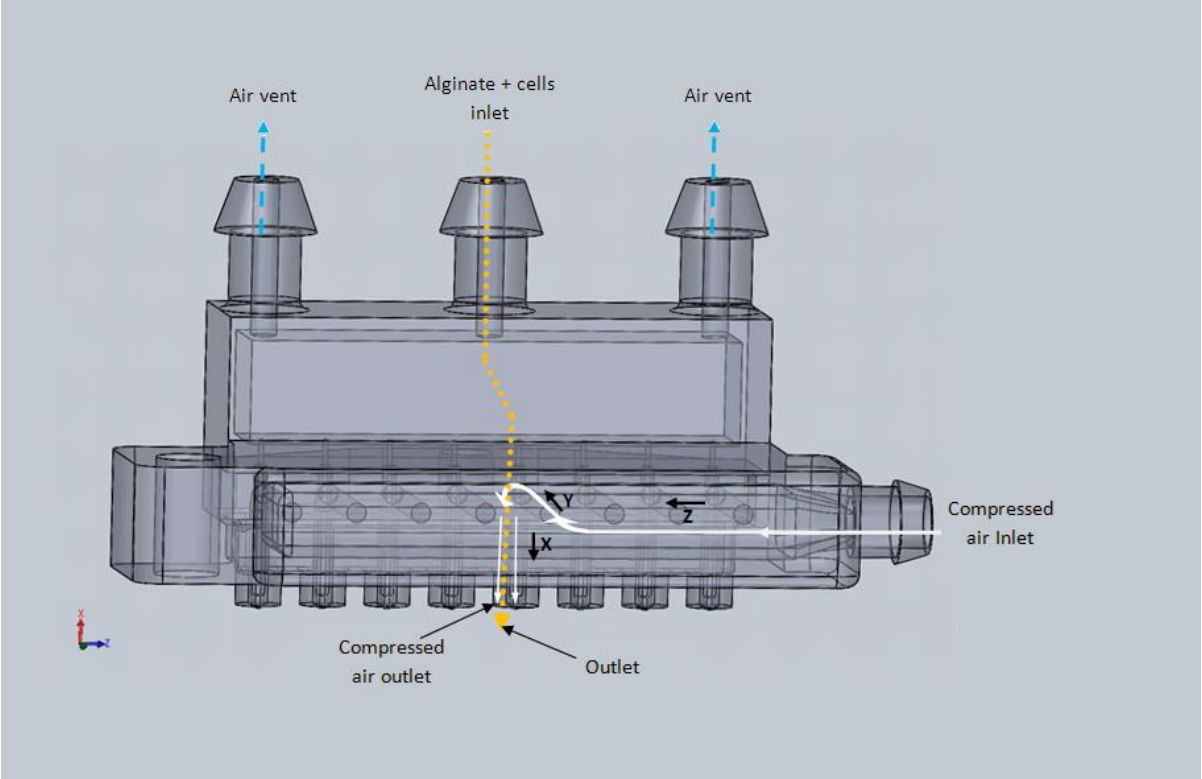

Figure 4.2: Shows the flow of alginate-cell mixture and compressed air through the microfluidic device.

The microfluidic device was designed using SolidWorks 2008™ (Dassault Systemes SolidWorks Corp., MA, USA), a commercially available CAD package. The CAD file is saved as STL file which is the standard format for stereo lithography applications. After the CAD file is converted to STL file, it is analyzed for defects and features that may not form. It is then prepared for high resolution build using 3D Lightyear software for the Viper si2 SLA System (3D Systems Corporation, South Carolina, USA). The parts were then built in the

machine by UV curing of layers 0.002″ thick into a vat of liquid polymer. As the part is built in a vat of liquid resin, appropriate supports are provided to support the structure. DSM Somos ProtoTherm 12120 polymer (3D Systems Corporation, South Carolina, USA) is the liquid resin used to build this device. After the build is complete, the excess liquid resin that is clinging to the parts is cleaned off by using a two-step process. The first step comprises of cleaning using solvent called 'Polyflush' a type of propanol which removes bulk of the uncured resin. In the second step, isopropyl alcohol is used to remove Polyflush residue, which evaporates quickly and leaves the part clean and residue-free. After the part is cleaned it is then post cured in a UV oven for an hour. Following post cure, the supports break off easily from the part. After sanding, the parts can be sand blasted to provide a better surface finish.

4.2.2 Experimental setup

The schematic diagram of the experimental setup is shown in Figs. 4.3 and 4.4. As the alginate solution is pumped into the microfluidic device, it fills up the chamber and then starts flowing out through the internal alginate nozzle. The air flowing through the outer nozzle then shears off the alginate solution and form droplets which are collected in a calcium chloride bath where the hydrogel microcapsules crosslink to form microcapsules as shown in Fig. 4.3. These droplets thus formed are then further analyzed for shape, size, etc. under a high resolution microscope. The relative air/alginate flow ratios can be used to control the size of the droplets formed.

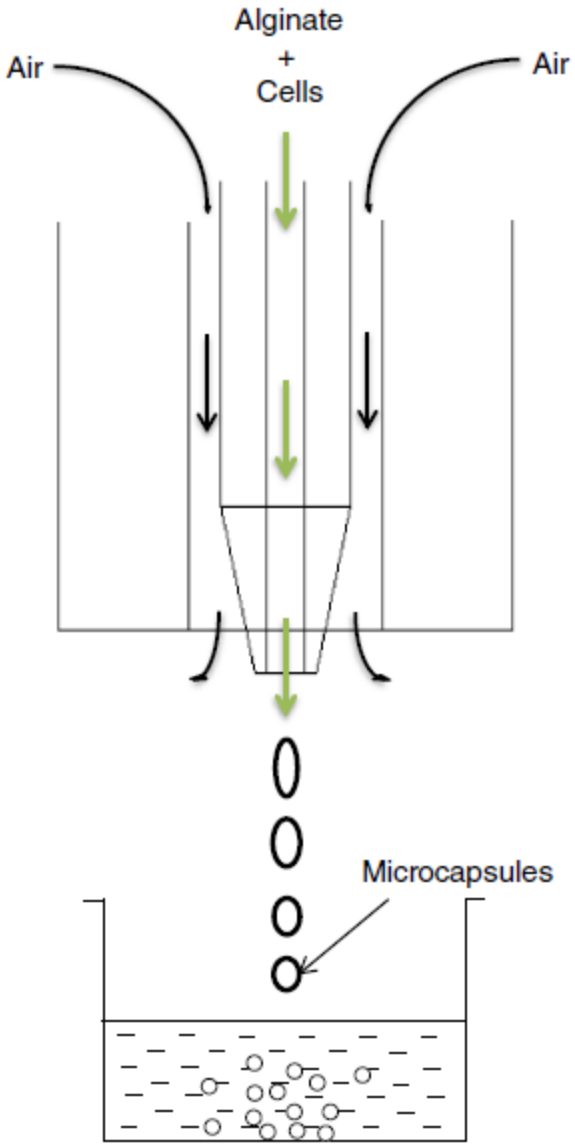

Figure 4.3: 2D Schematic of the droplet forming region of the microfluidic device

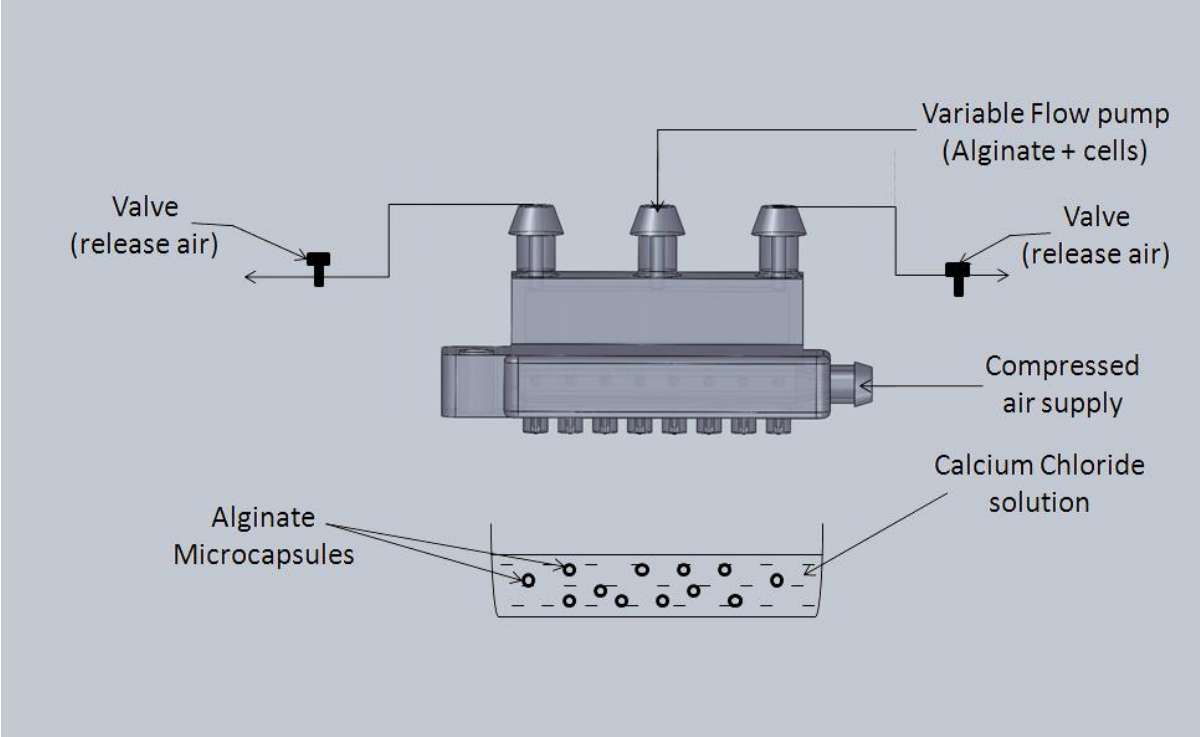

Figure 4.4: Schematic of a complete encapsulation system using the microfluidic device.

4.3 Parametric Study

4.3.1 Effect of Flow rate of Alginate

It was observed that the size of the hydrogel microcapsules decreases with reduction in the flow rate of alginate. Figure 4.5 is an illustration of the distribution of microcapsule size relative to alginate flow rate. As the flow rate of alginate is increased from 49.08 ml/h to 79.79 ml/hr., the average diameter of the microspheres increases from 654 μm to 707 μm.

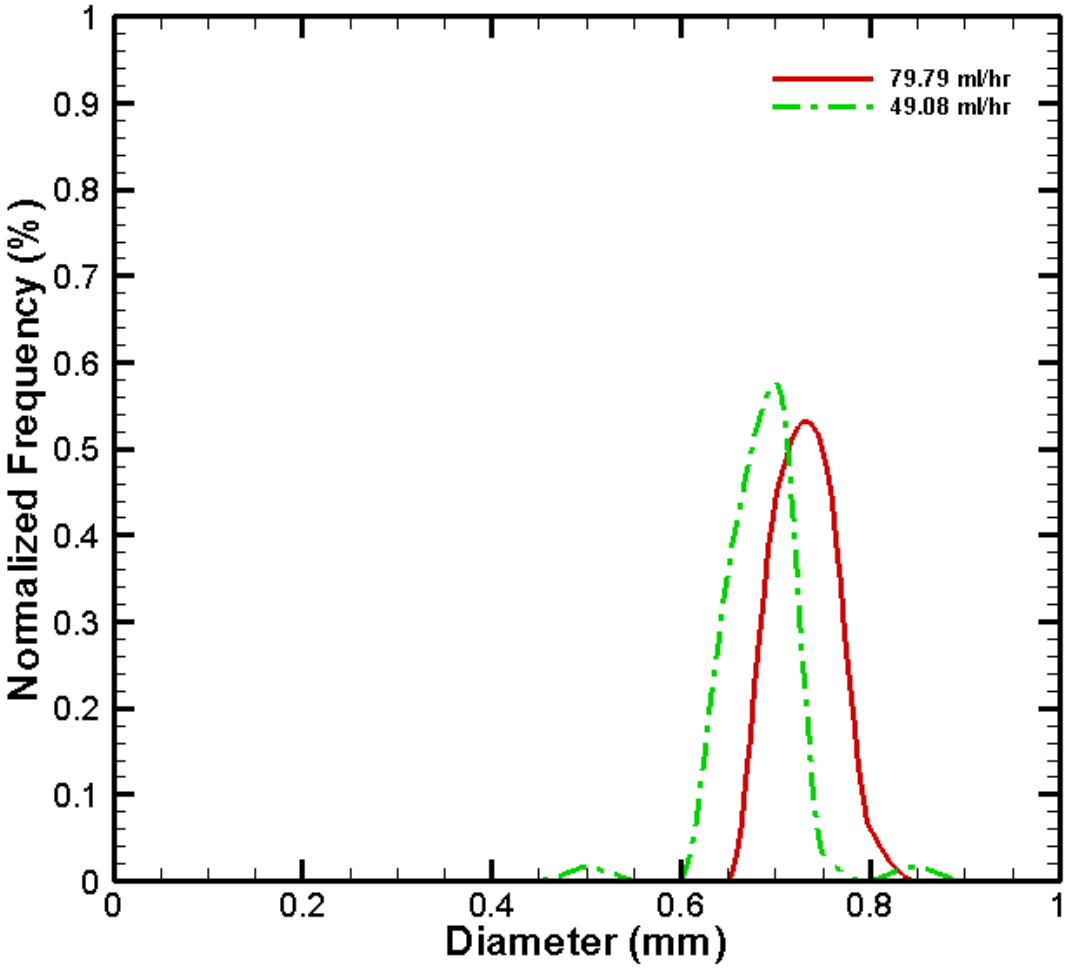

Figure 4.5: Effect of flow rate of Alginate on droplet diameter distribution.

4.3.2 Effect of Air Pressure

The size of the alginate hydrogel microcapsules is reduced with increase in the air pressure. Figure 4.6 illustrates the distribution of size with change in the air pressure from 5 psi (34.473 kPa) to 2 psi (13.789 kPa) at an alginate flow rate of 42 ml/hr. As the air pressure increased from 2 psi (13.789 kPa) to 5 psi (34.473 kPa) the average diameter of the hydrogel microcapsules decreased from 624 μm to 584 μm.

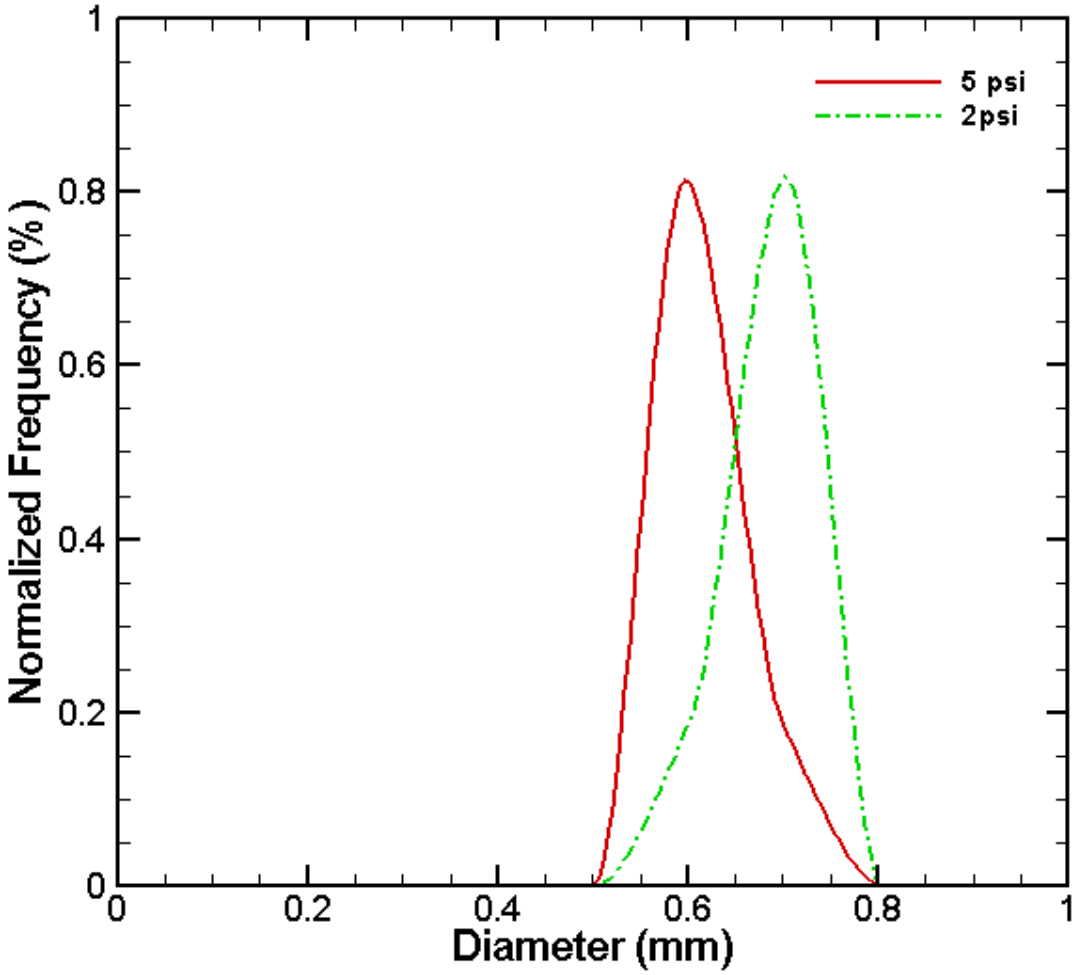

Figure 4.6: Effect of air pressure on droplet diameter distribution.

4.3.3 Effect of change in concentration of alginate

Figure 4.7 shows the effect of varying the alginate concentration at a fixed air pressure of 5 psi (34.473 kPa) and alginate flow rate of 42 ml/h on size distribution. As the concentration of alginate is increased from 1.5% to 3%, the average diameter of the hydrogel microcapsules increased from 587 μm to 672 μm.

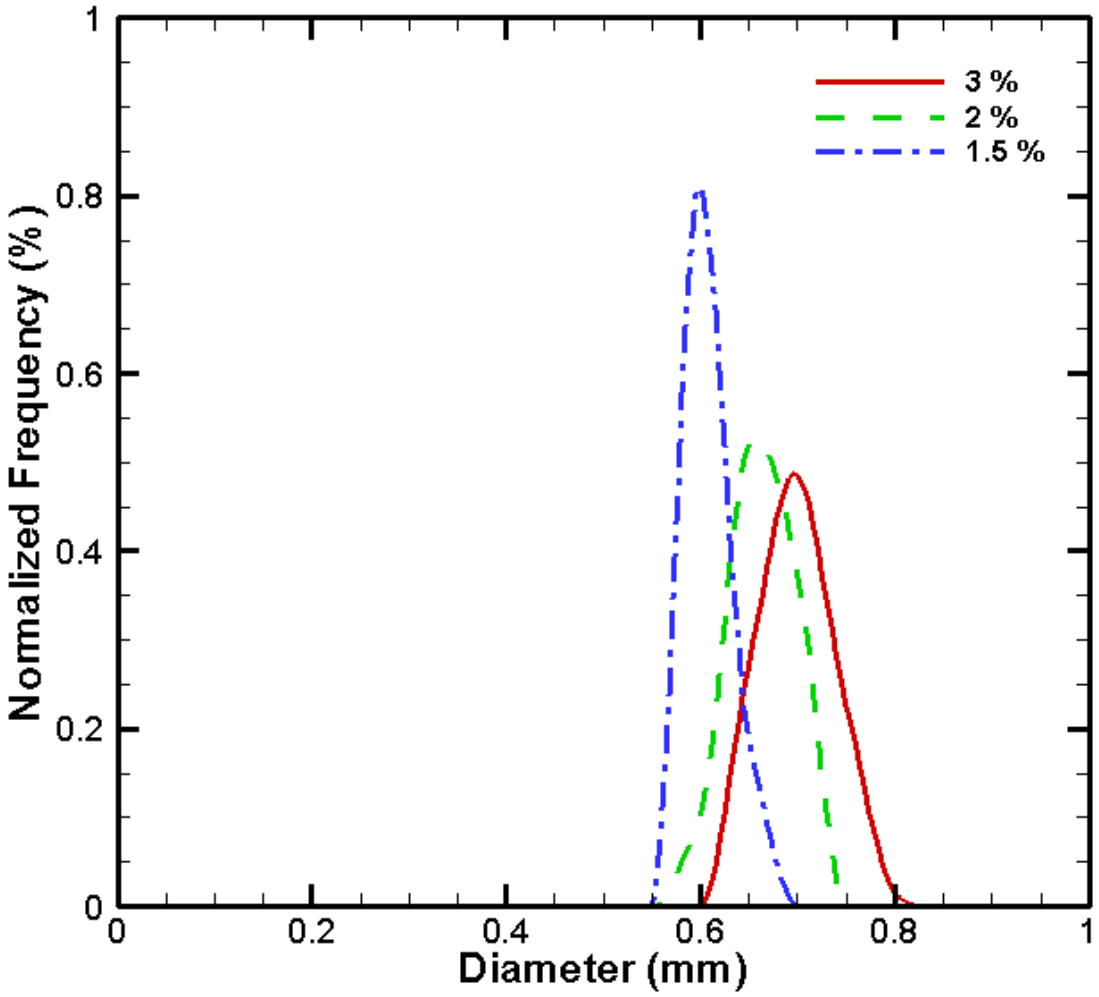

Figure 4.7: Effect of concentration of alginate on droplet diameter distribution.

4.3.4 Effect of change in distance

As the distance of the collection plate from the outlet nozzles is reduced below 0.24 m, the shape of the microcapsules changed from circular to tear drop to random shapes. The optimum distance range observed was 0.24– 0.29 m. As the distance increases beyond 0.29 m, the shape of the microcapsules is spherical; however, it leads to the coalescence of the

hydrogel microcapsules from adjacent nozzles as they fall into the collection plate. Figure 4.8(a), (b) and (c) show images taken with an optical microscope at 5x magnification.

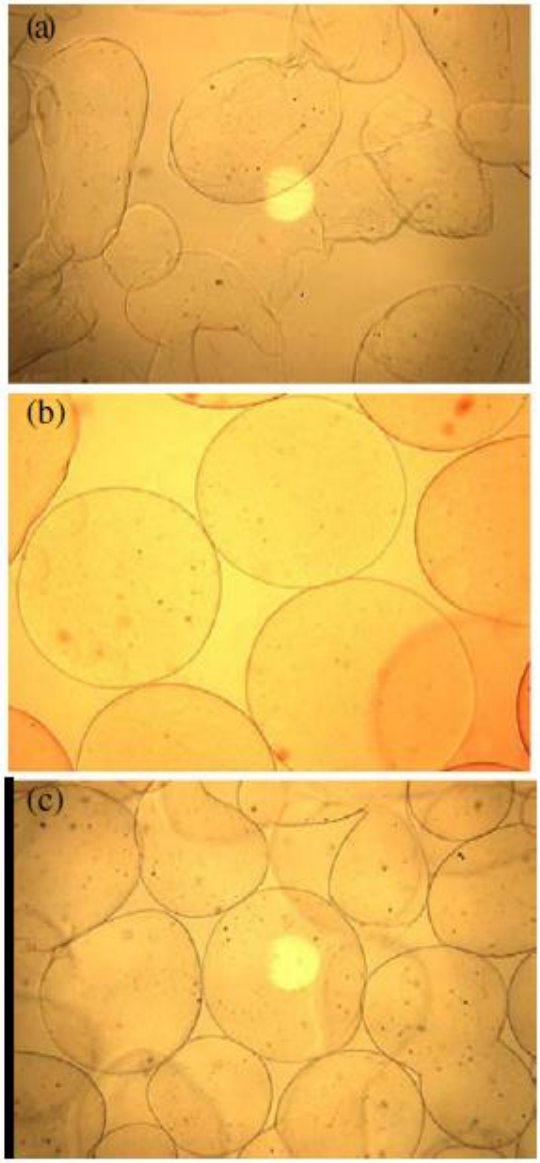

Figure 4.8: Effect of distance of Calcium Chloride (CaCl2) bath from tip of microfluidic device on droplet shape (a) 0.19 m—Irregular shapes (b) 0.25 m—Spherical droplets (c) 0.33 m—Irregular shapes.

4.4 High speed video analysis

High speed video analysis was conducted on the high throughput 8 channel microfluidic device to gain in depth understanding of the physics occurring in the droplet formation zone. A high speed video camera (HotShot Mega Sc, NAC Image Technology, CA, USA) was used to capture the formation of microcapsules at frame rates ranging from 1000-8000 frames per second (fps). A macro zoom lens Computar® MLH 10X 13-130mm (CBC Corp., NY, USA) was used to record the high speed videos. Figure 4.9 shows the various stages of droplet formation recorded at 6000 fps. For the purpose of this high speed video study, the concentration of the aqueous solutions of sodium alginate was varied from 0.75% to 3% (wt. / vol.); flow rate of air was varied from 0.1 to 3 psi (0.689 to 20.684 kPa) and flow rate of alginate solutions was varied from 15 to 90ml/hr.

In the study of co-flow microfluidic systems, the three main dimensionless numbers used are Reynolds number (Re), Capillary number (Ca) and Weber number (We). These numbers are defined as follows:

$$Re = \frac{\rho U D}{\mu} \quad \textbf{4.4.1}$$

$$Ca = \frac{\mu U}{\sigma} \quad \textbf{4.4.2}$$

$$We = \frac{\rho U^2 l}{\sigma} \quad \textbf{4.4.3}$$

$$\rho_c = \frac{\rho_{alginate}}{\rho_{air}} \quad \textbf{4.4.4}$$

$$\mu_c = \frac{\mu_{alginate}}{\mu_{air}} \qquad \textbf{4.4.5}$$

where ρ is density, U is velocity of the fluid, D is the diameter, μ is the viscosity of the fluid, σ is the interfacial tension, l is the characteristic length (in this case the droplet diameter), ρ_c is the density ratio and μ_c is the viscosity ratio.

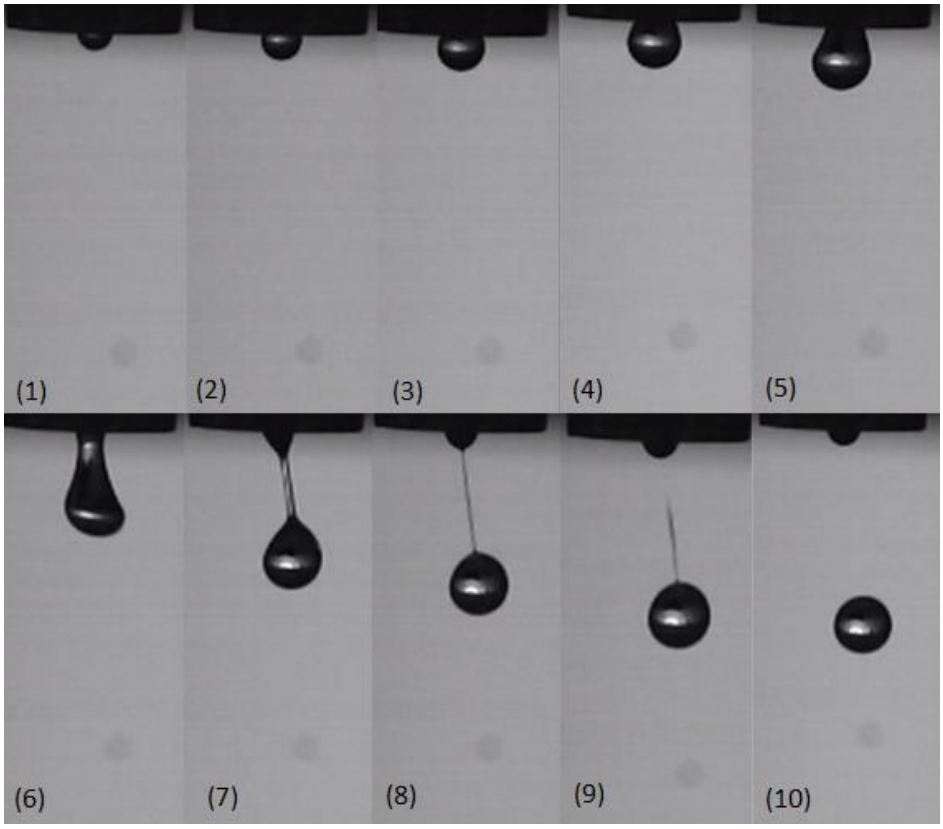

Figure 4.9: Shows the different stages of drop formation recorded at 6000 fps. The encapsulation conditions used were 0.75% wt. /vol. concentration aqueous solution of alginate at compressed air pressure of 0.6 psi (4.136 kPa) and alginate flow rate of 5ml/min.

The Reynolds number is the ratio of the inertial forces to the viscous forces and provides more information about the flow regime of the fluid flow. Capillary number is the ratio of viscous forces to interfacial tension forces acting across the interface between a

liquid and a gas or between two immiscible liquids. Weber number is the ratio of fluids inertial forces to interfacial tension and is important in the analysis of free surface or droplet formation flows. Since we have two fluids in our system namely air and aqueous solutions of sodium alginate, we have two sets of the above mentioned numbers. For the purpose of the high speed video study, the dimensionless numbers were varied as follows:

$800 < Re_{air} < 7050;\ 0.1 < Re_{alg} < 11; 1 < We_{air} < 250;$

$0.001 < We_{alg} < 0.05; 0.001 < Ca_{air} < 0.02;\ 0.001 < Ca_{alg} < 0.3;$

$1400 < \mu_c < 37000;\ \rho_c = 1000$

Based on the flow regimes of the fluids in the microfluidic device for the high speed video study, namely for air (Re>>1) and for alginate (Re<<1), only two of the above mentioned dimensionless numbers per fluid phase have significance from the point of view of the physics of droplet formation, Weber number for air (We_{air}) and Capillary number for Alginate (Ca_{alg}). These two numbers help to describe and understand the behavior observed during droplet formation in the microfluidic device and will be discussed in detail below.

4.4.1 Effect of change in Weber Number (We_{air})

The Weber number for air was varied for the three different concentrations of sodium alginate solutions namely 1%, 2% and 3% and its effect on droplet formation was observed. It was observed that as the Weber number of air increased, the droplet size reduced. Figures 4.10, 4.11, 4.12 depict the diameter of droplets produced by the microfluidic device as a function of the Weber number of air for varying concentrations of alginate solutions (1%, 2%, 3%).

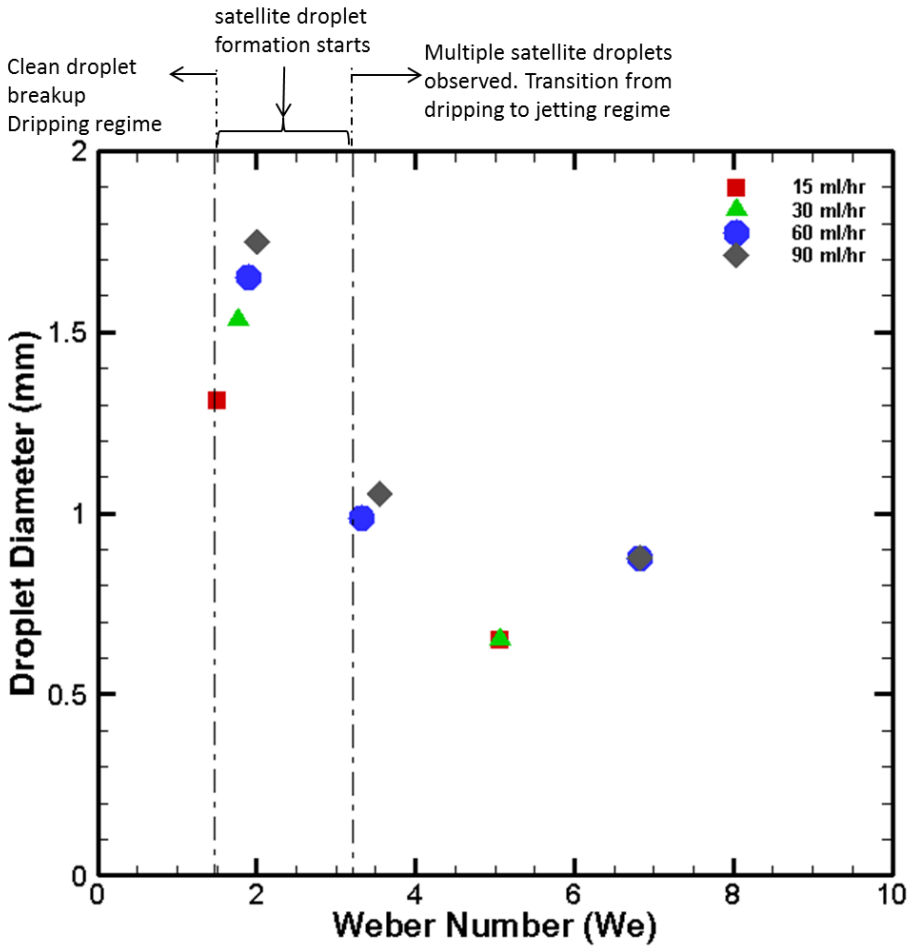

Figure 4.10: Effect of change in We_{air} on the droplet diameter for 1% aqueous solution of sodium alginate.

The plots show expected trend as the Weber number of air increased, the drag force exerted by air on the droplet increased thus sheared them faster from the alginate nozzle and produced smaller droplets. The plots show drop formation observed at four different flow rates of alginate solutions namely 15, 30, 60, 90 ml/hr. and it can be observed that the plots for each flow rate follow the same trend i.e. as the We_{air} increases, the diameter of the droplet formed decreases.

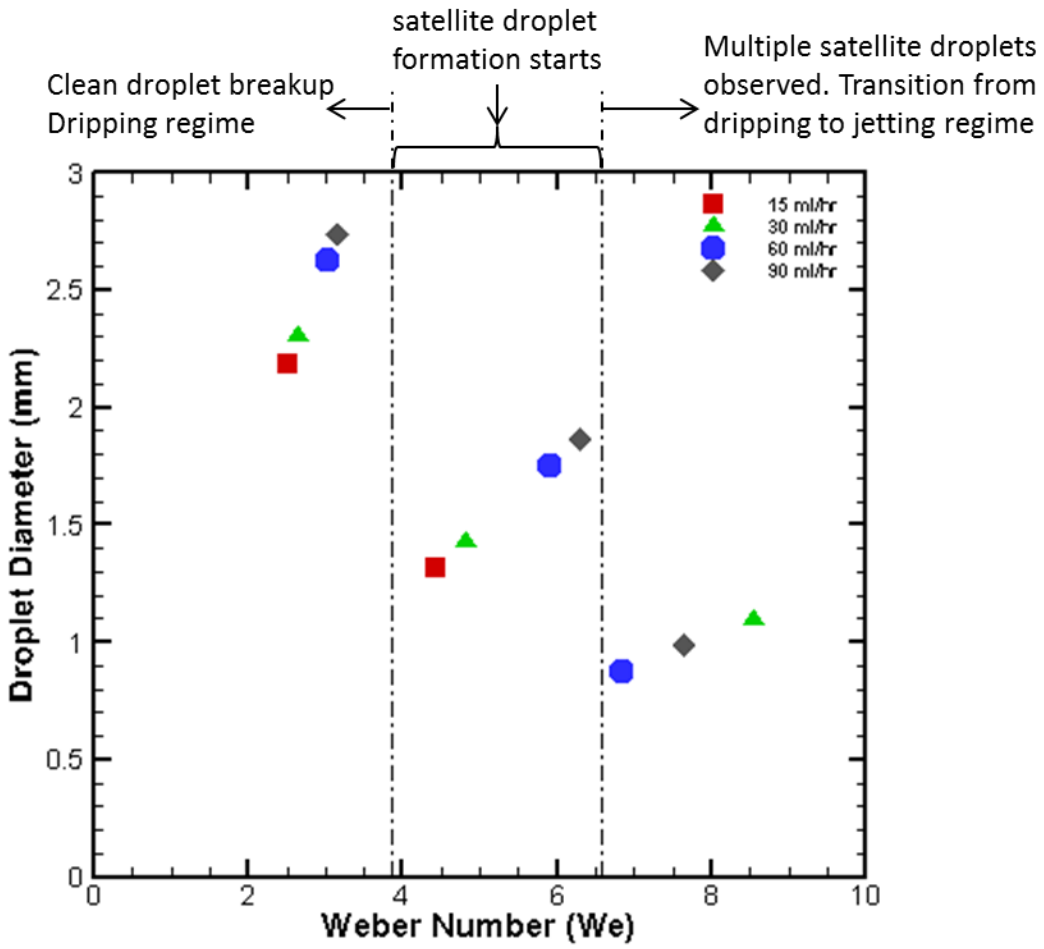

Figure 4.11: Effect of change in We_{air} on the droplet diameter for 2% aqueous solution of sodium alginate.

It was also observed that at lower Weber numbers the drop formation of the nozzle occurs in the dripping regime. However, as the We_{air} increased, the drop formation regime starts transitioning towards jetting. In this transitioning zone, satellite droplet formation is observed. The satellite droplet formation observed in the transition zone changes as the Weber number increases. At the start of the transition zone, i.e. at lower Weber numbers a single satellite droplet is observed as the Weber number is increased; further multiple

satellite droplets are formed along with the primary droplet. In this range of Weber numbers as the satellite droplet formation increases, the primary droplet size reduces. As the Weber number is increased, further droplet formation becomes unstable and fluid volume breaks off from the nozzle which later breaks into random number of droplets based on Rayleigh instabilities produced in the fluid volume due to the co-flowing jet of air. It was also observed that as the concentration of the alginate solution increases, the satellite droplet formation zone shifts to the right as shown in figures 4.10, 4.11 and 4.12.

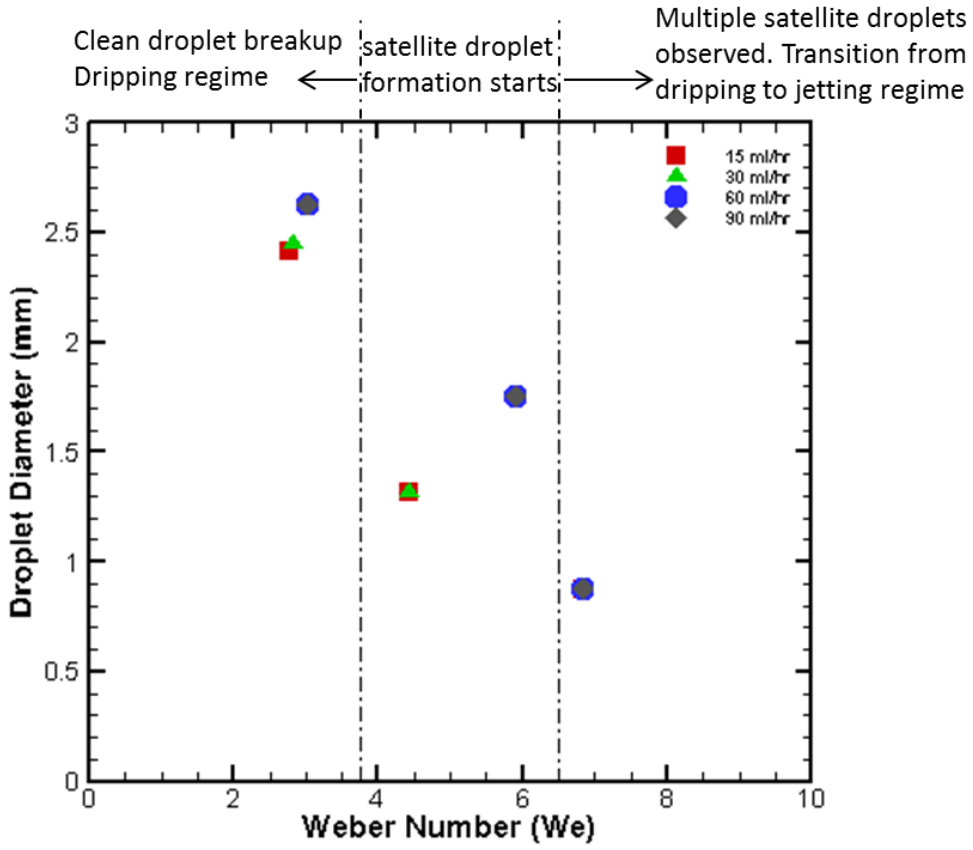

Figure 4.12: Effect of change in We_{air} on the droplet diameter for 3% aqueous solution of sodium alginate.

4.4.2 Effect of change in Capillary number (Ca_{alg})

The capillary number of alginate was varied for the three different concentrations of sodium alginate solutions at 1%, 2% and 3% and its effect on droplet formation was observed. The capillary number was varied in two different ways (a) by changing the concentration of alginate solution (i.e. μ) and (b) by changing the flow rate of alginate (i.e. V). It was observed that as the capillary number was increased the diameter of the droplet produced by the microfluidic device increased. Figures 4.13, 4.14, 4.15 depict the diameter of droplets produced by the microfluidic device as a function of the capillary number of alginate for varying concentrations of alginate solutions (1%, 2%, 3%). Plots show the drop formation observed at flow rates of air varying from 0.1 - 0.5 psi (0.689 - 3.447 kPa).

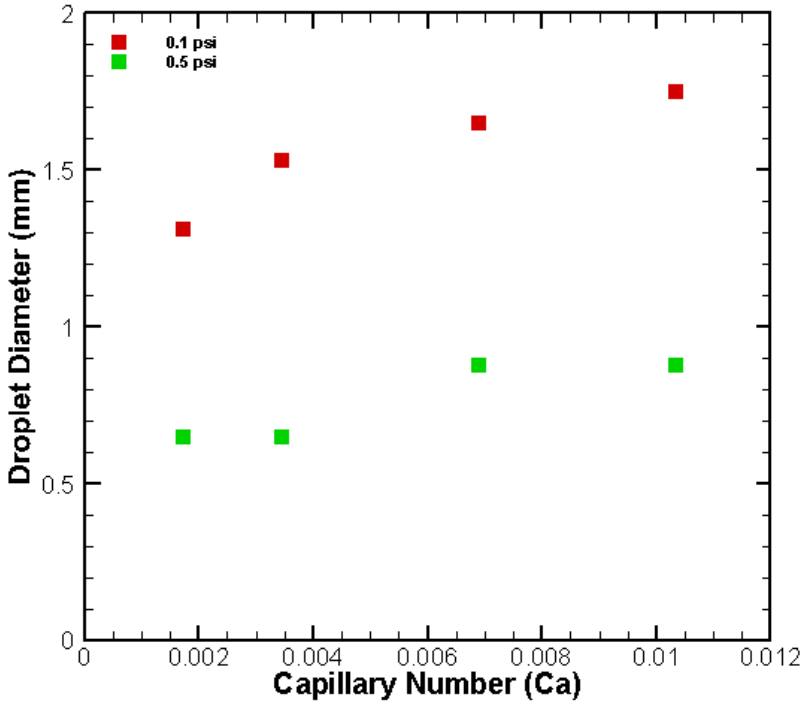

Figure 4.13: Effect of change in Ca_{alg} on the droplet diameter for 1% aqueous solution of sodium alginate.

This follows the expected trend, as the capillary number of the alginate solution is increased, the viscous forces become more dominant. This increase in viscous forces adds to the damping effect at the nozzle for droplet formation, thus reducing the disturbances produced in alginate fluid column due to the co-flowing air thereby stabilizing the drop against the growth of Rayleigh instabilities which lead to the formation of bigger droplets. For the purpose of this high speed video study and equipment constraints (flow rate limit of the syringe pump), the droplet formation controlled by capillary number of alginate was restricted to the dripping regime. However, if the capillary number of alginate (Ca_{alg}) is kept on increasing further then the flow regime would eventually transition to jetting and finally one would observe two co-flowing jets i.e. alginate-air core-annular flow respectively.

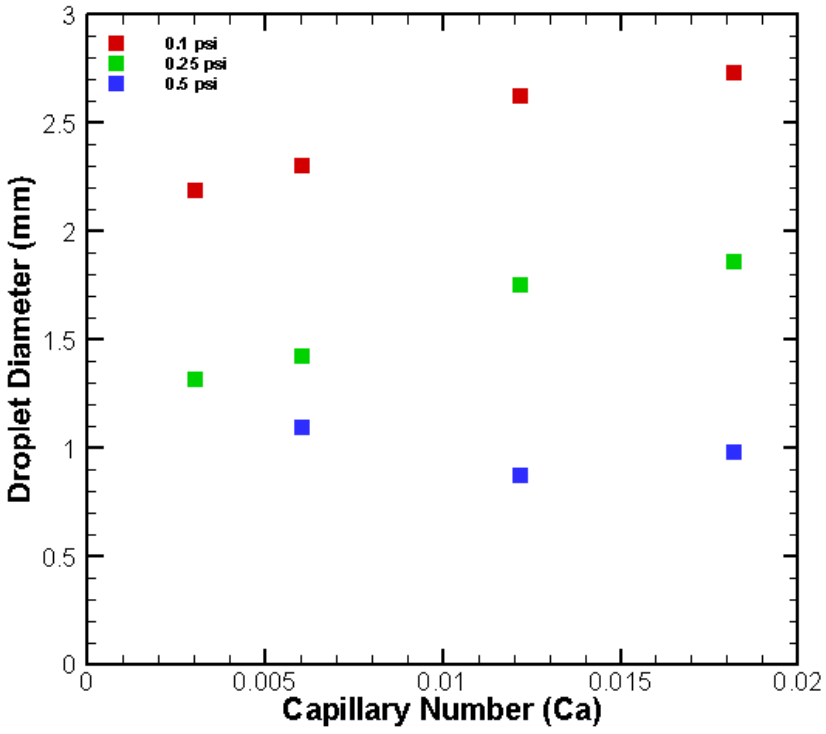

Figure 4.14: Effect of change in Ca_{alg} on the droplet diameter for 2% aqueous solution of sodium alginate.

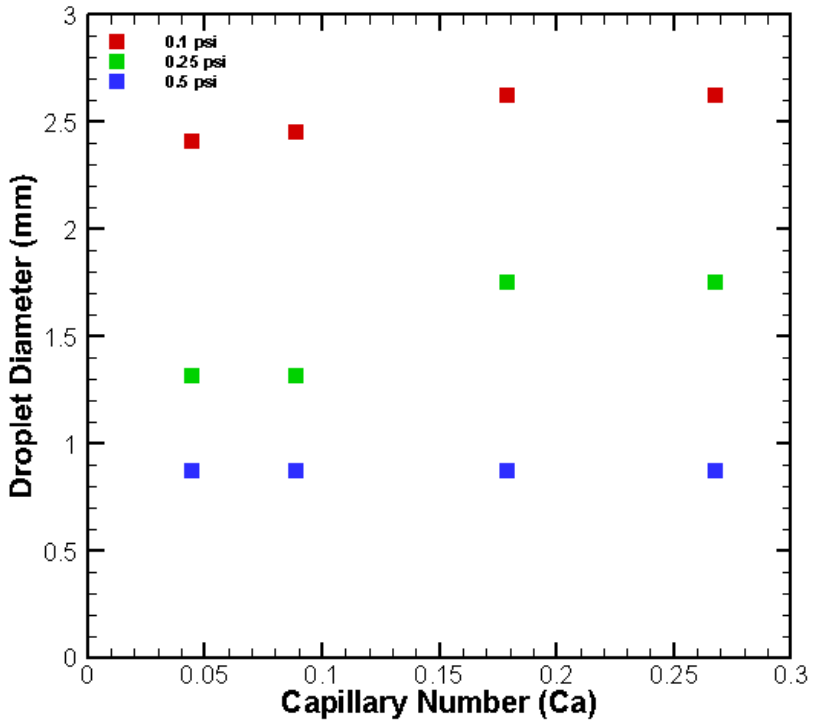

Figure 4.15: Effect of change in Ca_{alg} on the droplet diameter for 3% aqueous solution of sodium alginate.

4.5 Defects observed in mass production of microcapsules

As with regards to any high throughput/mass production process, a percentage of the final output is defective. In the microencapsulation process too, one comes across capsules that have certain defects. Defects include empty capsules, cells at the surface of the capsule and exposed, non-spherical capsules, surface cracks that will accelerate deterioration of capsules when put to use, satellite particles and capsules too large in dimension required. Of these defects the most concerning ones namely formation of satellite droplets and observation of stress lines are discussed in more detail below.

4.5.1 Formation of satellite droplets

Uniform microcapsule size distribution is always desirable for encapsulation, drug delivery and release, etc. Generally speaking, any liquid jet breaks into droplets due to the Rayleigh instability induced by the co-flowing fluid jet. Unfortunately, such a jet also has a tendency to form satellite droplets intermixed among the main drops (Pimbley & Lee 1977). The existence and behavior of these satellite droplets depend on the droplet formation conditions and their existence leads to the difficulty in the size control of the microcapsules. Thus, it is desirable to reduce/suppress if not eliminate the formation of the satellite droplets during the microencapsulation process. Formation of the satellite droplets as observed for the 8 channel microfluidic device is as shown in figure 4.16.

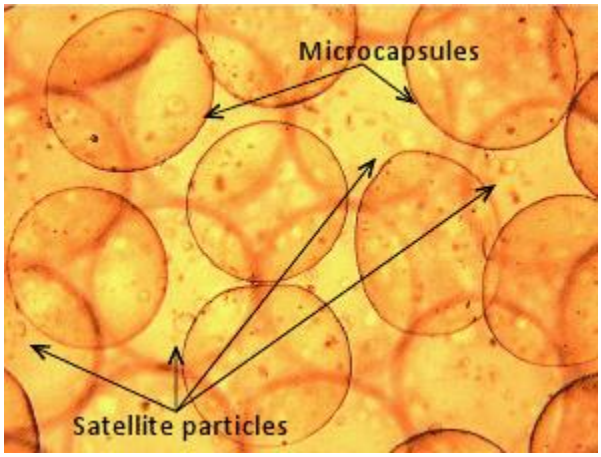

Figure 4.16: Satellite droplet formation observed during encapsulation using the high throughput 8 channel microfluidic device.

During the high speed video study, it was observed that as the Weber number of air (We_{air}) increased, the drop formation regime started transitioning from dripping to jetting regime and satellite droplet formation was observed. At lower Weber numbers, only a single

small satellite droplet was observed. However as Weber number of air was increased further, multiple satellite droplets were observed. The factors affecting the formation of satellite droplets are flow regime of the continuous phase, concentration of alginate solution and the alginate nozzle tip finish of the microfluidic device. These factors are discussed below in detail.

4.5.1.1 Flow regime of the Continuous phase

The flow regime of the continuous phase near droplet formation zone at the time of droplet break up is a critical factor affecting the formation of satellite droplets. As the Weber number of air is increased, the flow regime of air transitions from laminar to turbulent. However, a closer look at the droplet formation zone shows that just near droplet break up when the droplet size is at its maximum, the local Reynolds number would increase as the droplet blocks more and more area of the air channel outlet, thus causing local turbulence in the droplet formation zone. This phenomenon is observed in the high speed video analysis, as the droplet starts to oscillate with small oscillations first during the droplet growth period and as it grows bigger and starts blocking more area of the air channel near outlet, the droplet oscillations increase and finally the droplet breaks from the nozzle. These observations concur with observations by Ganan-Calvo (Ganan-Calvo 1998). Figure 4.17 depicts the various stages of droplet formation using the high speed video analysis taken at different stages of drop formation. One can also observe the formation of satellite droplet shown in figure 4.17 (h).

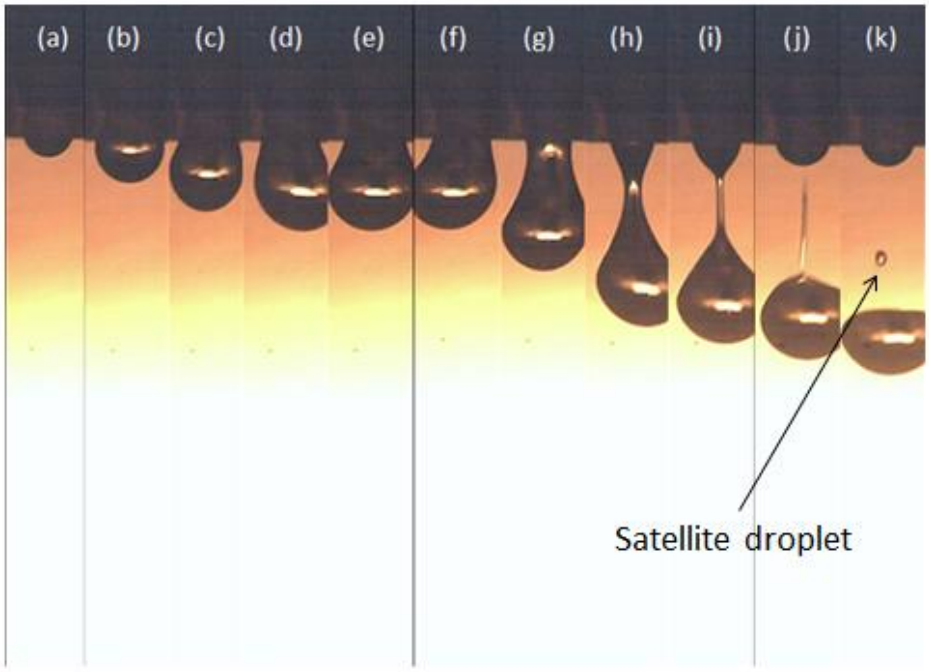

Figure 4.17: (a)-(k) Shows various stages of droplet formation using the 8 channel microfluidic device for 1% alginate solution flow rate of 15ml/hr. at 0.1 psi (0.689 kPa) air pressure.

4.5.1.2 Concentration of Alginate solution

The concentration of the alginate solution also affects the formation of satellite droplets. It was observed that as the concentration of the aqueous solution of sodium alginate increased from 1% to 3% (wt. / vol.) the formation of satellite droplets occurred at higher Weber number. This trend is expected as the concentration of the alginate solution increases, its apparent viscosity increases. This viscosity acts as a damping factor and thus reduced the disturbances induced in the alginate phase by the continuous phase fluid. Thus at the point of droplet formation for the same Weber number of air, the droplet formation is more stable and satellite droplets are observed at much higher values of Weber number for air as the concentration of the alginate solution increases. This shift in the start of satellite droplet

formation zone with increase in concentration of sodium alginate can be observed in figures 4.10, 4.11, 4.12.

4.5.1.3 Alginate nozzle tip finish

As the eight - channel microfluidic device is fabricated using the rapid prototyping technique of 3D printing, the tip of the alginate nozzle does not have a good clean finish as depicted in figure 4.18. To understand the effect of this alginate nozzle tip finish on the formation of satellite droplets, we fabricated a single channel needle based design using the needle tip shown in figure 4.19 as the alginate nozzle thus providing a clean flat finish to the alginate nozzle outlet. Satellite droplet formation was observed for very low Ca_{alg} for 1% aqueous solution of sodium alginate (same as that for the 8-channel microfluidic device); however, one anomaly was that as the capillary number was increased, the satellite droplet formation was not observed in case of the steel needle based design. For higher concentration of the alginate solutions, the behavior of both the devices was same.

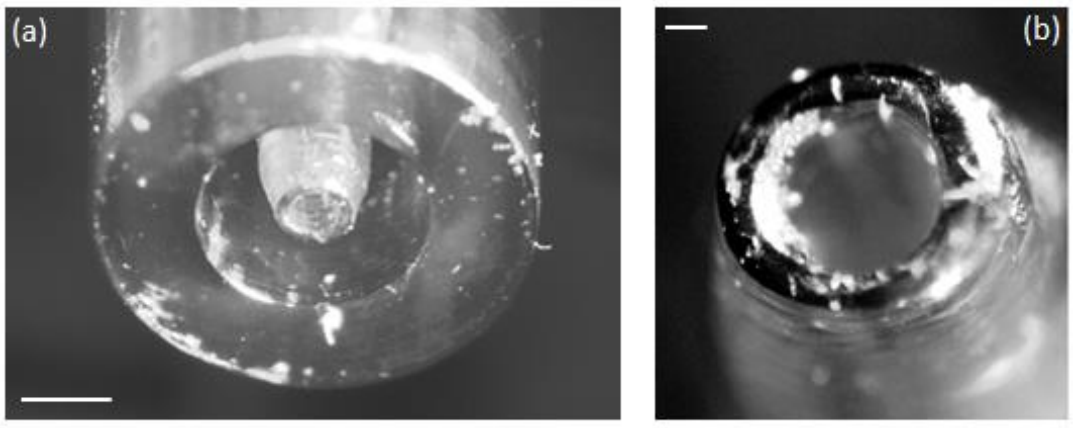

Figure 4.18: Alginate nozzle tip of the 8-channel microfluidic device. (a) Scale bar 500 microns. (b) Scale bar 50 microns.

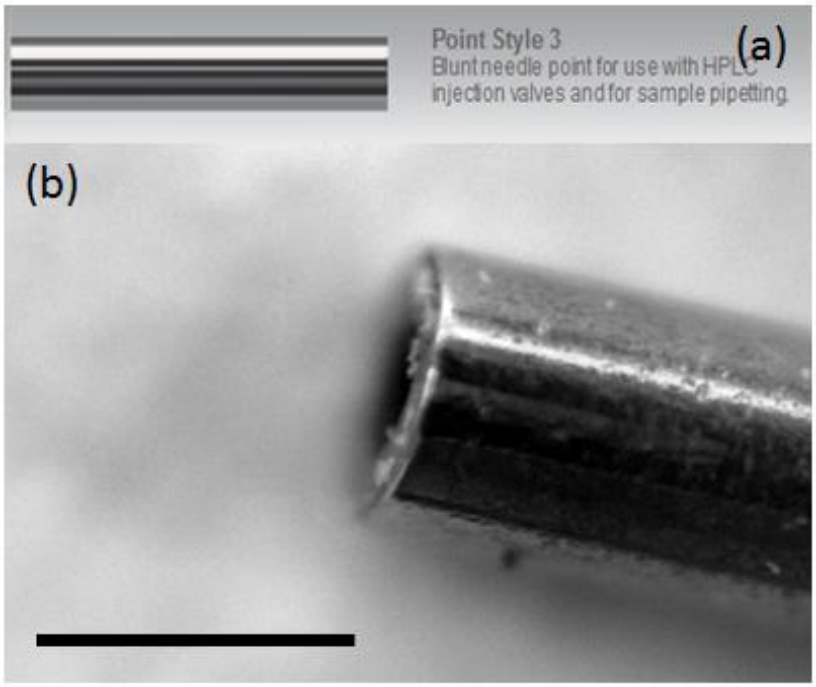

Figure 4.19: (a) Needle tip used for fabrication of alginate nozzles (b) A higher magnification image of the micro needle, scale bar 500 microns.

4.5.2 Stress lines on surface of microcapsules

Another major defect observed in microcapsules is the formation of stress lines on the surface. The two main factors contributing to the occurrence of this phenomenon are first shear force exerted by the continuous phase (air) on alginate and secondly material properties of sodium alginate. Figure 4.20 depicts the stress lines observed on the surface of microcapsules produced using the high throughput microfluidic device.

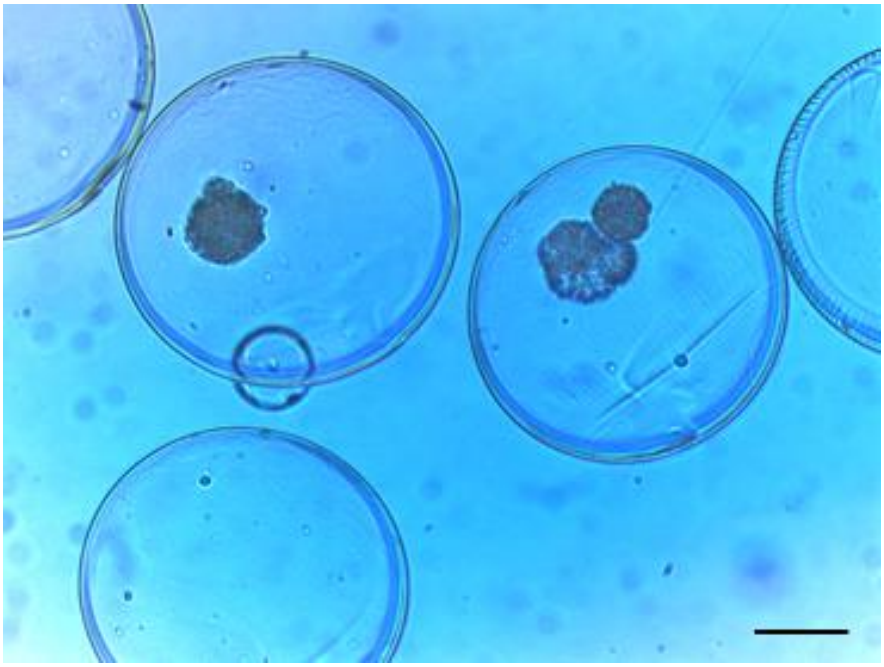

Figure 4.20: Stress lines observed on microcapsules produced by the encapsulation process during encapsulation of pancreatic islets. Scale bar = 100µm.

The formation of stress lines on the surface of microcapsules is not desirable and should be avoided as they basically indicate the regions where there are residual stress concentrations on the surface of the microcapsules. If such a microcapsule was transplanted inside the body it would rupture and release the cell/ biological material inside the body thus leaving it exposed to the host immune system. This would not only compromise the exposed cell, but would also the cause the host immune system to attack the remaining transplant graft thereby affecting the viability of the remaining graft and reducing the effectiveness of the transplant procedure. In case of sustained drug delivery, a rupture of micro capsule with stress lines would result in quick release of the drug thereby defeating the original purpose of encapsulating the drug for sustained release.

Increasing the flow rate of air reduces the droplet diameter; however the increase in flow rate of air means a corresponding increase in the shear force exerted by air on the droplet surface, which causes more prominent stress lines to develop on the capsules. This effect is similar to the sharkskin effect observed during extruding on a polymer surface (Miller & Rothstein 2004). Figure 4.21(a) and (b) shows microcapsules produced at 12ml/hr. of alginate flow rate and air pressure of 0.25 psi (1.724 kPa) and 0.5 psi (3.447 kPa) respectively. It can be observed that the droplet diameter reduced as the air pressure was increased, however the stress lines become more prominent in figure 4.21 (b) as compared to 4.21 (a).

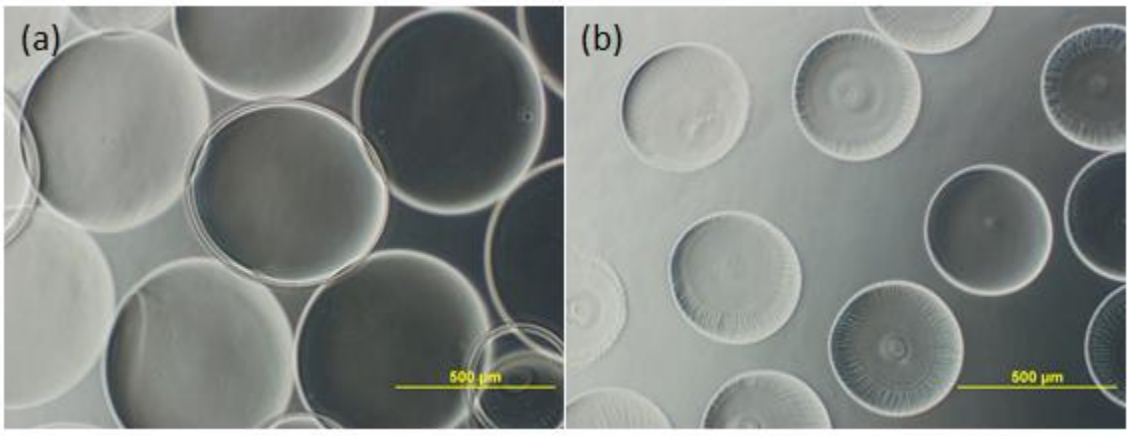

Figure 4.21: Increasing the flow rate of air increases the shear force on the droplets leading to smaller capsules however more prominent stress lines. Microcapsules produced at 12ml/hr. and (a) 0.25 psi (1.724 kPa) (b) 1.0 psi (3.447 kPa).

The second reason for the formation of stress lines depends on the material properties of the sodium alginate. As shown in figure 4.22, the same encapsulation conditions produced different levels of stress lines on alginate solutions made from sodium alginate acquired from

two different sources. The ultrapure LVM alginate procured from Novamatrix® (Sandvika, Norway) showed more stress lines as compared to crude alginate procured from Acros Organics (Fair Lawn, NJ). This can be attributed to the fact that the alginate obtained from Novamatrix® was more purified, thus having more cross linking units as compared to the crude alginate from Acros. However this then becomes a purely material science oriented question as then one also needs to consider the gelling kinetics i.e. diffusion and concentration of calcium ions present in the $CaCl_2$ bath, number of 'G' and 'M' units present in alginate, Molecular weight, etc. which are outside the scope of this dissertation and hence will not be discussed here.

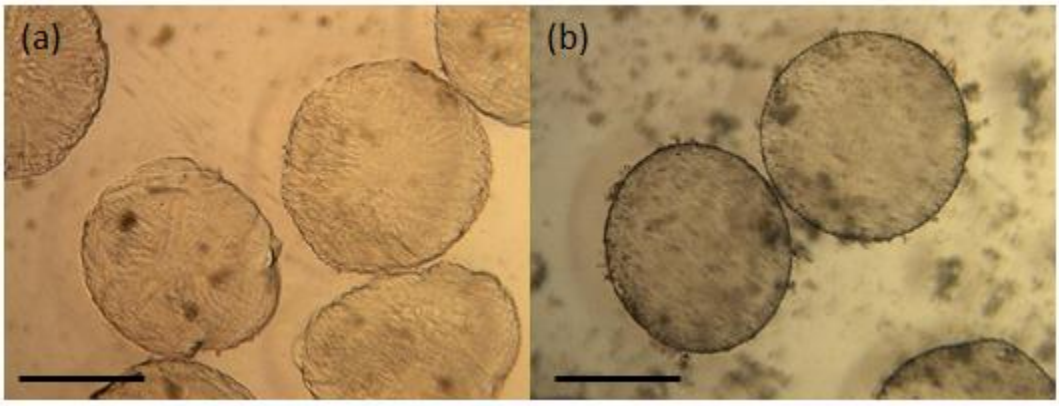

Figure 4.22: Microcapsules with stress lines on the surface. Scale bars = 500µm. Encapsulations conditions used were 0.75% (wt. / vol.) of alginate solution, 0.1 psi (0.689 kPa), at flow rate of 3 ml/hr. cross linked in 3% CaCl2 solution (a) Ultrapure LVM alginate (b) Acros Organics alginate.

4.6 Conclusion

In this chapter, we have conducted thorough testing of the scaled up microfluidic device designed in chapter 3 and discussed in detail the various parameters affecting the

process of droplet formation. Also the major defects observed during the high throughput manufacturing of the microcapsules have been discussed and careful experiments were conducted to understand the effect of the droplet formation parameters resulting in occurrence of the defects. Thus, the droplet formation process involving air and alginate in a co-flow system is a complex process due to the high viscosity ratio and high density ratio between the two fluids. The knowledge gained in this chapter will be applied towards developing a computational model of the droplet formation process to predict the most optimal conditions for formation of droplets and be able to better address the aforementioned defects observed during microcapsule formation.

Chapter 5 Computational Model of the Microfluidic device

5.1 Introduction

The single channel needle based microfluidic device fabricated during the high speed video analysis to test the effect of the finish of the needle tip on formation of satellite droplet was selected for computational modeling to gain more fundamental understanding of the droplet formation process for our co-axial air flow design. In this chapter, we discuss the computational model developed to simulate the droplet formation process and validate it. The effect of various parameters namely concentration of alginate, flow rate of alginate, and flow rate of air on droplet formation are studied using the computational model and the results are discussed.

5.2 Background

The precise control of microcapsules and microspheres size and size distribution in fabrication is of great manufacturing interest for microencapsulation and controlled release drug delivery applications as their size distribution critically impacts not only the allowable routes of administration (i.e. transplants and implants) but also the release rate of encapsulated compounds. The effects of microcapsule size on efficient drug delivery for different targets and drug composition have been reported in literature (Tabata, Inoue & Ikada 1996; Barrow et al. 1998; Berkland et al. 2004; Berkland et al. 2004). In order to achieve this uniform microcapsule size distribution and to have precise control over it, an in depth understanding of the microcapsule fabrication process is necessary. Microcapsule fabrication using co-axial air flow process as reported in the earlier chapters is the process

used for microcapsule fabrication and is the focus of this study (Tendulkar et al. 2012). The microcapsule formation process using co-axial air flow can be further modeled and optimized based on the understanding of a single nozzle co-axial air flow device.

It is well known that the breakup of a liquid jet is closely associated with the instability of the jet. Since the pioneering jet instability study by Rayleigh (Rayleigh 1879; Rayleigh 1892), there have been numerous theoretical and experimental efforts to study the effects of various flow parameters to further understanding of jetting dynamics (Eggers 1997; Stone 1994; Tomotika 1935; Nayfeh 1970; Lee 1974; Ganan-Calvo 1998; Pimbley & Lee 1977; Rallison 1984). Two different modes have been distinguished: one is Rayleigh mode (Rayleigh 1879) and the other is the Taylor mode (Taylor 1962) . In Rayleigh mode the size of the droplets generated is comparable to the jet diameter in size while in Taylor mode the size of droplets is much smaller than that of the jet diameter. It was found that for uniform velocity profiles of liquid and gas the spatial instability results are in good accordance with the temporal analysis, except at sufficiently large jet velocities (Si, Li & Yin 2009). Lin & Lian (Lin & Ibrahim 1990; Lin & Lian 1993) and Lin & Chen (Lin & Chen 1998) investigated the linear instability of a cylindrical viscous liquid jet surrounded by a viscous gas in a circular pipe, where the basic velocity profiles of the liquid and gas exactly satisfy the Navier–Stokes equations. It was demonstrated that the mechanism of the Rayleigh mode is capillary pinching, and the mechanism of the Taylor mode is the interfacial shear and pressure fluctuation. Richards et al. and Zhang used the VOF–continuum surface force ‘CSF’ method to estimate the droplet size of liquid jet surrounded by a liquid medium (Richards, Beris & Lenhoff 1995; Zhang 1999; Zhang 1999). Eggers and Dupont applied the second-

order finite-difference scheme and slender jet approximation for breakup physics (Eggers 1997). Su et al. and Herran et al. showed that the VOF-CSF method can also be applied to piezo-electrically actuated drop on demand systems and predicted droplet diameters from their models showed good comparison with experiments (Su, Longest & pidaparti 2010; Herran, Wang & Huang 2010). Other experimental studies include the investigation of the scaling law of the jet diameter at the hole exit, the influence of *We* on the dispersion of particle size and various applications of co-flow and flow focusing devices in drug encapsulation, dye-labeled particles and microfluidic systems (Ganan-Calvo 1998; Anna, Bontoux & Stone 2003). Recently, Si et al. theoretically modeled the flow focusing experiments of a liquid jet forced by a high-speed air stream (Si, Li & Yin 2009; Si et al. 2010). Temporal and spatio-temporal instability analysis and the resulting prediction of the most unstable wavelength and the AI/CI boundary showed good agreement with the experimental results. They observed that the Weber number and velocity at interface have the significant influences on the transition between axisymmetric and non-axisymmetric instabilities while other parameters like density ratio, viscosity ratio, and Reynolds number hardly induce the transition.

While there are numerous efforts in understanding the droplet formation dynamics, the systematic understanding of droplet/microsphere as a function of material properties and operating conditions is still missing. To date, no one has studied the effect of co-axial air stream on the microcapsule formation involving non-Newtonian fluids. This study aims to understand the underlying relationship that controls the microcapsule size in dripping mode with coaxially flowing air stream in order to optimize the single nozzle co-axial air flow

droplet generation system. The knowledge gained from this study would also help towards scale-up of the microcapsule production.

In this study, a single channel needle based device (see figure 5.1) is designed and fabricated using the rapid prototyping process of 3D printing as reported in chapter 4. The formulation of the problem, governing equations and validation of the numerical model are discussed in the numerical model of droplet formation section. The effects of various parameters for microcapsule generation are discussed in the Results and Discussion section and finally conclusions and future work are discussed in the Conclusions section.

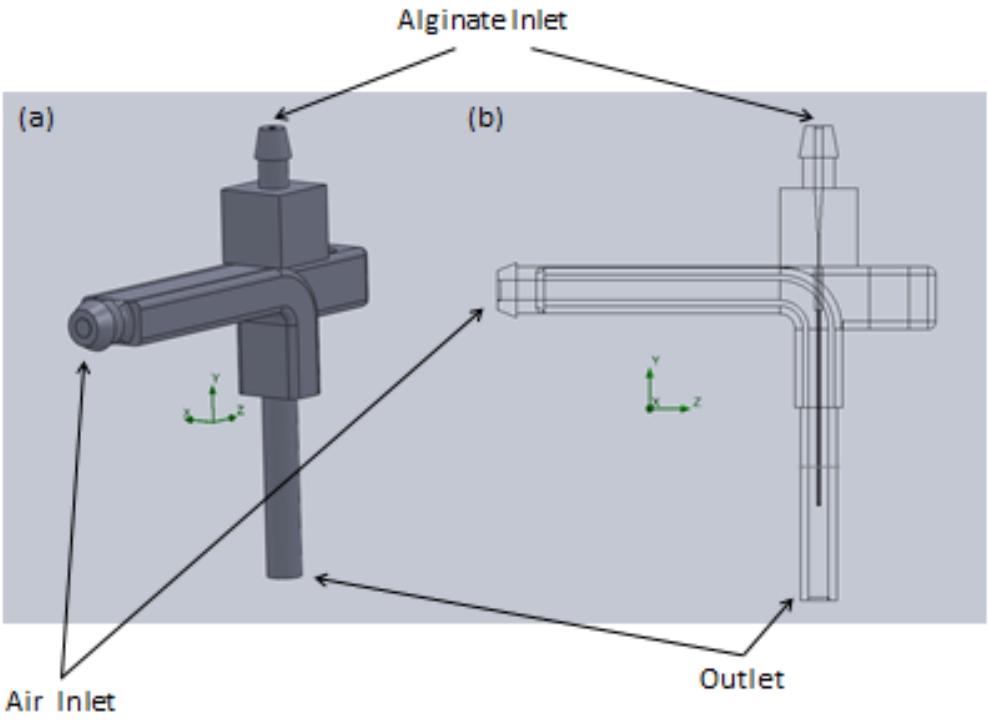

Figure 5.1: CAD model of the single nozzle co-axial air device (a) Isometric view (b) Side view.

5.3 Numerical Model of Single nozzle device

5.3.1 Formulation

The droplet generation problem for the single channel co-axial air flow device was solved in two parts. Part (A) involved separate steady state simulations of the air part and alginate part and Part (B) involved the actual transient droplet formation simulation. Part (A) was modeled using SolidWorks® and the numerical study was performed using SolidWorks® Flow Simulation tool. This study was similar to the one performed in chapter 3 and hence only the parts which were different between the two studies have been reported in this chapter. For details about governing equations and parameters used, please refer to chapter 3 section 3.3.3.1 Governing equations. Part (B) was modeled in general purpose commercial CFD solver Fluent 14 (ANSYS, Inc.). The details on modeling of the device are provided as follows:

5.3.1.1 Part (A)

Figure 5.1 shows the CAD model of the single nozzle co-axial air flow device designed in SolidWorks® (Dassault Systemes, MA, USA). For this study, the flow rate of alginate was varied from 0.05 ml/hr. to 15 ml/hr. The air pressure was varied from 0.05 psi to 0.6 psi (0.345 to 4.136 kPa). The concentration of alginate solutions was varied from 1% to 3%. The final mesh was determined by refining the mesh until grid independence of the results was achieved. The final mesh comprised of 498,957 and 504,764 rectangular parallelepiped elements for air part and alginate head, respectively. Figure 5.2 shows the final mesh used for the steady state simulations for both the air and alginate parts respectively in SolidWorks® Flow simulation tool.

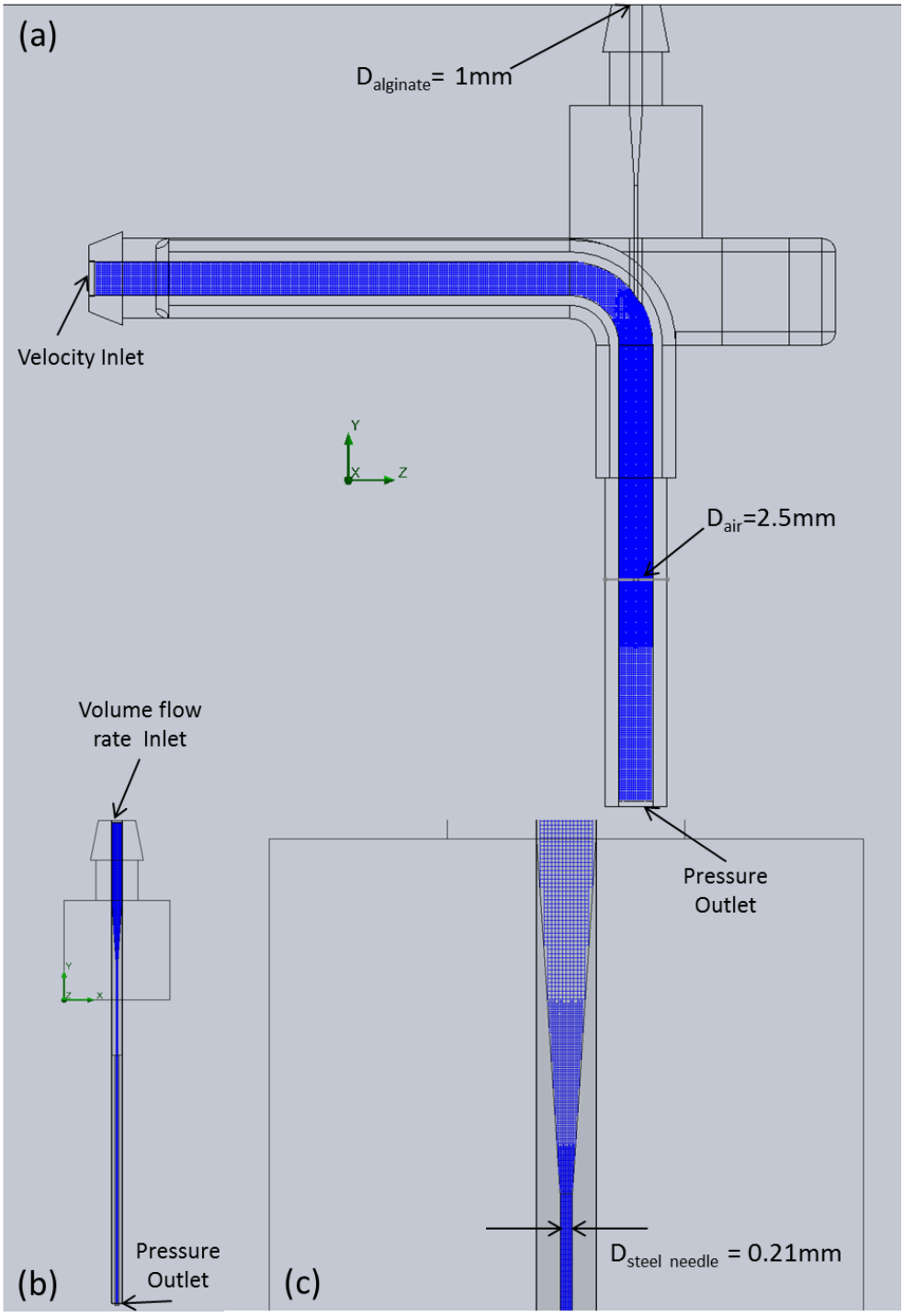

Figure 5.2: Final Mesh used for the numerical study of (a) Air channel (b) Alginate head & (c) Close up of the mesh in the alginate head.

5.3.1.2 Part (B)

Figure 5.3 shows the schematic of the region of interest for droplet formation for the single nozzle co-axial air flow system. Droplet formation from a needle in co-axial air flow is a typical problem in two-phase flow and can be solved using CFD simulations by tracking the volume fraction of each of the fluids throughout the computational domain using the Volume of Fluid (VOF) method. The details of this method can be found here (Hirt & Nichols 1981; ANSYS Inc. 2011). The computational domain consists of the inner alginate channel which contains alginate and drug mixture or alginate and cells suspension and the air stream flows co-axially around it. Alginate solution was modeled using the material models developed in chapter 2. Flow of air stream was modeled using the material properties reported in chapter 3 Table 3.1.

5.3.1.3 Governing Equations

The Navier-Stokes equations are used to model the flow in both the alginate and air channel. The flow in both the channels is assumed to be isothermal and incompressible. It is also assumed that the diffusion between the alginate solution and the co-flowing air stream is negligible. The flow of alginate in the channel is laminar. The flow of the co-axial air stream starts in the laminar region and with the growth of droplet becomes turbulent. As the droplet formation region is symmetrical, the problem was modeled at 2D axis-symmetric as shown in figure 5.3 and 5.4. The following equations were used to generate the transient solutions of the flow field in the droplet formation zone.

For mass conservation, the continuity equation can be expressed as

$$\frac{D(\alpha_i \rho_i)}{Dt} + \nabla.\left(\alpha_i \rho_i \vec{V}\right) = 0 \quad \textbf{5.1}$$

where α_i is the volume fraction of the i[th] phase, which is subjected to

$$\sum_{i=1}^{n} \alpha_i = 1 \quad \textbf{5.2}$$

The volume fraction is each cell is tracked by using

$$\rho = \alpha_1 \rho_1 + \alpha_2 \rho_2 \quad \textbf{5.3}$$

The momentum equation is expressed as follows

$$\frac{D\left(\rho \vec{V}\right)}{Dt} + \nabla.\left(\rho \vec{V} \vec{V}\right) = -\nabla P + \nabla.\left(\mu\left(\nabla \vec{V} + \nabla \vec{V}^T\right)\right) + \vec{F} + \rho \vec{g} \quad \textbf{5.4}$$

Where $\vec{V}$ is the velocity vector, P is the pressure, ρ is the density, and μ is the dynamic viscosity. The body force term at the interface comes from the interfacial surface tension and is based on continuum surface force model by Brackbill et al. (Brackbill, Kothe & Zemach 1992) in which the surface forces on the interface are transformed to volume forces in regions near the interface as

$$F = \sigma \, \kappa \, \nabla \alpha \quad \textbf{5.5}$$

where σ is the interfacial tension co-efficient and κ is the interfacial curvature.

The turbulence kinetic energy and dissipation transport equations for the $k - \varepsilon$ model read

$$\frac{\partial \rho k}{\partial t} + \frac{\partial}{\partial x_i}(\rho u_i k) = \frac{\partial}{\partial x_i}\left(\left(\mu + \frac{\mu_t}{\sigma_k}\right)\frac{\partial k}{\partial x_i}\right) + G_k + G_b - \rho\varepsilon - Y_M + S_k \quad \textbf{5.6}$$

$$\frac{\partial \rho \varepsilon}{\partial t} + \frac{\partial}{\partial x_i}(\rho u_i \varepsilon)$$

$$= \frac{\partial}{\partial x_i}\left(\left(\mu + \frac{\mu_t}{\sigma_\varepsilon}\right)\frac{\partial \varepsilon}{\partial x_i}\right) + C_{1\varepsilon}\frac{\varepsilon}{k}(G_k + C_{3\varepsilon}G_b) - C_{2\varepsilon}\rho\frac{\varepsilon^2}{k} + S_\varepsilon \quad \textbf{5.7}$$

where G_k represents the generation of turbulence kinetic energy due to the mean velocity gradients, G_b generation of turbulent kinetic energy due to buoyancy, Y_M represents the contribution of the fluctuating dilatation in compressible turbulence to the overall dissipation rate, $C_{1\varepsilon}$, $C_{2\varepsilon}$ and $C_{3\varepsilon}$ are constants, σ_k and σ_ε are turbulent Prandtl numbers for k and ε respectively. S_k and S_ε are user defined source terms.

The turbulent eddy viscosity μ_t is defined using two basic turbulence properties, namely the turbulent kinetic energy (k) and the turbulent dissipation (ε),

$$\mu_t = \rho C_\mu \frac{k^2}{\varepsilon} \quad \textbf{5.8}$$

where $C_\mu$is a constant.

$$G_k = -\rho\overline{u_i' u_j'}\frac{\partial u_j}{\partial x_i} \quad \textbf{5.9}$$

$$G_b = \beta g_i \frac{\mu_t}{Pr_t}\frac{\partial T}{\partial x_i} \quad \textbf{5.10}$$

where Pr_t is the turbulent Prandtl number for energy and g_i acceleration due to gravity in the i[th] direction. $Pr_t = 0.85$ for standard $k - \varepsilon$ models.

$$\beta = -\frac{1}{\rho}\left(\frac{\partial \rho}{\partial T}\right)_p \quad \textbf{5.11}$$

The degree to which ε is affected depends on constant $\boldsymbol{C_{3\varepsilon}}$ which is given as

$$C_{3\varepsilon} = \tanh\left|\frac{v}{u}\right| \quad \textbf{5.12}$$

where v is the component of velocity parallel to gravitational vector, and u is the component of velocity perpendicular to the gravitational vector.

$$Y_M = 2\rho\varepsilon M_t^2 \quad \textbf{5.13}$$

where M_t is the turbulent Mach number, defined as

$$M_t = \sqrt{\frac{k}{a^2}} \quad \textbf{5.14}$$

where a is the speed of sound.

$$C_\mu = 0.09, C_{1\varepsilon} = 1.44, C_{2\varepsilon} = 1.92, \sigma_\varepsilon = 1.3, \sigma_k = 1$$

To obtain the transient solution of the flow field, the governing equations were solved numerically on commercially available CFD solver Fluent 14 (ANSYS Inc. 2011) with the finite volume method using explicit time marching technique in order to use geometric reconstruction scheme which bests captures the interface between the two phases. A first order implicit transient formulation is used to accelerate convergence. The solutions at each time step were assumed to be converged when the dimensionless mass and momentum residuals were less than 0.001. Improving the convergence criteria to 0.00001 had negligible effect on the simulation results. A second order spatial discretization scheme was selected for solving momentum equation while first order upwind was used for the turbulence kinetic energy and turbulence dissipation in the $k-\varepsilon$ model. The SIMPLE algorithm was used for solving the pressure-velocity coupling. The basic boundary conditions were: volume flow rate boundary condition at inlet of the alginate channel, velocity boundary condition at the

inlet of air channel and a static pressure boundary condition (atmospheric pressure) was set at the outlet of the single channel co-flow device while the walls of the air and alginate channels were modeled as no-slip, smooth boundaries as shown in figure 5.3 and 5.4. The material properties used for the simulation of both the alginate and air part are same as that used in chapter 3, Table 3.1.

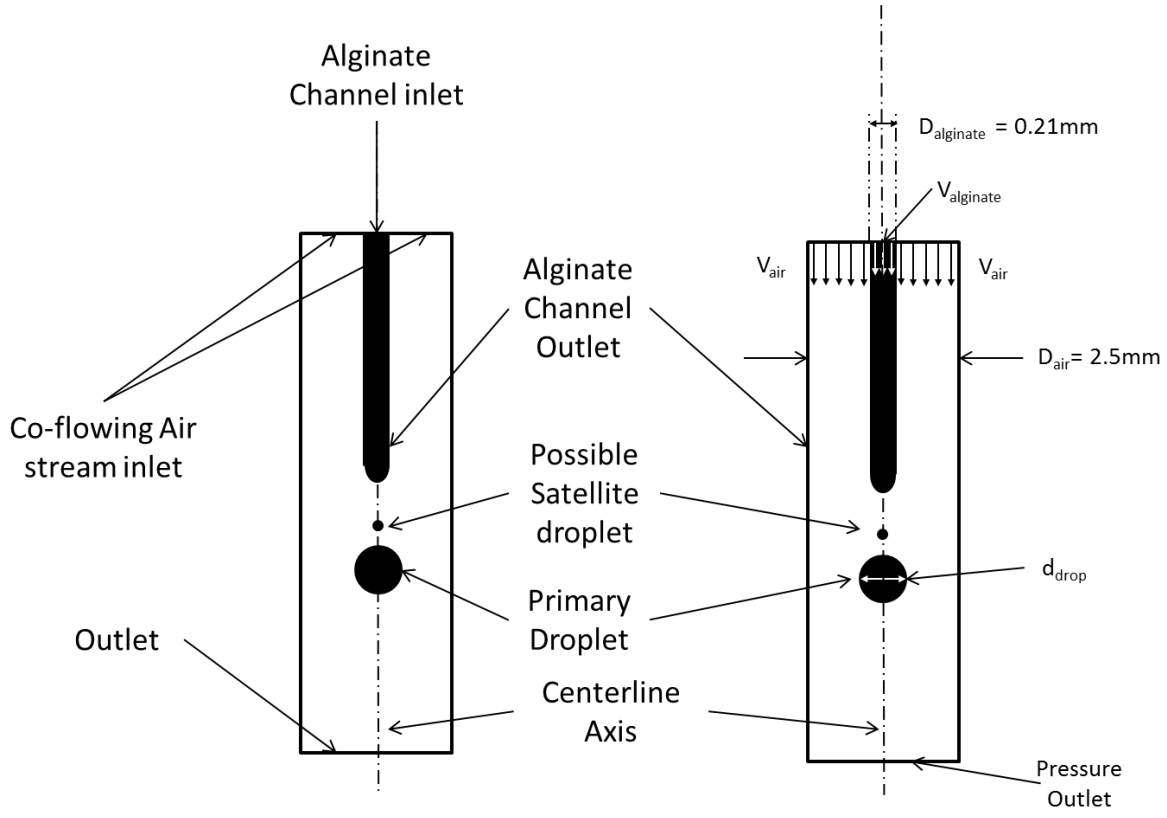

Figure 5.3: Schematic Diagram of the Co-axial air flow system (a) Part (B) modeled in Fluent and (b) schematic of the computational setup

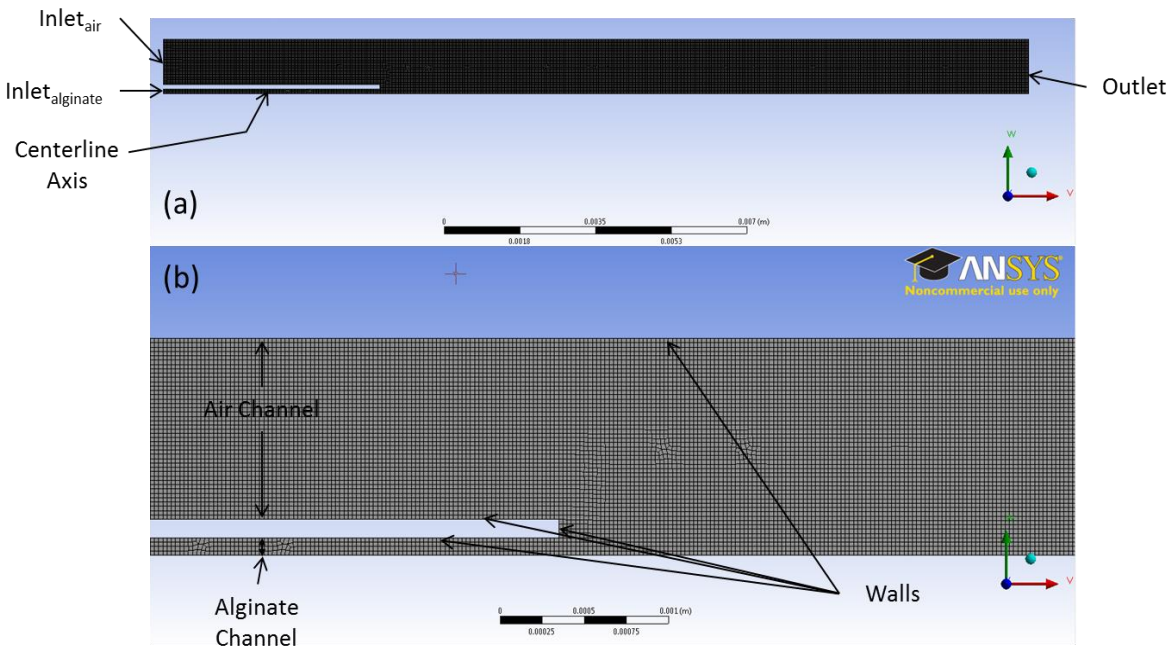

Figure 5.4: Schematic for CFD analysis (a) Final Mesh used for simulating single nozzle co-axial air flow device Part (B), (b) Close-up of the mesh near the droplet formation zone.

5.4 Results and Discussion

In order to validate the numerical approach described above, simulations performed were compared with the experimental data generated from high speed video analysis of the droplet formation region for the single nozzle co-axial air flow device. High speed video experiments were performed as described in chapter 4 section 4.5. The values of the droplet diameter for the numerical model were measured from the grid used for solving the model while the data from experiments was measured from the individual frames recorded during high speed video analysis. Figure 5.5 (a)-(g) and 5.6 (a)-(g) depict the various stages of droplet formation as observed during the high speed video analysis and predicted by the numerical model respectively. Red and blue colors indicate volume fractions of alginate and

air respectively. These figures provide a qualitative comparison between the experimental droplet diameter and the predicted droplet diameter by the numerical model. The conditions used were alginate flow rate of 9ml/hr. and air pressure of 0.1 psi (0.689 kPa) and 0.75% concentration of alginate solution. The high speed video was captured at 8000 frames per second.

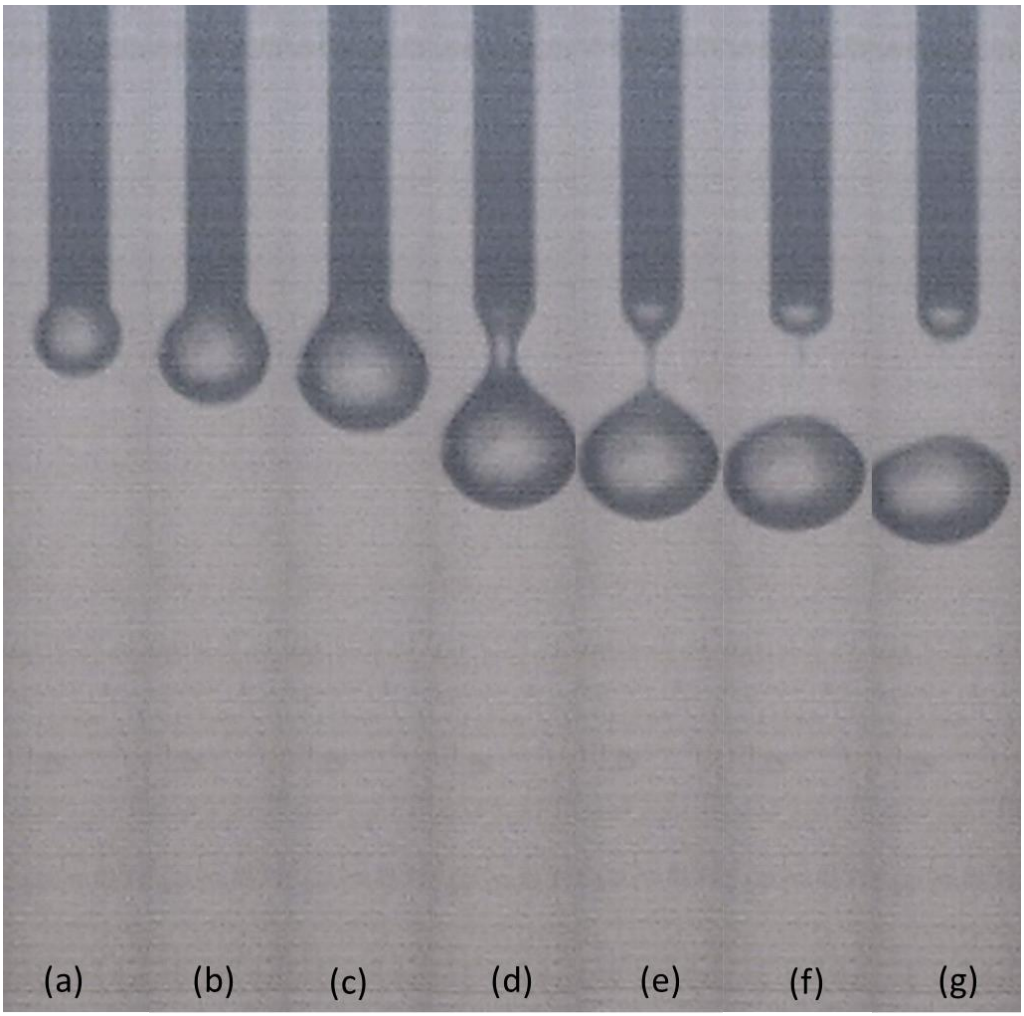

Figure 5.5: (a)-(g) show the various stages of droplet formation as observed on the high speed video.

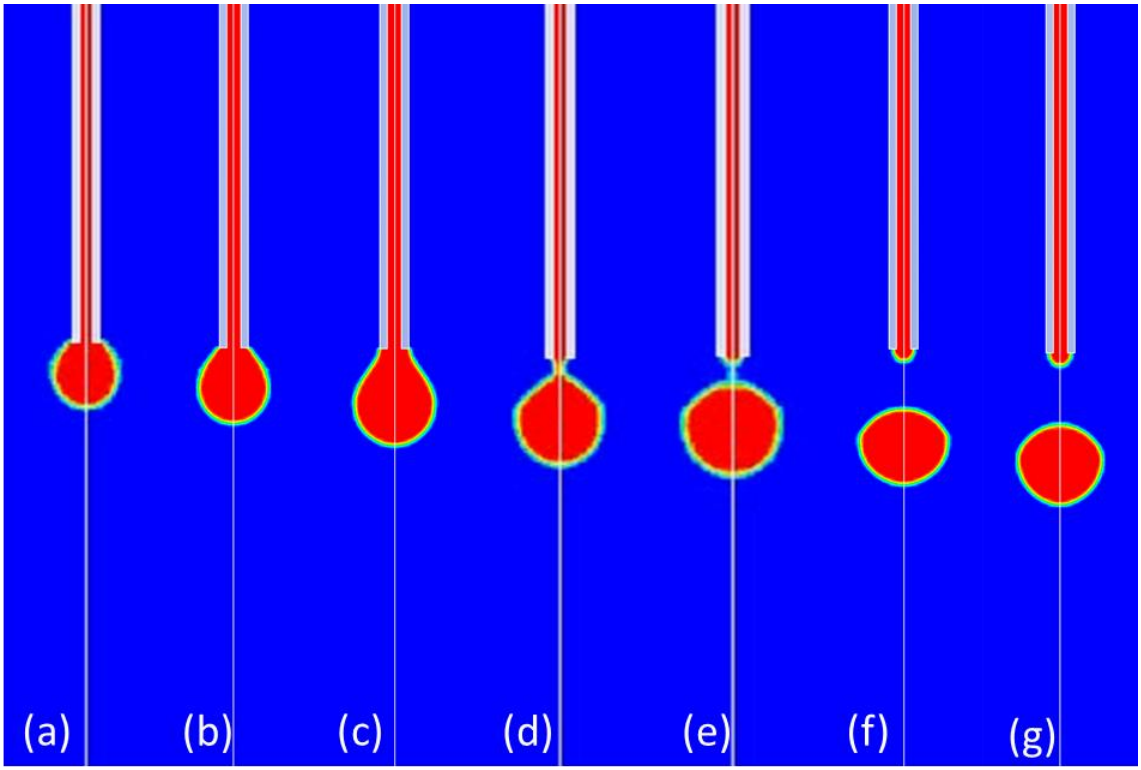

Figure 5.6: (a)-(g) show the various stages of droplet formation as predicted by the numerical model of the single nozzle co-axial microfluidic device.

5.4.1 Effect of Weber number (We_{air})

Figure 5.7 depicts the effect of Weber number of air on droplet diameter. As the Weber number increases, the drag force due to air on the droplet increases and the droplet diameter decreases. At low values of Weber number the droplet shape becomes spherical soon after its breakup from the nozzle. As the Weber number increases, the distance before the droplet shape becomes spherical increases. Both the experimental and modeling results show the same trend. At lower values of Weber number, the droplet diameter predicted by the numerical model shows good agreement with the experimental data. At higher values of Weber number, the model predictions of droplet diameter of the primary droplet are much

higher as compared to the experimental data. This can be attributed to a couple of reasons (a) the simulated droplets were not exactly spherical, (b) As the Weber number increases the droplet formation transitions from dripping to jetting. As the droplet experiences higher drag forces a transition between axisymmetric and non-axisymmetric instabilities is observed which agrees with the findings reported by Si et al. (Si, Li & Yin 2009) and are not captured entirely by the 2D axisymmetric numerical model used for this study.

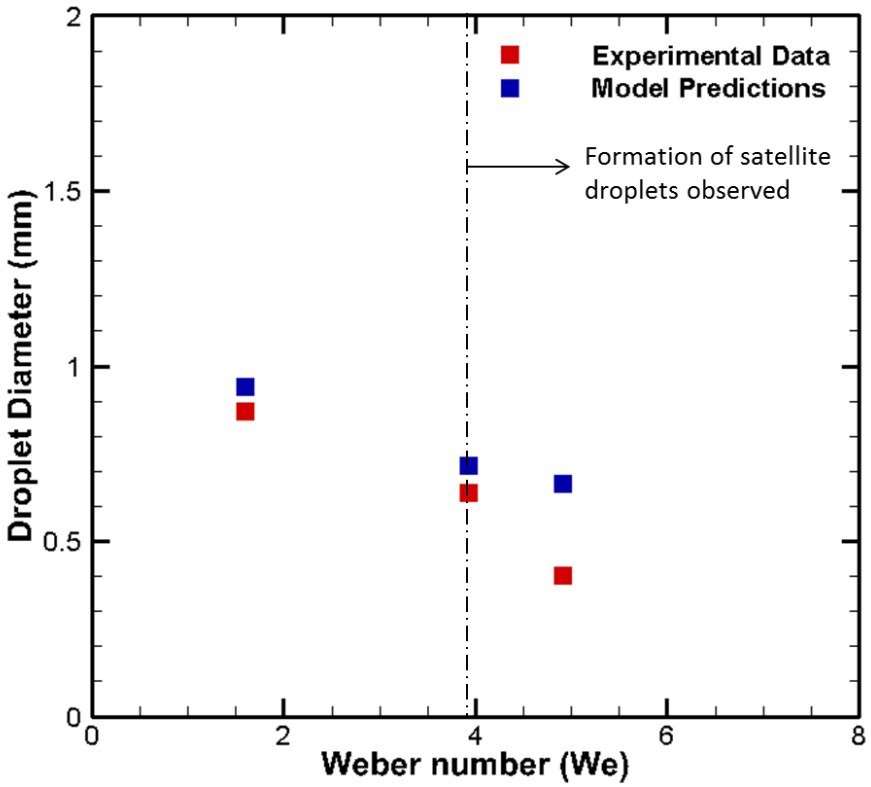

Figure 5.7: Shows the droplet diameter as a function of the Weber number of air for 1% concentration of alginate solution.

5.4.2 Effect of Capillary number (Ca_{alg})

Figure 5.8 depicts the droplet diameters obtained as a function of capillary number of alginate (Ca_{alg}) at 0.1 psi (0.689 kPa) air pressure for 1% concentration of alginate solution. As capillary number increases, the viscous forces acting on the droplet increase. This increase in viscous forces adds to the damping effect at the nozzle for droplet formation, thus reducing the disturbances produced in alginate fluid column due to the co-flowing air thereby stabilizing the drop against the growth of Rayleigh instabilities which lead to the formation of bigger droplets. From figure 5.8 it can be observed that the proposed numerical model and the experimental results follow the expected trend.

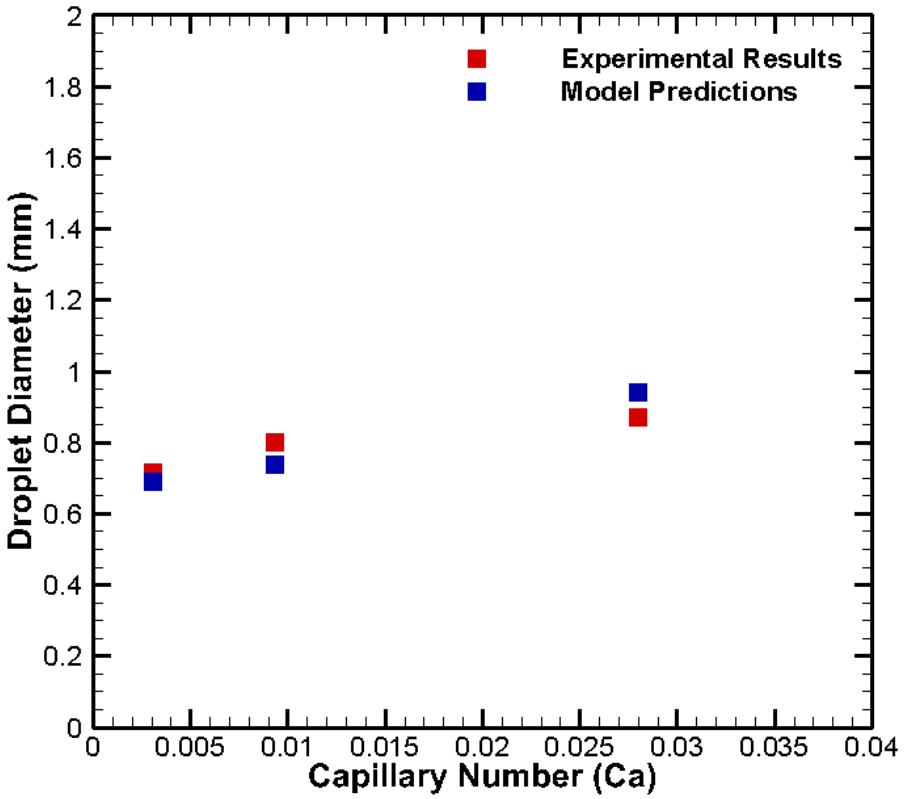

Figure 5.8: Shows the droplet diameter as a function of the capillary number of alginate for 1% concentration of alginate solution.

Figure 5.9 (a)-(g) and 5.10 (a)-(g) depict the various stages of droplet formation as observed on high speed video experiments and predicted by the numerical model for Capillary number of 0.083. The numerical model closely predicts the different stages of droplet development namely drop growth, extension and then break up. The numerical model also correctly predicted the tail of the droplet breaking off and retracting back to the alginate nozzle. A qualitative comparison thus shows good agreement between the experimental results and the numerical model of the single nozzle co-axial air flow device.

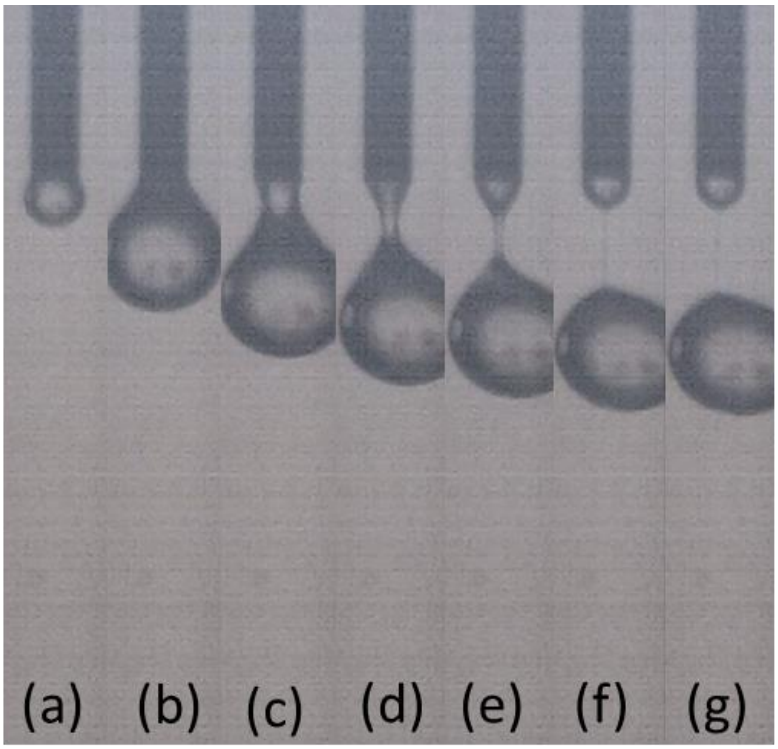

Figure 5.9: (a)-(g) shows the various stages of droplet generation as observed on high speed video for Ca=0.083.

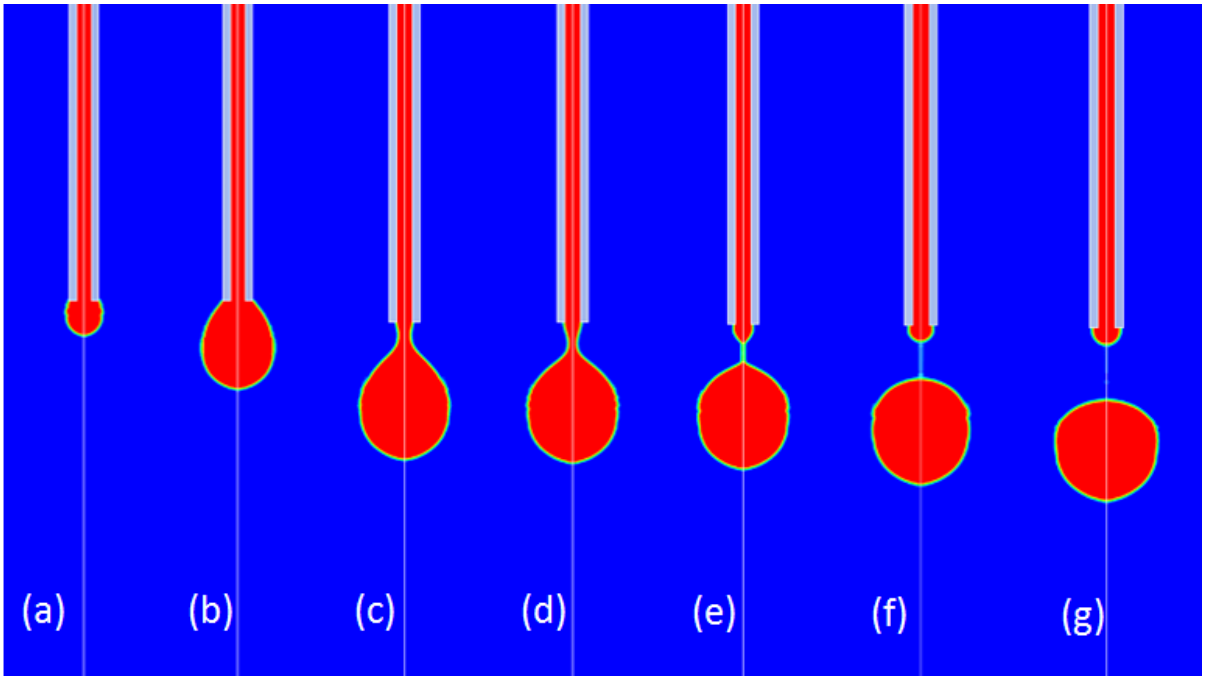

Figure 5.10: (a)-(g) shows the various stages of droplet formation as predicted by the numerical model for Ca=0.083.

5.5 Conclusion

In summary, a single nozzle co-axial airflow device was numerically modeled using commercially available CFD tools namely SolidWorks® flow simulation and Fluent 14 solver. A parametric study is performed to understand the effects of physical parameters namely flow rate of air, flow rate of alginate and concentration of alginate using dimensionless numbers namely Capillary number and Weber number on the droplet diameter to better understand the physics in the droplet formation zone. Based on the data, it is observed that the droplet diameter decreased with the increase in Weber number while the increase in capillary number led to a subsequent increase in the droplet diameter. The numerical model shows good agreement with the results for various capillary numbers and

lower values of Weber number. At high Weber number, the droplet experiences higher drag forces and a transition between axisymmetric and non-axisymmetric instabilities is observed. The 2D axisymmetric numerical model is able to predict the subsequent reduction in droplet diameter due to increase in the drag forces; however it is unable to capture entirely the effect of the non-axisymmetric instabilities on droplet formation.

Chapter 6 Microencapsulation towards Transplantation

6.1 Introduction

In the preceding chapters, details about the prototype 8-channel device used for encapsulation including design stages, various factors affecting the process of microencapsulation and the effect of each parameter on the microcapsule production have been provided. In this chapter, details about the application of the microcapsules produced using the prototype microfluidic device towards encapsulation of islets, including the isolation of islets to the preparation of microcapsules and the actual transplantation have been discussed in detail. Additionally, details of the application of the prototype microfluidic device towards encapsulation of proteins and other biological materials have also been provided. All the biological functionality of the current prototype microfluidic device, including the isolation of pancreatic islets, labeling of proteins and functional testing were performed in Dr. Opara's lab at Wake Forest Institute of Regenerative Medicine (WFIRM) Winston-Salem, NC, USA.

6.2 Preparation of the Islets and other biological materials for encapsulation

6.2.1 Isolation of islets from rat pancreas

Islets were isolated from the pancreas of Lewis rats (300 – 400 g) using the protocol of collagenase digestion of pancreatic tissue (Lacy & M. 1967) with modifications (Field, Farney & Sutherland 1996). Following euthanasia according to IACUC guidelines, the common bile duct was cannulated and 10 mL of 1 mg/mL Collagenase P (Roche,

Indianapolis) in HEPES-buffered Hanks balanced salt solution (HBSS) was infused to distend the pancreas prior to incubation at 37°C for 20 min. The digestion was stopped with the addition of 15 mL ice-cold wash solution (HEPES-buffered HBSS with 10% fetal bovine serum (FBS), and then shaken for 45 s to dissociate the digested pancreas. The digest was filtered through a 500 μm mesh filter and then washed three times with wash solution and centrifuged at 200 g for 3 min. Islets were then handpicked under a stereomicroscope, or purified on an Optiprep gradient prior to handpicking, and cultured overnight at 37°C, 5% CO2 in RPMI-1640 with 3.3 mM glucose and 10% FBS at a concentration of approximately 100 islets per mL. The above protocol was used by Dr. Opara's lab to provide us with isolated islets.

6.2.2 Fluorescence Labeling of protein for encapsulation

Alexa 568-carboxy was coupled to bovine serum albumin (BSA) by taking 435 μl of 2.3 mg/ml of BSA in PBS in a 2 ml flip cap vial, and adding 28.8 μl of 1 mg/ml of EDAC (Sigma), 32.6 μl of 1 mg/ml of sulpho- NHS (Pierce), 3 μl of AlexaFlor568-carboxy-succinimide (in DMF). This mixture was allowed to react overnight at room temperature on stir plate and covered with aluminum foil. The above solution was dialyzed exhaustively with 4 buffer changes (1 L PBS buffer solution) using a 3.5 kDa dialysis tubing, 0.5–3 ml capacity. The Bio-Rad protein assay was used to determine the concentration of BSA after dialysis.

6.3 Microencapsulation Procedure

Islets were microencapsulated as previously described (Darrabie, Kendall & C. 2005) using the 8-channel microfluidic device. Following purification, islets were suspended in 3%

alginate solution (ultrapure low-viscosity high-mannuronic acid (LVM) sodium alginate, NovaMatrix, Oslo, Norway), and microspheres (<600 μm) containing one islet/microsphere were collected in 100 mM CaCl2 bath where they were gelled during 15 min incubation. Following two washings with normal saline, the microspheres were incubated in 0.1% (w/v) Poly-L-Ornithine (PLO, Sigma-Aldrich, St. Louis, MO) for 10 min to provide them with perm-selectivity. In order to prevent electrostatic interactions between the positive charges on the polycationic PLO and the negative charges on cells and proteins in the body when the PLO-coated microcapsules are used for in vivo experiments, the PLO is covered by a final coating with the biocompatible poly-anionic alginate. Therefore, after two washings in normal saline, the PLO-coated microcapsules were incubated in 0.25% alginate solution for 4 min followed by two saline washes. The microcapsules were then incubated in 55 mM sodium citrate for 10 min to liquefy the inner alginate core prior to two final washes with normal saline. The liquefaction of the inner alginate core is performed in order to enhance the diffusion of nutrients, oxygen, and insulin, as previously shown by Garfinkel et al. (Garfinkel, Harland & Opara 1998).

6.4 Histological tests of encapsulated islet viability

Following encapsulation, islets were fluorescently labeled for viability with carboxyfluorescein diacetate (CFDA) and propidium iodide (PI) to demonstrate live and necrotic cells respectively. Briefly, capsules were incubated with 200 μL 25 μM CFDA in serum-free RPMI 1640 for 15 min at 37°C, and then 30 minutes in RPMI 1640 with 10% FBS, followed by washes in normal saline and a two-minute incubation with 50 μg/mL PI, prior to fixation with 4% paraformaldehyde and nuclear counterstaining with 4′, 6-diamidino-

2-phenylindole (DAPI). Student's *t*-test was used to evaluate the significance of difference in percent viability of encapsulated versus unencapsulated islet cells, and a value of $p<0.05$ was accepted as significant.

6.5 Statistical Evaluation of Data for insulin release

The basal rate of insulin secretion at 5.5 mMol/L glucose was compared to the maximal rate of secretion at 27.5 mMol/L glucose using Student *t*-test, and a value of $P<0.05$ was accepted as significant.

6.6 Encapsulation of Bovine Serum Albumin (BSA)

BSA was encapsulated in capsules to demonstrate the encapsulation of protein using the microfluidic device. Figure 6.1 shows fluorescence images of BSA encapsulated in alginate microcapsules. The bright red spots show the encapsulated protein. Figure 6.1 (a) & (b) show images taken at 10x magnification. It has been previously shown that alginate microspheres can be used to encapsulate therapeutic proteins for controlled drug delivery (Wee & Gombotz 1998; Moya et al. 2009) and in this study it has been shown that the microfluidic device can also be used to encapsulate proteins, thus making it useful for pharmaceutical scale manufacture of microcapsules for controlled drug delivery.

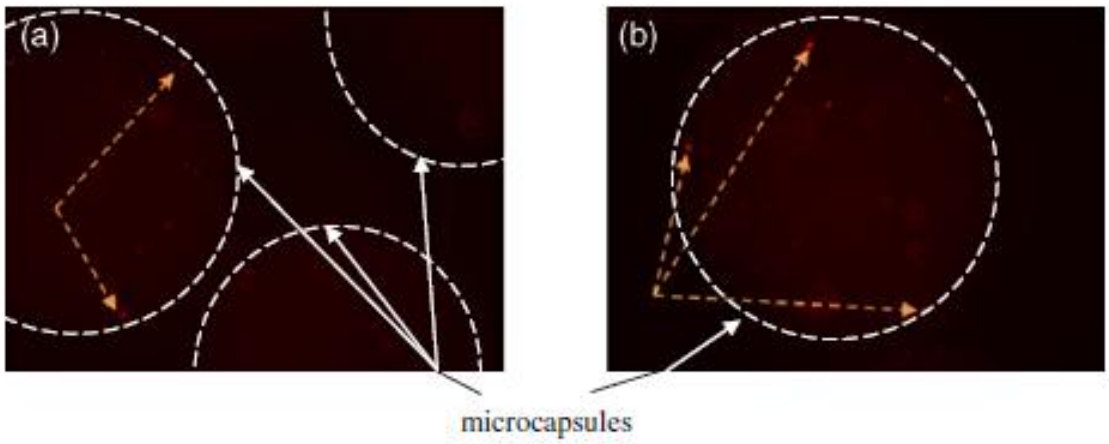

Figure 6.1: (a) and (b) Protein (BSA) encapsulated hydrogel microcapsules. Arrows indicate the location of protein in the image (Tendulkar et al. 2012).

6.7 Encapsulation of Islets and their functional testing

For proof of concept, pancreatic islets isolated from normal Lewis rats were encapsulated using the high throughput microfluidic device. Under low magnification, pancreatic islets can be observed within the capsules as white spheroids approximately 100–200 μm in size, with one islet per capsule (Fig. 6.2(a), (b)). We also examined the effect of the encapsulation procedure on the viability of the pancreatic islets shown in Fig. 6.2(c) where live cells are green and necrotic (dead) cells are red within the islet (Fig. 6.2(c)). We incubated unencapsulated islets and encapsulated islets in RPMI-1640 for 3 h, after which they were stained with the live-dead assay and the images quantitatively assessed for live and dead cells under a confocal microscope using Image J software (NIH) on the z-stack confocal images. Interestingly, statistical analysis of the percent viability of cells indicated that the % mean ± SD encapsulated islet viability (60.4±3.6) was significantly higher than that of the unencapsulated islets (40.3±1.8, $p<0.001$, $n=3$). This data are consistent with the

observations by other investigators who have examined the effect of encapsulation on the viability of other cell types (Chin et al. 2008; Moya et al. 2010). During the functional testing of the microencapsulated islets, insulin secretion increased from a mean standard deviation basal rate of 0.165 ± 0.059 ng/10 islets/min to a stimulated rate of 0.422 ± 0.095 ng/10 islets/min ($P < .05, n = 3$), which was not different from the response of unencapsulated islets to glucose stimulation under same conditions (Tendulkar et al. 2011).

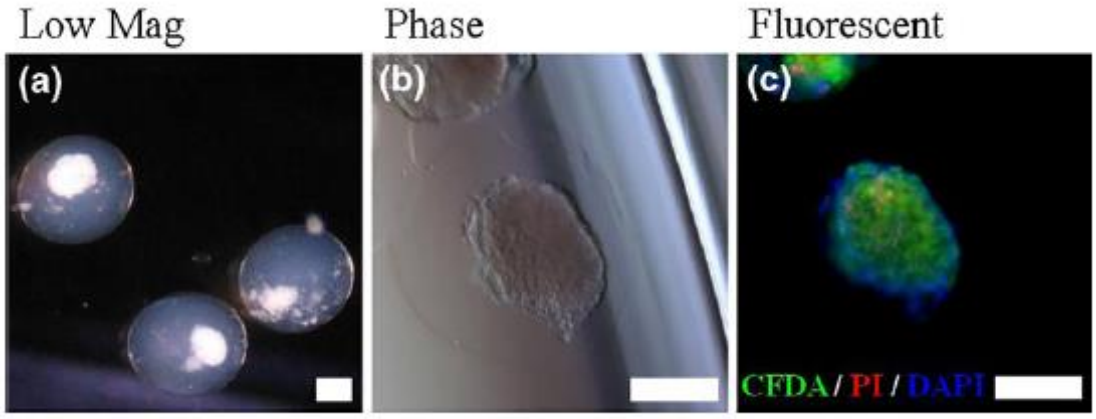

Figure 6.2: Encapsulation of rat pancreatic islets with microfluidic device. (a) Islets seen within the alginate capsules; (b) parallel phase contrast and (c) fluorescently labeled pancreatic islets for live and dead cells, stained with carboxyfluorescein diacetate (CFDA; green) and propidium iodide (PI; red) respectively, and nuclear counterstain 4′, 6-diamidino-2-phenylindole (DAPI; blue). Scale bars=200 μm (Tendulkar et al. 2012).

6.8 Conclusion

In summary, the prototype 8-channel microfluidic device was used to encapsulate pancreatic islets and Bovine Serum Albumin (BSA). Cell viability and insulin response studies show that the pancreatic islets are viable and show response to insulin stimulation after encapsulation. Thus successful microencapsulation of various biological materials using the 8 channel prototype microfluidic device has been presented in this chapter.

Chapter 7 Conclusion

7.1 Introduction

This dissertation describes a scalable co-axial air flow based high throughput microfluidic device containing eight droplet formation zones capable of producing microcapsules at 8 times the current production rates. This research was motivated by the fact that the two most widely used devices for microencapsulation namely the air-syringe droplet generator and the electrostatic bead generator each of which fitted with a single needle through which microcapsules containing cells and other biological materials are incapable of producing sufficient number of microcapsules in a short-period of time to permit mass production of encapsulated and viable cells for transplantation in large animals and humans. As such there is an urgent need for a new approach to producing viable encapsulated cells in sufficient quantities rapidly for routine application in human cell therapy. In this work, an 8 channel co-axial air flow based high throughput microfluidic device was developed which can be scaled up to even 16, 32, 64 droplet formation zones. In this chapter, a summary of design problem, the approach and the applications of the high throughput microfluidic device are presented. This is followed by suggestions for future work.

7.2 Summary and Conclusions

As a part of developing a new approach to producing viable encapsulated cells in sufficient quantities rapidly, a high throughput scalable microfluidic microencapsulation device has been presented. Various encapsulation materials were researched into and use of sodium alginate as the encapsulation material is preferred due to its availability (abundance),

biocompatibility and ability to tailor its properties according to the application. Various material models to describe the non-Newtonian behavior of aqueous solutions of sodium alginate of concentration varying from 0.75% - 3% (wt. /vol.) were investigated and the Carreau model was chosen for its good agreement with the experimental data. CFD analysis using commercial CFD solvers (SolidWorks® Flow simulation) was used to design and model the high throughput scalable microfluidic device. The final design of the microfluidic device was then fabricated using the rapid prototyping technology of 3D printing as a monolithic device. A comparative study was performed to understand the parameters affecting the process of droplet formation and effect of each parameter has been documented. The effect of flow rates of air and alginate, concentration of alginate, distance of the $CaCl_2$ bath from the alginate nozzle on the droplet diameter was observed. The droplet diameter increased as the flow rate of alginate and concentration of alginate increased. The increase in the flow rate of air led to the reduction in the droplet size produced. The change in the distance of the collection plate from the alginate outlet led to observation of an optimal distance required for good formability of capsules and to reduce polymorphism.

High speed video filming was carried out to observe the effect of dimensionless numbers namely capillary number and Weber number. It was observed that the increase in capillary number led to a corresponding increase in the droplet diameter while the increase in Weber number led to reduction in the droplet diameter. At higher Weber number the droplet formation regime starts transition from dripping to jetting and formation of satellite droplets was observed. The defects in the mass manufacturing of microcapsules were identified and the most critical namely satellite droplet formation and observation of stress lines on the

surface of microcapsules were investigated further. It was observed that with the increase in Weber number of air the satellite droplet formation increased. It starts with a single satellite droplet being generated and accounting for a very small fraction of the primary droplet to multiple satellite droplets at higher Weber numbers where by the output of the microfluidic device is no longer monodisperse. A 2-D axisymmetric numerical model was created to model the droplet formation region in a single channel co-axial flow device and qualitative analysis showed good agreement with the experimental high speed video results. Finally the high throughput microfluidic device was used to encapsulate pancreatic islets and protein (Bovine Serum Albumin) to show applicability towards encapsulation of cells and biological materials. Viability studies showed that the islets were viable after encapsulation process and insulin response to glucose stimulation. Thus it can be concluded that the scalable 3-D high throughput microfluidic device is capable of increasing the production rates of microcapsules to 8 times as compared to a single co-flow device and can be used towards successful encapsulation of pancreatic islets and other biological materials for treatment of type1 diabetes and controlled drug delivery applications.

7.3 Future Work

The current work has examined high throughput microencapsulation of pancreatic islets and other biological material using a 3-D scalable microfluidic device. There is ample of scope to expand on this work by considering the following problems:

7.3.1 Sorting of microcapsules

As discussed in chapter 4, section 4.6, the various defects observed in the mass manufacturing of the microcapsules include, production of satellite droplets, observation of

stress lines, empty capsules, etc. In order to maintain higher quality of output to meet the strict guidelines of large animal and human transplants in the medical industry ideally speaking one would want to reduce if not entirely eliminate the above mentioned defects from the final product. For this a high throughput sorting device can be implemented in line to sort the defective microcapsules from the good ones as close to the droplet formation region as possible to help towards improving the quality of the transplant. There is no present work on sorting microcapsules in the size range of 350 – 600 μm and the results obtained from the parametric studies would be a good starting point for development in this direction.

7.3.2 Stress lines observation on the surface of the microcapsules: Material properties and gelling kinetics

As observed in chapter 4 and chapter 5 the material properties of sodium alginate have a significant effect on the droplet formation, gelling of the microcapsules and stress lines observed on the surface of the microcapsules. The parametric study data provided in chapter 4 could be used as a starting point for research in this direction. It was observed that the stress lines observed on the surface of the microcapsules were a result of the shear force exerted on the surface of the capsules during droplet formation. In order to reduce the shearing force acting on the droplet investigation can be carried out into use of additional elements for example electrostatic force in conjunction with air. Use of ultra-hydrophobic alginate nozzles could also be looked into towards reducing the amount of shear exerted on the alginate solution during droplet formation.

Additionally, it was observed that the source of alginate also affected the formation of stress lines. Looking at the formation of stress lines from a material science point of view

would be a good research problem where the study of molecular weight of alginate, composition of alginate (G:M ratio), gelling kinetics during cross linking, are other interesting aspects to be considered.

7.3.3 Scalability and Applications to other cell types

The current study shows the design steps to the scale up from one droplet formation zone to 8 droplet formation zones for a co-flow device. Similar design study can be undertaken to scale up the design to 16, 32, 64 nozzles. Application of the device to pancreatic islets and proteins (Bovine Serum Albumin) have been demonstrated and further investigations can be carried out to improve the applicability of the device to different strains of cells and viruses towards applications in controlled drug release and cancer treatment.

REFERENCES

Abdelgawad, M & Wheeler, AR 2008, 'Low-cost, rapid-prototyping of digital microfluidics devices', *Microfluidics and Nanofluidics*, vol 4, pp. 349-355.

Aebischer, P, Goddard, M, Signore, AP & Timpson, RL 1994, 'Functional Recovery in Hemiparkinsonian Primates Transplanted with Polymer-Encapsulated PC12 Cells', *Experimental Neurology*, vol 126, no. 2, pp. 151-158.

Aebischer, P, Russell, PC, Christenson, L, Panol, G, Monchik, JM & Galletti, PM 1986, 'A bioartificial parathyroid.', *American Society for Artificial Internal Organs*, vol 32, no. 1, pp. 134-137.

Anilkumar, AV, Lacik, I & Wang, TG 2001, 'A novel reactor for making uniform capsules', *Biotechnology and Bioengineering*, vol 75, no. 5, pp. 581-589.

Anna, SL, Bontoux, N & Stone, HA 2003, 'Formation of dispersions using "flow focusing" in microchannels', *Applied Physics Letters*, vol 82, no. 3, pp. 364-366.

ANSYS Inc. 2011, 'ANSYS FLUENT User's Guide', ANSYS, Inc., Canonsburg, PA, USA.

Arnanthigo, Y, Yurteri, CU, Biskos, G, Marijnissen, JCM & Schmidt-Ott, A 2011, 'Out-scaling electrohydrodynamic atomization systems for the production of well-defined droplets', *Powder Technology*, vol 214, no. 3, pp. 382-387.

Arnanthigo, Y, Yurteri, CU, Marijnissen, JM & Schmidt-Ott, A 2009, 'Multiple Electrospray Unit with Circular Symmetry', *European Aerosol Conference 2009*, Karlsruhe.

Baharudin, L 2008, 'Microfluidics: Fabrications and Applications', *Instrumentation Science and Technology*, vol 36, pp. 222-230.

Barrow, ELW, Winchester, GA, Staas, JK, Quenelle, DC & Barrow, WW 1998, 'Use of Microsphere Technology for Targeted Delivery of Rifampin to Mycobacterium tuberculosis-Infected Macrophages', *Antimicrobial Agents and Chemotherapy*, vol 42, no. 10, pp. 2682-2689.

Beck, J, Angus, R, Madsen, B & Britt, D 2007, 'Islet Encapsulation: Strategies to Enhance Islet Cell Functions', *Tissue Engineering*, vol 13, no. 3, pp. 589-599.

Becker, H & Gartner, C 2000, 'Polymer microfabrication methods for microfluidic analytical applications', *Electrophoresis*, vol 21, pp. 12-26.

Becker, H & Gartner, C 2008, 'Polymer microfabrication technologies for microfluidic systems', *Analytical and Bioanalytical Chemistry*, vol 390, no. 1, pp. 89-111.

Ben-Tzvi, P & Rone, W 2010, 'Microdroplet generation in gaseous and liquid environments', *Microsystem Technologies*, vol 16, no. 3, pp. 333-356.

Berkland, C, Kipper, MJ, Narasimhan, B, Kim, KK & Pack, DW 2004, 'Microsphere size, precipitation kinetics and drug distribution control drug release from biodegradable polyanhydride microspheres', *Journal of Controlled Release*, vol 94, no. 1, pp. 129-141.

Bertsch, A, Lorenz, H & Renaud, P 1999, '3D microfabrication by combining microstereolithography and thick resist UV lithography', *Sensors and Actuators A: Physical*, vol 73, no. 1-2, pp. 14-23.

Bisceglie, V 1933, 'Uber die antineoplastische immunitat; heterologe Einpflnzung von Tumoren in Huhner-embryonen', *Ztschr. Krebsforsch*, vol 40, pp. 122-140.

Brackbill, JU, Kothe, DB & Zemach, C 1992, 'A Continuum Method for modelling surface tension', *Journal of Computational Physics*, vol 100, pp. 335-354.

Brandenberger, H & Widmer, F 1998, 'A new multinozzle encapsulation/immobilisation system to produce uniform beads of alginate', *Journal of Biotechnology*, vol 63, no. 1, pp. 73-80.

Bugarski, B, Li, Q, Goosen, MFA, Poncelet, D, Neufeld, RJ & Vunjak, G 1994, 'Electrostatic droplet generation: Mechanism of polymer droplet formation', *AIChE Journal*, vol 40, no. 6, pp. 1026-1031.

Burns, MA, Johnson, BN, Brahmasandra, SN, Handique, K, Webster, JR, Krishnan, M, Sammarco, TS, Man, PM, Jones, D, Heldsinger, D, Mastrangelo, CH & Burke, DT 1998, 'An Integrated Nanoliter DNA Analysis Device', *Science*, vol 282, no. 5388, pp. 484-487.

Cai, X, Lin, Y, Ou, G, Luo, E, Man, Y, Yuan, Q & Gong, P 2007, 'Ectopic osteogenesis and chondrogenesis of bone marrow stromal stem cells in alginate system', *Cell Biology International*, vol 31, pp. 776-783.

Carrilho, E, Martinez, AW & Whitesides, GM 2009, 'Understanding Wax Printing: A Simple Micropatterning Process for Paper-Based Microfluidics', *Analytical Chemistry*, vol 81, no. 16, pp. 7091-7095.

Chabbra, RP 2006, *Bubbles, Drops, and Particles in Non-newtonian Fluids*, 2nd edn, CRC Press.

Chabert, M & Viovy, J-L 2008, 'Microfluidic high-throughput encapsulation and hydrodynamic self-sorting of single cells', *PNAS*, vol 105, no. 9, pp. 3191-3196.

Chang, TMS 1964, 'Semipermeable Microcapsules', *Science*, vol 146, no. 3643, pp. 524-525.

Chang, P, Shen, N & Westcott, A 1993, 'Delivery of recombinant gene products with microencapsulated cells in vivo', *Human Gene Therapy*, vol 4, no. 4, pp. 433-440.

Chaudhary, A, Harma, H, Hanninen, P, McShane, MJ & Srivastava, R 2011, 'Glucose Response of Near-Infrared Alginate-Based Microsphere Sensors Under Dynamic Reversible Conditions', *Diabetes Technology & Therapeutics*, vol 13, no. 8, pp. 827-835.

Chick, WL, Like, AA & Lauris, V 1975, 'Beta Cell Culture on Synthetic Capillaries: An Artificial Endocrine Pancreas', *Science*, vol 187, no. 4179, pp. 847-849.

Chin, K, Khattak, SF, Bhatia, SR & Roberts, SC 2008, 'Hydrogel-perfluorocarbon composite scaffold promotes oxygen transport to immobilized cells', *Biotechnology Progress*, vol 24, no. 2, pp. 358-366.

Chinnayelka, S & McShane, MJ 2005, 'Microcapsule Biosensors Using Competitive Binding Resonance Energy Trasnfer Assays Based on Apoenzymes', *Analytical Chemistry*, vol 77, no. 17, pp. 5501-5511.

Cieslinski, DA & Humes, HD 1994, 'Tissue engineering of a bioartificial kidney', *Biotechnology and Bioengineering*, vol 43, pp. 678-381.

Cihakova, 2001, *Type 1 Diabetes Mellitus: Autoimmune Disease Research Center*, viewed 16 May 2012, <http://autoimmune.pathology.jhmi.edu/diseases.cfm?systemID=3&DiseaseID=23>.

Cirone, P, Bourgeois, JM, Austin, RC & Chang, PL 2002, 'A Novel Approach to Tumor Suppression with Microencapsulated Recombinant Cells', *Human Gene Therapy*, vol 13, no. 10, pp. 11157-1166.

Comiskey, B, Albert, JD, Yoshizawa, H & Jacobson, J 1998, 'An electrophoretic ink for all-printed reflective electronic displays', *Nature*, vol 394, pp. 253-255.

Cross, MM 1965, 'Rheology of non-Newtonian fluids: a new flow equation for viscoelastic systems', *Journal of Colloid Science*, vol 20, no. 5, pp. 417-437.

Dai, C, Wang, B & Zhao, H 2005, 'Microencapsulation peptide and protein drugs delivery system', *Colloids and Surfaces B: Biointerfaces*, vol 41, no. 2-3, pp. 117-120.

Darrabie, MD, Kendall, WFJ & C., OE 2005, 'Characteristics of Poly-L-Ornithine-coated alginate microcapsules', *Biomaterials*, vol 26, no. 34, pp. 6846-6852.

De Vos, P, Haan, BJD & Schilfgaarde, RV 1997, 'Upscaling the production of microencapsulated pancreatic islets', *Biomaterials*, vol 18, no. 16, pp. 1085-1090.

Dean, SK, Yulyana, Y, Williams, G, Sidhu, KS & Tuch, BE 2006, 'Differentiation of Encapsulated Embryonic Stem Cells After Transplantation', *Transplantation*, vol 82, no. 9, pp. 1175-1184.

Deng, W, Klemic, JF, Li, X, Reed, MA & Gomez, A 2006, 'Increase of electrospray throughput using multiplexed microfabricated sources for the scalable generation of monodisperse droplets', *Aerosol Science*, vol 37, no. 6, pp. 696-714.

Donaldson, PEK 1976, 'The Encapsulation of Microelectronic Devices for Long-Term Surgical Implantation', *IEEE Transactions on Biomedical Engineering*, vol 23, no. 4, pp. 281-285.

Draget, KI, Skjak-Braek, G & Smidsrod, O 1994, 'Alginic Acid gels: the effect of alginate chemical composition and molecular weight', *Carbohydrate Polymers*, vol 25, pp. 31-38.

Draget, KI & Taylor, C 2011, 'Chemical, Physical and biological properties of alginates and their biomedical implications', *Food Hydrocolloids*, vol 25, no. 2, pp. 251-256.

Eggers, J 1997, 'Nonlinear dynamics and breakup of free-surface flows', *Reviews of Modern Physics*, vol 69, pp. 865-930.

Esch, MB, Kapur, S, Irizarry, G & Genov, V 2003, 'Influence of master fabrication techniques on the characteristics of embossed microfluidic channels', *Lab on a Chip*, vol 3, pp. 121-127.

Eun, Y-J, Utada, AS, Copeland, MF, Takeuchi, S & Weibel, DB 2011, 'Encapsulating Bacteria in Agarose Microparticles Using Microfluidics for High-Throughput Cell Analysis and Isolation', *ACS Chemical Biology*, vol 6, no. 3, pp. 260-266.

Field, J, Farney, A & Sutherland, DER 1996, 'Improved Islet Isolation From Rat Pancreas Using 35% Bovine Serum Albumin in Combination With Dextran Gradient Separation', *Transplantation*, vol 61, no. 10, pp. 1554-1556.

Fiorini, GS & Chiu, DT 2005, 'Disposable microfluidic devices: fabrication, function and application', *BioTechniques*, vol 38, no. 3, pp. 429-446.

Fisher, SM 2006, 'A Method for the Encapsulation of MicroSpherical Particles', PhD Thesis, North Carolina State University, Raleigh.

Florian-Algarin, V & Acevedo, A 2010, 'Rheology and Thermotropic Gelation of Aqueous Sodium Alginate Solutions', *Journal of Pharmaceutical Innovation*, vol 5, no. 1-2, pp. 37-44.

Fu, S, Thacker, A, Sperger, DM, Boni, RL, Velankar, S, Munson, EJ & Block, LH 2010, 'Rheological Evaluation of Inter-grade and Inter-Batch Variability of Sodium Alginate', *AAPS PharmSciTech*, vol 11, no. 4, pp. 1662-1674.

Ganan-Calvo, AM 1998, 'Generation of Steady Liquid Microthreads and Micron-Sized Monodisperse Sprays in Gas Streams', *Physical Review Letters*, vol 80, no. 2, pp. 285-288.

Gañán-Calvo, AM & Gordillo, JM 2001, 'Perfectly Monodisperse Microbubbling by Capillary Flow Focusing', *Physical Review Letters*, vol 87, no. 27, p. 274501.

Ganan-Calvo, AM, Lopez-Herrera, JM & Riesco-Chueca, P 2006, 'The combination of electrospray and flow focusing', *Journal of Fluid Mechanics*, vol 566, pp. 421-455.

Garfinkel, MR, Harland, RC & Opara, EC 1998, 'Optimization of the Microencapsulated Islet for Transplantation', *Journal of Surgical Research*, vol 76, no. 1, pp. 7-10.

Garg, T, Singh, O, Arora, S & Murthy, R 2011, 'Patented Microencapsulation Techniques And Its Application', *Journal of Pharmacy Research*, vol 4, no. 7, pp. 2097-2102.

Garstecki, P, Fuerstman, MJ, Stone, HA & Whitesides, GM 2006, 'Formation of droplets and bubbles in a microfluidic T-junction—scaling and mechanism of break-up', *Lab on a Chip*, vol 6, pp. 437-446.

Ghosh, SK 2006, 'Functional Coatings and Microencapsulation: A General Perspective', in *Functional Coatings by Polymer Microencapsulation*, Wiley-VCH, Hoboken, NJ, USA.

Graessley, WW, Hazleton, RL & Lindeman, LR 1967, 'The ShearRate Dependence of Viscosity in Concentrated Solutions of NarrowDistribution Polystyrene', *Journal of Rheology*, vol 11, no. 3, pp. 267-285.

Gu, H, Duits, MHG & Mugele, F 2011, 'Droplets Formation and Merging in Two-Phase Flow Microfluidics', *International Journal of Molecular Sciences*, vol 12, pp. 2572-2597.

Guttman, A & Khandurina, J 2004, 'Chapter 11 Microfabricated analytical devices', in E Heftmann (ed.), *Chromatography*, Elsevier.

Haberger, K & Feil, M 2006, 'Ultra-Flat "Mounted" Electronics', *Electronics Systemintegration Technology Conference*, Dresden.

Hashimoto, M, Shevkoplyas, SS, Zasońska, B, Szymborski, T, Garstecki, P & Whitesides, GM 2008, 'Formation of Bubbles and Droplets in Parallel, Coupled Flow-Focusing Geometries', *Small*, vol 4, no. 10, pp. 1795-1805.

He, P, Kim, H, Luo, D, Marquez, M & Cheng, Z 2010, 'Low-frequency ac electro-flow-focusing microfluidic emulsification', *Applied Physics Letters*, vol 96, no. 17, p. 174103.

Herran, CL, Wang, W & Huang, Y 2010, 'Parametric study of Acoustic Excititation-Based Glycerol-Water Microsphere Fabrication in Single Nozzle Jetting', *Journal of Manufacturing Science and Engineering*, vol 132, pp. 051001 1-7.

Hirt, CW & Nichols, BD 1981, 'Volume of fluid (VOF) method for the dynamics of free boundaries', *Journal of Computational Physics*, vol 39, pp. 201-225.

Hsu, B, Chen, H, Fu, S, Huang, Y & Huang, H 1994, 'The use of field effects to generate calcium alginate microspheres and its application in cell transplantation.', *Journal of Formosan Medical Association*, vol 93, no. 3, pp. 240-245.

Hunt, NC & Grover, LM 2012, 'Cell encapsulation using biopolymer gels for regenerative medicine', *Biotechnology Letters*, vol 32, pp. 733-742.

Iliescu, C, Taylo, H, Avram, M, Miao, J & Franssila, S 2012, 'A practical guide for the fabrication of microfluidic devices using glass and silicon', *Biomicrofluidics*, vol 6, no. 1, p. 016505.

Ishii, S, Tago, K & Senoo, K 2010, 'Single-cell analysis and isolation for microbiology and biotechnology: methods and applications', *Applied Microbiology and Biotechnology*, vol 86, no. 5, pp. 1281-1292.

Joki, T, Machluf, M, Atala, A, Zhu, J, Seyfried, NT, Dunn, IF, Abe, T, Carroll, RS & Black, PM 2001, 'Continuous release of endostatin from microencapsulated engineered cells for tumor therapy', *Nature Biotechnology*, vol 19, pp. 35-39.

Jyothi, NVN, Prasanna, PM, Sakarkar, SN, Prabha, KS, Ramaiah, PS & Srawan, GY 2010, 'Microencapsulation techniques, factors influencing encapsulation efficiency ', *Journal of Microencapsulation*, vol 27, no. 3, pp. 187-197.

Kaigala, GV, Ho, S, Pentermanb, R & Backhouse, CJ 2007, 'Rapid prototyping of microfluidic devices with a wax printer', *Lab on a Chip*, vol 7, pp. 384-387.

Kaigler, D, Krebsbach, PH, Wang, Z, West, ER, Horger, K & Mooney, DJ 2006, 'Transplanted Endothelial Cells Enhance Orthotopic Bone Regeneration', *Journal of Dental Research*, vol 85, no. 7, pp. 633-637.

Kandansamy, K & Somasundaram, PD 2012, 'Microencapsulation of Colors by Spray Drying - A Review', *International Journal of Food Engineering* , vol 8, no. 2, pp. 1-17.

Kendall, MR, Bardin, D, Shih, R, Dayton, PA & Lee, AP 2012, 'Scaled-up production of monodisperse, dual layer microbubbles using multi-array microfluidic module for medical imaging and drug delivery', *Bubble Science, Engineering and Technology*, vol 4, no. 1, pp. 12-20.

Keshavarz, T, Ramsden, G, Phillips, P, Mussenden, P & Bucke, C 1992, 'Application of electric field for production of immobilized biocatalysts', *Biotechnology Techniques*, vol 6, no. 5, pp. 445-450.

Kimerling, TE, Liu, W, Kim, BH & Yao, D 2006, 'Rapid hot embossing of polymer microfeatures', *Microsystem Technologies*, vol 12, no. 8, pp. 730-735.

Kim, BI, Jeong, SW, Lee, KG, Park, TJ, Park, JY, Song, JJ, Lee, SJ & Lee, C-S 2012, 'Synthesis of Bioactive Microcapsules Using a Microfluidic Device', *Sensors*, vol 12, pp. 10136-10147.

Kim, DS, Lee, SH, Ahn, CH, Leed, JY & Kwon, TH 2006, 'Disposable integrated microfluidic biochip for blood typing by plastic microinjection moulding', *Lab on a Chip*, vol 6, pp. 794-802.

Kim, C, Lee, KS, Kim, YE, Lee, K-J, Lee, SH, Kim, TS & Kang, JY 2009, 'Rapid exchange of oil-phase in microencapsulation chip to enhance cell viability', *Lab on a Chip*, vol 9, pp. 1294-1297.

Kizilel, S, Scavone, A, Liu, X, Nothias, J-M, Ostrega, D, Witkowski, P & Millis, M 2010, 'Encapsulation of Pancreatic Islets Within Nano-Thin Functional Polyethylene Glycol Coatings for Enhanced Insulin Secretion', *Tissue Engineering: Part A*, vol 16, no. 7, pp. 2217-2228.

Koo, J & Chang, T 1993, 'Secretion of erythropoietin from microencapsulated rat kidney cells: preliminary results.', *International Journal of Artificial Organs*, vol 16, no. 7, pp. 557-560.

Koo, SK, Kim, SC, Wee, YM, Kim, YH, Jung, EJ, Choi, MY, Park, YH, Park, KT, Lim, DG & Han, DJ 2008, 'Experimental Microencapsulation of Porcine and Rat Pancreatic Islet Cells With Air-Driven Droplet Generator and Alginate', *Transplantation Proceedings*, vol 40, no. 8, pp. 2578-2580.

Lacy, PE & M., K 1967, 'Method for the isolation of intact islets from the pancreas', *Diabetes*, vol 16, pp. 35-39.

Lee, HC 1974, 'Drop Formation in a Liquid Jet', *IBM Journal of Research and Development*, vol 18, no. 4, pp. 364-369.

Lim, F & Sun, AM 1980, 'Microencapsulated islets as bioartificial endocrine pancreas', *Science*, vol 210, no. 4472, pp. 908-910.

Lim, GJ, Zare, S, Dyke, MV & Atala, A 2010, 'Cell Microencapsulation', in JL Pedraz, G Orive (eds.), *Therapeutic Applications of Cell Microencapsulation*, Springer New York.

Lin, SP & Chen, JN 1998, 'Role played by the interfacial shear in the instability mechanism of a viscous liquid jet surrounded by a viscous gas in a pipe', *Journal of Fluid Mechanics*, vol 376, pp. 37-51.

Lin, SP & Ibrahim, EA 1990, 'Instability of a viscous liquid jet surrounded by a viscous gas in a vertical pipe', *Journal of Fluid Mechanics*, vol 218, pp. 641-658.

Lin, Y-H, Lee, C-H & Lee, G-B 2008, 'Droplet Formation Utilizing Controllable Moving-Wall Structures for Double-Emulsion Applications', *Journal of Microelectromechanical Systems*, vol 17, no. 3, pp. 573-581.

Lin, SP & Lian, ZW 1993, 'Absolute and convective instability of a viscous liquid jet surrounded by a viscous gas in a vertical pipe', *Physics of Fluids*, vol 5, no. 3, pp. 771-773.

Liu, H, Ofosu, F & Chang, P 1993, 'Expression of human factor IX by microencapsulated recombinant fibroblasts', *Human Gene Therapy*, vol 4, no. 3, pp. 291-301.

Li, W, Young, EWK, Seo, M, Nie, Z, Garstecki, P, Simmons, CA & Kumacheva, E 2008, 'Simultaneous generation of droplets with different dimensions in parallel integrated microfluidic droplet generators', *Soft Matter*, vol 4, no. 2, pp. 258-262.

Löhr, M, Hoffmeyer, A, Kröger, J-C, Freund, M, Hain, J, Holle, A, Karle, P, Knöfel, WT, Liebe, S, Müller, P, Nizze, H, Renner, M, Saller, RM, Wagner, T, Hauenstein, K, Günzburg,

WH & Salmons, B 2001, 'Microencapsulated cell-mediated treatment of inoperable pancreatic carcinoma', *The lancet*, vol 357, no. 9268, pp. 1591-1592.

Lorenz, RM, Fiorini, GS, Jeffries, GDM, Lim, DSW, He, M & Chiu, DT 2008, 'Simultaneous generation of multiple aqueous droplets in a microfluidic device', *Analytica Chimica Acta*, vol 630, pp. 124-130.

Machluf, M, Orsola, A & Atala, A 2000, 'Controlled release of therapeutic agents: slow delivery and cell encapsulation', *World Journal of Urology*, vol 18, no. 1, pp. 80-83.

Malek, CGK 2006, 'Laser processing for bio-microfluidics applications (part I)', *Analytical and BioAnalytical Chemistry*, vol 385, no. 8, pp. 1351-1361.

Malek, CGK 2006, ' Laser processing for bio-microfluidics applications (part II)', *Analytical and Bioanalytical Chemistry*, vol 385, no. 8, pp. 1362-1369.

Mancini, M, Moresi, M & Sappino, F 1996, 'Rheological Behaviour of Aqueous Dispersions of Algal Sodium Alginates', *Journal of Food Engineering*, vol 28, no. 3-4, pp. 283-295.

Manojlovic, V, Djonlagic, J, Obradovic, B, Nedovic, V & Bugarski, B 2006, 'Immobilization of cells by electrostatic droplet generation: a model system for potential application in medicine', *International Journal of Nanomedicine*, vol 1, no. 2, pp. 163-171.

Martinez, AW, Phillips, ST & Whitesides, GM 2008, 'Three-dimensional microfluidic devices fabricated in layered paper and tape', *PNAS*, vol 105, no. 50, pp. 19606-19611.

Martinez, AW, Phillips, ST, Whitesides, GM & Carrilho, E 2010, 'Diagnostics for the Developing World: Microfluidic Paper-Based Analytical Devices', *Analytical Chemistry*, vol 82, no. 1, pp. 3-10.

Maruo, S, Ikuta, K & Korogi, H 2003, 'Submicron manipulation tools driven by light in a liquid', *Applied Physics Letters*, vol 82, no. 1, pp. 133-135.

Matte, U, Lagranha, VL, Carvalho, TGD, Mayer, FQ & Giugliani, R 2011, 'Cell microencapsulation: a potential tool for the treatment of neuronopathic lysosomal storage diseases', *Journal of Inherited Metabolic Disease*, vol 34, no. 5, pp. 983-990.

McCormick, RM, Nelson, RJ, Alonso-Amigo, MG, Benvegnu, DJ & Hooper, HH 1997, 'Microchannel Electrophoretic Separations of DNA in Injection-Molded Plastic Substrates', *Analytical Chemistry*, vol 69, no. 14, pp. 2626-2630.

McDonald, JC, Duffy, DC, Anderson, JR, Chiu, DT, Wu, H, Schueller, OJA & Whitesides, GM 2000, 'Fabrication of Microfluidic systems in poly(dimethylsiloxane)', *Electrophoresis*, vol 21, pp. 27-40.

McShane, M & Ritter, D 2010, 'Microcapsules as optical biosensors', *Journal of Materials Chemistry*, vol 20, pp. 8189-8193.

Metz, S, Bertsch, A, Bertrand, D & Renaud, P 2004, 'Flexible polyimide probes with microelectrodes and embedded microfluidic channels for simultaneous drug delivery and multi-channel monitoring of bioelectric activity.', *Biosensors and Bioelectronics*, vol 19, no. 10, pp. 1309-1318.

Mikos, AG, Papadaki, MG, Kouvroukoglou, S, Ishaug, SL & Thomson, RC 1994, 'Mini-Review: Islet Transplantation to Create a Bioartificial Pancreas', *Biotechnology and Bioengineering*, vol 43, no. 7, pp. 673-677.

Miller, E & Rothstein, JP 2004, 'Control of the sharkskin instability in the extrusion of polymer melts using induced temprature gradients', *Rheologica Acta*, vol 44, no. 2, pp. 160-173.

Moya, ML, Cheng, MH, Huang, JJ, Francis-Sedlak, ME, Kao, S, Opara, EC & Brey, EM 2010, 'The effect of FGF-1 loaded alginate microbeads on neovascularization and adipogenesis in a vascular pedicle model of adipose tissue engineering.', *Biomaterials*, vol 31, no. 10, pp. 2816-2826.

Moya, ML, Lucas, S, Francis-Sedlak, M, Liu, X, Garfinkel, MR, Huang, J-J, Cheng, M-H, Opara, EC & Brey, EM 2009, 'Sustained delivery of FGF-1 increases vascular density in comparison to bolus administration', *Microvascular Research*, vol 78, no. 2, pp. 142-147.

Murua, A, Portero, A, Orive, G, Hernández, RM, Castro, MD & Pedraz, JL 2008, 'Cell microencapsulation technology: Towards clinical application', *Journal of Controlled Release*, vol 132, pp. 76-83.

Nayfeh, AH 1970, 'Nonlinear Stability of a Liquid Jet', *Physics of Fluids*, vol 13, no. 4, pp. 841-847.

Nedović , VA, Manojlović, V, Pruesse, U, Bugarski, B, Đonlagić, J & Vorlop, KD 2006, 'Optimization of the electrostatic droplet generation process for controlled microbead production: Single nozzle system', *Chemical Industry and Chemical Engineering Quarterly*, vol 12, no. 1, pp. 53-57.

Nelson, G 2002, 'Application of microencapsulation in textiles', *International Journal of Pharmaceutics*, vol 242, pp. 55-62.

Nisisako, T & Torii, T 2007, 'Microfluidic large-scale integration on a chip for mass production of monodisperse droplets and particles', *Lab on a Chip*, vol 8, pp. 287-293.

Nussinovitch, A 2010, 'Bead Formation, Strengthening and Modification', in *Polymer Macro- and Micro-Gel Beads: Fundamentals and Applications*, 1st edn, Springer.

Opara, EC 1998, 'The therapeutic potential of islet cell transplant in the treatment of diabetes', *Expert Opinion on Investigational Drugs*, vol 7, no. 5, pp. 785-795.

Opara, EC & Kendall Jr, WF 2002, 'Immunoisolation techniques for islet cell transplantation', *Expert Opinion on Biological Therapy*, pp. 503-511.

Opara, EC, Mirmalek-Sani, S-H, Khanna, O, Moya, ML & Brey, EM 2010, 'Design of a bioartificial pancreas', *Journal of Investigative Medicine*, vol 58, no. 7, pp. 831-837.

Orive, G, Gascon, AR, Hernandez, RM, Igartua, M & Pedraz, JL 2003, 'Cell microencapsulation technology for biomedical purposes: novel insights and challenges', *Trends in Pharmacological Sciences*, vol 24, no. 5, pp. 207-210.

Orive, G, Hernández, RM, Gascón, AR, Calafiore, R, Chang, TMS, Vos, PD, Hortelano, G, Hunkeler, D, Lacík, I & Pedraz, JL 2004, 'History, challenges and perspectives of cell microencapsulation', *Trends in Biotechnology*, vol 22, no. 2, pp. 87-92.

Orive, G & Pedraz, JL 2010, 'Highlights and Trends in Cell Encapsulation', in *Therapeutic Applications of Cell Microencapsulation*, Springer New York.

Pareta, RA, McQuilling, JP, Farney, A & Opara, EC 2012, 'Bioartificial Pancreas: Evaluation of Crucial Barriers to Clinical Application', in *Organ Donation*, INTECH Publishers, <http://cdn.intechopen.com/pdfs/27738/InTech-Bioartificial_pancreas_evaluation_of_crucial_barriers_to_clinical_application.pdf>.

Park, J, Ye, M & Park, K 2005, 'Biodegradable Polymers for Microencapsulation of Drugs', *Molecules*, vol 10, no. 1, pp. 146-161.

Pimbley, WT & Lee, HC 1977, 'Satellite Droplet Formation in a Liquid Jet', *IBM Journal of Research and Development*, vol 21, no. 1, pp. 21-30.

Poncelet, D, Neufeld, R, Bugarski, B, Amsden, BG, Zhu, J & Goosen, MFA 1994, 'A Parallel plate electrostatic droplet generator: Parameters affecting microbead size', *Applied Microbiology and Biotechnology*, vol 42, no. 2-3, pp. 251-255.

Poncelet, D, Neufeld, RJ, Goosen, MFA, Burgarski, B & Babak, V 1999, 'Formation of Microgel Beads by Electric Dispersion of Polymer Solutions', *AIChE Journal*, vol 45, no. 9, pp. 2018-2023.

Prüsse, U, Bilancetti, L, Bučko, M, Bugarski, B, Bukowski, J, Gemeiner, P, Lewińska, D, Manojlovic, V, Massart, B, Nastruzzi, C, Nedovic, V, Poncelet, D, Siebenhaar, S, Tobler, L, Tosi, A & A. Vikartovská, K-DV 2008, 'Comparison of different technologies for alginate beads production', *Chemical Papers*, vol 62, no. 4, pp. 364-374.

Prüsse, U, Bruske, F, Breford, J & Vorlop, K-D 1998, 'Improvement of the Jet Cutting Method for the Preparation of Spherical Particles from Viscous Polymer Solutions', *Chemical Engineering and Technology*, vol 21, no. 2, pp. 153-157.

Qin, D, Xia, Y & Whitesides, GM 1996, 'Rapid prototyping of complex structures with feature sizes larger than 20 μm', *Advanced Materials*, vol 8, no. 11, pp. 917-919.

Rallison, JM 1984, 'The Deformation of Small Viscous Drops and Bubbles in Shear Flows', *Annual Review of Fluid Mechanics*, vol 16, pp. 45-66.

Ramasubramanian, MK 2004, 'Methods and Devices for Microencapsulation of Cells', *US7482152 B2*.

Rayleigh, L 1879, 'On the Capillary Phenomena of Jets', *Proceedings of the Royal Society of London*, vol 29, no. 196-197, pp. 71-97.

Rayleigh, L 1892, 'On the instability of a cylinder of viscous liquid under capillary force', *Philisophical Magazine Series 5*, vol 34, no. 107, pp. 145-154.

Richards, JR, Beris, AN & Lenhoff, AM 1995, 'Drop Formation in Liquid-liquid Systems Before and After Jetting', *Physics of Fluids*, vol 7, no. 11, pp. 2617-2630.

Ricordi, C, Lacy, PE, Finke, EH, Olack, BJ & Scharp, DW 1988, 'Automated Method for isolation of human pancreatic islets', *Diabetes*, vol 37, pp. 413-420.

Seemann, R, Brinkmann, M, Pfohl, T & Herminghaus, S 2012, 'Droplet based microfluidics', *Reports on Progress in Physics*, vol 75, no. 1, p. 016601.

Sheeran, PS & Dayton, PA 2012, 'Phase-Change Contrast Agents for Imaging and Therapy', *Current Pharmaceutical Design*, vol 18, no. 15, pp. 2152-2165.

Sheeran, PS, Wong, VP, McFarland, RJ, Ross, WD, Feingold, SG, Matsunaga, TO & Dayton, PA 2010, 'Efficacy of Perfluorobutane as a Phase-Change Contrast Agent for Low-Energy Ultrasonic Imaging', *Ultrasonics Symposium (IUS)*, San Diego, California.

Si, T, Li, F & Yin, X-Z 2009, 'Modes in flow focusing and instability of coaxial liquid-gas jets', *Journal of Fluid Mechanics*, vol 629, pp. 1-23.

Si, T, Li, F, Yin, X-Y & Yin, X-Z 2010, 'Spatial instability of coflowing liquid-gas jets in capillary flow focusing', *Physics of Fluids*, vol 22, pp. 112105 1-7.

Skjak-Braek, G, Smidsrod, O & Larsen, B 1986, 'Tailoring of algintes by enzymatic modification in vitro', *International Journal of Biological Macromolecules*, vol 8, no. 6, pp. 330-336.

SolidWorks 2011, *Technical Reference*.

Soon-Shiong, , Heintz, RE, Merideth, N, Yao, QX, Yao, Z, Zheng, T, Murphy, M, Moloney, MK, Schmehl, M & Harris, MM 1994, 'Insulin independence in a type 1 diabetic patient after encapsulated islet transplantation', *Lancet*, vol 343, no. 8903, pp. 950-951.

Steigert, J, Haeberle, S, Brenner, T, uller, CM, Steinert, CP, Koltay, P, Gottschlich, N, Reinecke, H, R¨uhe, J, Zengerle, R & Ducr´ee, J 2007, 'Rapid prototyping of microfluidic chips in COC', *Journal of Micromechanics and Microengineering*, vol 17, no. 2, pp. 333-341.

Stone, HA 1994, 'Dynamics of Drop Deformation and Breakup in Viscous Fluids', *Annual Review of Fluid Mechanics*, no. 26, pp. 65-102.

Sugiura, S, Oda, T, Aoyagi, Y, Matsuo, R, Enomoto, T, Matsumoto, K, Nakamura, T, Satake, M, Ochiai, A, Ohkohchi, N & Nakajima, M 2007, 'Microfabricated airflow nozzle for microencapsulation of living cells into 150 micrometer microcapsules', *Biomedical Microdevices*, vol 9, no. 1, pp. 91-99.

Sugiura, S, Oda, T, Izumida, Y, Aoyagi, Y, Satake, M, Ochiai, A, Ohkohchi, N & Nakajima, M 2005, 'Size control of calcium alginate beads containing living cells using micro-nozzle array', *Biomaterials*, vol 26, pp. 3327-3331.

Su, G, Longest, PW & pidaparti, RM 2010, 'A Novel micropump droplet generator for aerosol drug delivery: Design Simulations', *Biomicrofluidics*, vol 4, pp. 044108 1-18.

Sun, Y & Kwok, YC 2006, 'Polymeric microfluidic system for DNA analysis', *Analytica Chimica Acta*, vol 556, no. 1, pp. 80-96.

Sun, Y, Ma, X, Zhou, D, Vacek, I & Sun, AM 1996, 'Normalization of diabetes in spontaneously diabetic cynomologus monkeys by xenografts of microencapsulated porcine islets without immunosuppression', *The Journal of Clinical Investigation*, vol 98, no. 6, pp. 1417-1422.

Tabata, Y, Inoue, Y & Ikada, Y 1996, 'Size effect on systemic and mucosal immune responses induced by oral administration of biodegradable microspheres', *Vaccine*, vol 14, no. 17-18, pp. 1677-1685.

Taylor, GI 1962, *Generation of ripples by wind blowing over viscous fluids*, Cambridge University Press, Cambridge.

Technologies, LC 2010, *LCT: The cell implant company*, viewed 24 September 2012, <http://www.lctglobal.com/>.

Teh, S-Y, Lin, R, Hung, L-H & Lee, AP 2008, 'Droplet microfluidics', *Lab on a Chip*, vol 8, pp. 198-220.

Tendulkar, S 2010, 'MAE 586 report', PhD Qualifiers report, North Carolina State University, Raleigh.

Tendulkar, S, McQuilling, JP, Childers, C, Pareta, R, Opara, EC & Ramasubramanian, MK 2011, 'A scalable microfluidic device for the mass production of microencapsulated islets', *Transplantation Proceedings*, vol 43, no. 9, pp. 3184-3187.

Tendulkar, S, Mirmalek-Sani, S-H, Childers, C, Saul, J, Opara, EC & Ramasubramanian, MK 2012, 'A three-dimensional microfluidic approach to scaling up microencapsulation of cells', *Biomedical Microdevices*, pp. 1-9.

Tewes, F, Boury, F & Benoit, AJ-P 2006, 'Biodegradable Microspheres: Advances in Production Technology', in S Benita (ed.), *Microencapsulation: Methods and Industrial Applications*, CRC Press, Boca Raton, Florida, US.

Thomas, MS, Millare, B, Clift, JM, Bao, D, Hong, C & Vullev, VI 2010, 'Print-and-Peel Fabrication for Microfluidics: What's in it for Biomedical Applications? ', *Annals of Biomedical Engineering*, vol 38, no. 1, pp. 21-32.

Thorsen, T, Roberts, RW, Arnold, FH & Quake, SR 2001, 'Dynamic Pattern Formation in a Vesicle-Generating Microfluidic Device', *Physical Review Letters*, vol 86, no. 18, pp. 4163-4166.

Tomotika, S 1935, 'On the Instability of a Cylindrical Thread of a Viscous Liquid surrounded by another Viscous Fluid', *Proceedings of the Royal Society of London*, vol 150, no. 870, pp. 322-337.

Umbanhowar, PB, Prasad, V & Weitz, DA 2000, 'Monodisperse Emulsion Generation Via Drop Break-Off in a Co-Flowing Stream', *Langmuir*, vol 16, no. 2, pp. 347-351.

Utada, AS, Fernandez-Nieves, A, Stone, HA & Weitz, DA 2007, 'Dripping to Jetting Transitions in Coflowing Liquid Streams', *Physical Review Letters*, vol 99, no. 9, p. 094502 (4).

Vaithilingam, V & Tuch, BE 2011, 'Islet Transplantation and Encapsulation: An Update on Recent Developments', *The Review of DIABETIC STUDIES*, vol 8, no. 1, pp. 51-67.

Wang, T, Lacík, I, Brissová, M, Anilkumar, AV, Prokop, A, Hunkeler, D, Green, R, Shahrokhi, K & Powers, AC 1997, 'An encapsulation system for the immunoisolation of pancreatic islets', *Nature Biotechnology*, vol 15, pp. 358-362.

Ward, T, Faivre, M, Abkarian, M & Stone, HA 2005, 'Microfluidic flow focusing: Drop size and scaling in pressure versus flow-rate-driven pumping', *Electrophoresis*, vol 26, no. 19, pp. 3716-3724.

Wee, S & Gombotz, WR 1998, 'Protein release from alginate matrices', *Advanced Drug Delivery Reviews*, vol 31, no. 3, pp. 267-285.

Wheatley, MA, El-Sherif, D, Basude, R, Shimp, R & Narayan, P 1998, 'Ultrasound Triggered Drug Delivery with Contrast Imaging: Effect of Microencapsulation Method', *Materials Research Society Proceedings*.

White, MA 1998, 'The Chemistry behind Carbonless Copy Paper', *Journal of Chemical Education*, vol 75, no. 9, pp. 1119-1120.

Whitesides, GM 2006, 'The origins and the future of microfluidics', *Nature*, vol 442, pp. 368-373.

Wolters, GHJ, Fritschy, WM, Gerrits, D & Schilfgaarde, RV 1992, 'A Versatile Alginate Droplet Generator Applicable for Microencapsulation of Pancreatic Islets', *Journal of Applied Biomaterials*, vol 3, no. 4, pp. 281-286.

Wong, H & Chang, TM 1986, 'Bioartificial liver: implanted artificial cells microencapsulated living hepatocytes increases survival of liver failure rats', *The International Journal of Artificial Organs*, vol 9, no. 5, pp. 335-336.

Wu, H-W, Huang, Y-C, Wu, C-L & Lee, G-B 2009, 'Exploitation of a microfluidic device capable of generating size-tunable droplets for gene delivery', *Microfluidics and Nanofluidics*, vol 7, no. 1, pp. 45-56.

Xu, W, Liu, L & Charles, IG 2002, 'Microencapsulated iNOS-expressing cells cause tumor suppression in mice', *FASEB*, vol 16, no. 2, pp. 213-215.

Yaniv, YR 2009, 'Rheological Characterization of Alginate Microbead Gels and Suspensions', (Doctoral Dissertation), North Carolina State University, Raleigh.

Yoshizawa, H 2004, 'Trends in Microencapsulation Research', *KONA Powder and Particle*, vol 22, pp. 23-31.

Zeng, Y, Novak, R, Shuga, J, Smith, MT & Mathies, RA 2010, 'High-Performance Single Cell Genetic Analysis Using Microfluidic Emulsion Generator Arrays', *Analytical Chemistry*, vol 82, no. 8, pp. 3183-3190.

Zhang, X 1999, 'Dynamics of drop formation in viscous flows', *Chemical Engineering Science*, vol 54, no. 12, pp. 1759-1774.

Zhang, X 1999, 'Dynamics of Growth and Breakup of Viscous Pendant Dropts into Air', *Journal of Colloid and Interfacial Science*, vol 212, pp. 107-122.

Zhang, A-L & Zha, Y 2012, 'Fabrication of paper-based microfluidic device using printed circuit technology', *AIP Advances*, vol 2, no. 2, p. 022171.